A NEW MODEL FOR THREE-DIMENSIONAL NONLINEAR DISPERSIVE LONG WAVES

Thesis by

Helene R. Schember

In Partial Fulfillment of the Requirements

for the Degree of

Doctor of Philosophy

California Institute of Technology

Pasadena, California

1982

(Submitted May 26, 1982)

ACKNOWLEDGEMENTS

My sincere thanks go to my advisor, Professor Theodore Y.-T. Wu, for his enthusiasm, encouragement and insight. The elegant long wave model which he first proposed has provided a sound and innovative foundation for this work. I gratefully acknowledge the many contributions which Dr. Wu has made to my personal and scientific development.

Professors Rolf Sabersky and James Knowles have helped me to feel more comfortable at Caltech and I appreciate their support during my years here. I also thank them for serving on both my candidacy and thesis committees.

My career was strongly influenced by my undergraduate advisor, Professor Timothy W. Kao, who generously expended time and energy in my behalf. I thank him for introducing me to fluid mechanics and for so solidly supporting my interest in this topic.

I appreciate the assistance I have received from other members of the Engineering Science Department. Dr. George Yates successfully transformed a number of last-minute projects into excellent results. Cecilia Lin also transformed some equally last-minute sketches into beautiful graphic artwork. And Helen Burrus, of course, is the key to this whole operation -- always in touch, organizing, and making the whole package turn out just right. My thanks go to each of them.

Carol Oken and Robin Stroll are two special friends. I thank them for their continuing support and confidence in me throughout my graduate work at Caltech.

The many conversations I have had with Dr. Sigrid McPherson have had a powerful positive influence on my life. I appreciate her wise counsel, insight into

Caltech, and interest in my well-being.

No matter what degree I have, or what my experience, a part of me will always be Joe and Helen's kid from Erie, Pa. Mom and Dad deserve full credit for the love, patience and encouragement that they have so freely supplied over these 27 years.

I have saved my most heartfelt thanks for Dr. Walter (Rick) Cook III. Rick has contributed so much to this thesis -- from a three-dimensional plotting package (and the movie!), to late-night strategy sessions, to a profound and unshakable confidence in me. There seems to be no way to adequately express my appreciation for the many loving contributions he has made to my research and to my whole life.

This research has been supported through grants from the National Science Foundation (PFR 77-16085, CME 77-21236) and the Office of Naval Research (N 00014-76-C-0157). I have received additional financial support through the California Institute of Technology in the form of Tuition Fellowships and Graduate Research and Teaching Assistantships.

ABSTRACT

A new formulation of the pair of Boussinesq-class equations for modelling the propagation of three-dimensional nonlinear dispersive long water waves is presented. This set of model equations permits spatial and temporal variations of the bottom topography. Further, the two resultant equations may be combined into a single equation through the introduction of an irrotational layer-mean velocity. An exact permanent-form solution is derived for the combined equation, which is still of the Boussinesq-class and includes reflection. This solution for the surface height is found to describe a slightly wider wave than the permanent form solution to the uni-directional Korteweg-deVries Equation.

A numerical scheme using an implicit finite-difference method is developed to solve the combined equation for propagation over fixed sloping bottom topography. The scheme is tested for various grid sizes using the permanent-form solution, and an oscillatory tail is seen to develop as a result of insufficient mesh refinement.

Several cases of wave propagation over a straight sloping ramp onto a shelf are solved using the permanent-form solution as initial conditions and the results are found to be in good agreement with previous results obtained by using either the Boussinesq dual-equation set or the single Korteweg-deVries equation. The combined equation is used to solve the related problem in two-horizontal dimensions of a wave propagating in a channel having a curved-ramp bottom topography. Depending on the specific topography, focussing or defocussing occurs and the crest is selectively amplified. Indications of cross-channel oscillation are presented. Linear, nondispersive theory is used to solve

a case with identical topographical features and initial condition. The solutions using the simplified theory are found to be considerably different from the results for nonlinear, dispersive theory with respect to the overall three-dimensional wave shape as well as in the areas of crest amplification, soliton formation and cross-channel effects.

TABLE OF CONTENTS

CHAPTER 1

Introduction

Waves travelling on the surface of water may be influenced by the bottom topography. In particular, waves possessing a wavelength which is large in comparison to the water depth are strongly affected by the lower boundary. To emphasize the large relative wavelength, these waves are called long waves, while to emphasize the small relative depth, they are alternately known as shallow-water waves. This thesis will explore a new formulation of classical long water wave theory originally developed over a century ago. The goal is to investigate the effects of three-dimensional bottom topography without sacrificing other interesting features of the propagation such as nonlinearity, dispersion and wave reflection.

Since the definition for long waves relies on the relative measure of wavelength to water depth, the kinds of waves considered here span a considerable range. For instance, the first oscillatory mode in a bathtub filled with a foot of water is a long wave. On another scale, the seismically generated sea waves known as tsunami† have wavelengths so long that even the deep ocean basin, averaging 3,500 meters in depth, seems shallow.

Much of the discussion in this paper will center on the effects of nonlinearity and dispersion in long waves. Nonlinearity is identified as the steepening of the front face of a wave. This steepening occurs when higher amplitudes travel at higher phase velocity. A wave which is strongly affected by

† The term tsunami has been adopted by scientists to denote an earthquake-generated wave. These waves are sometimes referred to as "tidal" waves, however, this term has been discarded in order to clearly separate tsunami from tides.

nonlinearity will overturn or break. Breaking waves are a special and difficult topic and will be excluded from the analysis presented here. We rely on the effects of dispersion -- the tendency of a wave to disperse into a train of waves -- to hold the effects of nonlinearity in check and prevent breaking. When nonlinearity and dispersion are balanced, we have a situation known as weak nonlinearity.

Nonlinear dispersive long water waves have been studied for over 100 years, beginning with Russell (1844) who observed a persistent, long-wavelength wave (a solitary wave) propagating in a canal. The simplest model for long wave propagation (described in many texts, for example, Lamb [1932]) assumes that the waves are of infinitesimal amplitude, linear and nondispersive. For constant depth situations, with no external forcing, this model reduces to the well-known wave equation. Airy (1845) developed a set of model equations (now bearing his name) which takes into account the finite amplitude of the wave, assuming that the effects of nonlinearity dominate dispersion. These equations predict that all waves steepen and break, a prediction which precludes the existence of permanent-form water waves. The classical model for finite amplitude long water waves in constant depth including nonlinear and dispersive effects was developed in three papers by Boussinesq (1871a,b, 1872). Rayleigh (1876) independently derived an equivalent set of equations. Both Boussinesq and Rayleigh derived the permanent form (solitary wave) solutions to these equations. Korteweg and deVries (1895), basing their work on the formulation of Rayleigh, restricted the equations to propagation in one direction only, combined them and found permanent form solutions (for both periodic and solitary waves). Their equation is known as the KdV equation. Miles (1981) gives a full account of the history of the KdV equation, with special emphasis on Boussinesq's contributions. Ursell (1953) clarified the relationship between the

Airy equations and the Boussinesq equations by establishing the importance of the relationship between the sizes of the dispersive and nonlinear effects. Some higher order formulations of the equations for finite amplitude long waves have been developed by Grimshaw (1971), Laitone (1960) and Fenton (1971). A method known as inverse scattering was used by Gardner, Green, Kruskal and Miura (1967) to solve the KdV initial-value problem. This method can be used to predict the number of solitary waves (solitons) which will emerge from arbitrary initial data. Madsen and Mei (1969) presented a derivation of Boussinesq-type equations for the propagation in one horizontal dimension of long waves over a bottom with slow spatial variation. Johnson (1972) developed a KdV equation with variable coefficients to described a wave progressing over a ramp and obtained the number and amplitude of the solitons produced on the shelf as a function of relative depth change and initial amplitude. Tappert and Zabusky (1971) independently obtained similar results.

In the past 20 years, it has become especially clear that research efforts concerned with the propagation of weakly nonlinear long waves over an uneven bottom has taken two distinct directions: One approach is to neglect reflection and proceed to combine the governing equations into a convenient, single equation of the KdV-type which is then solved either by inverse-scattering techniques or numerical methods. The other method is to leave the equations in their dual-equation form and solve these numerically. In this study, we present a description of weakly nonlinear shallow water waves which can conveniently accommodate three-dimensional variations in the bottom topography. Based on the model first put forward by Wu (1981), a single governing equation is derived for this system and a permanent form solution for constant depth is obtained. The governing equations are solved numerically for a series of cases of increasing complexity. One of our objectives in this study is

to establish some fundamental baseline information about this new equation, which has the potential to conveniently replace other single and multiple equation models while including effects that these models neglect.

Another goal of this thesis is to investigate some basic problems involving three-dimensional bottom topography, and this is accomplished through the development of a numerical method to solve the combined equation discussed above. Many computational models have been developed previously to solve the long wave equations, although most of these rely on the linear, nondispersive equations; see Goring (1978) for a discussion of criteria useful for determining when the linear, dispersive equations are appropriate. A computational model using two sets of difference equations was developed by Leendertse (1967) to study the propagation of long waves in two horizontal dimensions. The effects of the earth's rotation and bottom roughness were included; the water depths at certain points must be given as input to the numerical scheme. Peregrine (1967) numerically calculated solutions to the Boussinesq equation for a wave approaching a straight beach of constant slope. In addition, Peregrine obtained analytical solutions for wave reflected off the slope by using linear theory. The Boussinesq equations were solved numerically for the case of a solitary wave ascending a straight ramp by Madsen and Mei (1969). They cited experimental confirmation of the disintegration of the solitary wave on the shelf into two or more solitary waves. The variable-coefficient KdV equation has been solved, for cases involving ramp transitions from one depth to another, by Johnson (1972). Vliegenthart(1971) analyses a group of finite difference schemes used to solve initial-value problems for the KdV equation, including some schemes which are dissipative. Goring (1978) has solved the Boussinesq equation in one horizontal dimension using a finite element method. Lepelletier (1981) included dissipation in his finite-element solution to a Boussinesq-type model for basin excitation

and transient harbor excitation problems. A numerical model which propagates a cylindrical weakly nonlinear long waves was developed by Chwang and Wu (1976) to investigate the focussing of curved wavefronts. Their formulation solves the two-equation Boussinesq equations in cylindrical coordinates for spatially varying bottom topography.

The numerical methods required to solve the new combined equation which we present in this thesis are straightforward and need not be specific to the particularities of the situation under study since important effects such as nonlinearity, dispersion and wave reflection are included in the fundamental formulation. We employ an implicit finite-difference method to develop two computer programs to solve the combined equations. The basic problems investigated in this thesis concern the evolution of an initial solitary wave propagating down the length of a rectangular channel. The channel contains two regions of constant depth connected by a submerged ramp. In our numerical experiments, different ramp geometries are modelled. The simplest of these geometries (which reduces the problem to propagation in one horizontal dimension only) is the straight ramp with constant slope and no variation in the cross-channel direction. The other ramp geometries considered in this study retain the feature of constant longitudinal slope but incorporate curvature in the cross-channel direction. In all cases, the ramp configuration and wave motion are taken to be symmetric with respect to the centerplane of the channel. As the initial condition, we use the solitary wave solution appropriate to our combined equation. A single solitary wave, as opposed to a train of periodic waves, is useful in the context of our experiments for a number of reasons: (1) The solitary wave form can be derived as an exact solution to our governing equation for constant depth. (2) The solitary wave's extremely simple shape reduces the need for elaborate boundary conditions

which may influence the nature of the solution. (3) The solitary wave can be easily distinguished from the reflected wave when passing over a ramp. The final wave form resulting from the passage over the curving ramp is found to be strongly influenced by the bottom topography, and other methods based on simplified theories are found to be inadequate in these situations containing three-dimensional bottom topography.

CHAPTER 2

Derivation of the Governing Equations

The governing equations for long waves have been derived in many ways using different scalings, simplifying and restrictive assumptions, and choice of dependent variables. All methods arrive at similar, but not identical equations. (Compare for example: Boussinesq [1871], Korteweg and DeVries [1895], Lamb [1932], Madsen and Mei [1969], Whitham [1974], and Wu [1981].) In order to provide a clear and consistent understanding of the equations used in this study, we present the following derivation, based on the techniques used by Wu (1981). We also derive an exact permanent-form solution to a combined form of these new equations. This special solution proves useful in two ways: first, as an initial condition in our numerical studies and second, as a rigorous test on the accuracy of the numerical scheme.

2.1 The Basic Equations.

We start by considering three-dimensional, finite-amplitude waves of arbitrary wave number in both horizontal dimensions $(x,y) \equiv \mathbf{x}$. Figure 2.1 provides a reference sketch showing the placement of the coordinates $(x,y,z) \equiv \mathbf{X}$ and physical variables described below. The undisturbed ocean surface coincides with the plane $z=0$. The air-sea interface is assumed to span over the entire horizontal plane, and when perturbed is given by $z = \zeta(\mathbf{x},t)$. The impermeable lower boundary is prescribed by $z = -h(\mathbf{x},t)$, which will allow us to include movement of the ocean bed. The fluid is taken to be incompressible and inviscid, with a constant density ρ. Surface tension will be neglected. The governing equations are the Euler equations:

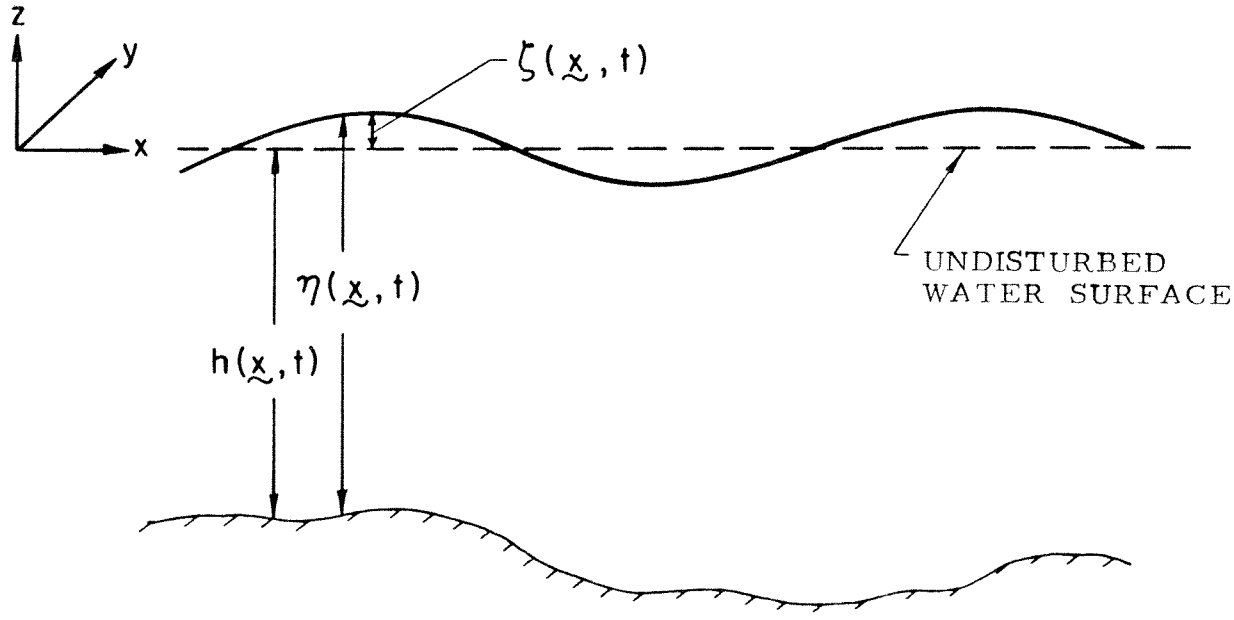

Figure 2.1 Definition sketch for the derivation of the governing equations.

$$\nabla_0 \cdot \mathbf{U} = 0 , \tag{2.1}$$

$$\frac{d\mathbf{U}}{dt} = \frac{\partial \mathbf{U}}{\partial t} + \mathbf{U}\cdot\nabla_0\mathbf{U} = -\frac{1}{\rho}\nabla_0 p - g\nabla_0 z \tag{2.2}$$

Here $\mathbf{U}(\mathbf{X},t) = (u,v,w)$ represents the flow velocity vector; $\nabla_0 \equiv (\frac{\partial}{\partial x}, \frac{\partial}{\partial y}, \frac{\partial}{\partial z})$; $p(\mathbf{X},t)$ is the pressure; and g is the acceleration due to gravity.

The boundary conditions for this system are:

- at the free surface:

$$w = \frac{\partial \zeta}{\partial t} + \mathbf{u}\cdot\nabla\zeta \qquad \text{on } z = \zeta(\mathbf{x},t), \tag{2.3}$$

$$p = p_0(\mathbf{x},t) \qquad \text{on } z = \zeta(\mathbf{x},t), \tag{2.4}$$

- at the lower (solid) boundary:

$$w = -\frac{\partial h}{\partial t} - \mathbf{u}\cdot\nabla h \qquad \text{on } z = -h(\mathbf{x},t), \tag{2.5}$$

where $\mathbf{u}(\mathbf{X},t) \equiv (u,v)$ is a vector which contains only the horizontal velocity components; $p_0(\mathbf{x},t)$ denotes the pressure at the free surface (here assumed to be prescribed); and $\nabla \equiv (\frac{\partial}{\partial x}, \frac{\partial}{\partial y})$.

An important set of layer-averaged equations can be obtained with application of the following transport theorem.

$$\int_{-h}^{\zeta} \frac{df}{dt} = \frac{\partial}{\partial t}\int_{-h}^{\zeta} f\, dz + \nabla\cdot\int_{-h}^{\zeta} \mathbf{u}\, f\, dz. \tag{2.6}$$

where $f(\mathbf{X},t)$ is any scalar, vector or tensor flow quantity; such operations with tensorial quantities can always be reduced to operations on the tensor's cartesian components which are scalar quantities. The validity of this theorem depends on the incorporation of the boundary conditions (2.3) and (2.5) as is shown in Appendix A. As a notational convenience we will use a bar to indicate the average of any quantity over the vertical layer, i.e., if q represents any vector or scalar quantity, then

$$\bar{q} = \frac{1}{\eta}\int_{-h}^{\zeta} q\, dz, \tag{2.7a}$$

where η is the layer thickness: $\eta=(\zeta+h)$. Using this notation, the transport theorem (2.6) may be rewritten as

$$\eta \overline{\frac{df}{dt}} = \frac{\partial}{\partial t}[\eta \bar{f}] + \nabla\cdot[\eta \overline{\mathbf{u}f}]. \tag{2.7b}$$

We may now proceed to use (2.7b) to investigate the transport of various quantities in the flow by replacing f with the physical variables of interest. Taking f=constant and f=**u** in (2.7b) yields, respectively,

$$\frac{\partial \eta}{\partial t} + \nabla\cdot[\eta\bar{\mathbf{u}}] = 0, \tag{2.8}$$

$$\frac{\partial}{\partial t}(\eta\bar{\mathbf{u}}) + \nabla\cdot[\eta\overline{\mathbf{uu}}] = -\eta\frac{\overline{\nabla p}}{\rho}, \tag{2.9}$$

where $\overline{\mathbf{uu}}$ denotes a tensor of the second order defined in the Euclidean space with the two horizontal dimensions ($x=x_1, y=x_2$) such that its ij^{th} component is $[\overline{\mathbf{uu}}]_{ij} = \overline{u_i u_j}$ and its i^{th} component of the divergence is $[\nabla\cdot\overline{\mathbf{uu}}]_i = \frac{\partial}{\partial x_j}[\overline{u_j u_i}]$. Equation 2.8 is an expression of layer-mean mass conservation (or volume conservation, since the density is constant), while Eq. 2.9, which is obtained by applying (2.7b) to the horizontal components of (2.2), governs the vertically-averaged horizontal momentum. These two equations form an important basis for describing the physical situation of interest.

Still using Eq. 2.7b, we may further take f=w and $f=E_d$, where E_d is defined as

$$E_d(\mathbf{X},t) = \frac{1}{2}\rho\mathbf{U}\cdot\mathbf{U} + \rho g z, \tag{2.10}$$

and making use of the vertical component of (2.2) and the mechanical energy equation derived from (2.1), we obtain

$$\frac{\partial}{\partial t}(\eta\bar{w}) + \nabla\cdot[\eta\overline{w\mathbf{u}}] = -g\eta - \frac{1}{\rho}[p_0 - p_{-h}] \tag{2.11}$$

$$\frac{\partial}{\partial t}(\eta\overline{E_d}) + \nabla\cdot[\eta\overline{(E_d + p)\mathbf{u}}] = -[p_0\frac{\partial\zeta}{\partial t} + p_{-h}\frac{\partial h}{\partial t}] \tag{2.12}$$

where p_{-h} indicates the pressure evaluated at z=-h. These equations, which we

show here for completeness, govern the layer-mean vertical momentum and energy, respectively. From Eq. 2.10, E_d may be seen to represent the sum of kinetic and potential energy densities.

Since the density ρ is constant, it follows from the principle of conservation of mass that the entire fluid volume remains constant over time. If we assume that certain physical quantities, such as ζ and $\mathbf{u}$, fall off sufficiently fast away from the region of interest, and if we take $h(\mathbf{x},t)$ in the form $h(\mathbf{x},t) = h_0(\mathbf{x}) + h_1(\mathbf{x},t)$ then the constant fluid volume is given by

$$\begin{aligned} \int_V dV &= \int_S dS \int_{-h}^{\zeta} dz \\ &= \int_S [\zeta + h_0(\mathbf{x}) + h_1(\mathbf{x},t)] dS \end{aligned} \tag{2.13}$$

for a sufficiently large but finite region V with a corresponding horizontal surface S over which $h(\mathbf{x},t)$ is assumed integrable (and beyond which $\zeta+h_1$ is assumed to have negligible integral effect). If we define the excess mass M_e as

$$M_e = \rho \int_S [\zeta + h_1] \, dS$$

then (2.13) implies M_e is constant over time. Furthermore, for a fixed lower boundary ($h_1 \equiv 0$) the mass above the undisturbed surface remains unchanged over time. This simple conservation law will later be used to check the accuracy of our numerical calculations.

2.2 Irrotational Long Waves; the Velocity Potential.

The system comprised of Eqs. 2.8 through 2.13 is exact and applies to both rotational and irrotational flow in an inviscid, incompressible fluid. We can simplify this system by assuming that the flow is irrotational, which is a good assumption for a homogeneous inviscid fluid starting from rest. This assumption allows us to introduce the velocity potential φ such that

$$\nabla_0 \varphi = \mathbf{U}. \tag{2.14}$$

If we substitute (2.14) into (2.1), we obtain the field equation for the potential as

$$\nabla_0^2 \varphi = 0 \tag{2.15}$$

which is the Laplace equation. Furthermore, if we introduce the velocity potential into (2.2) and integrate, we obtain the Bernoulli equation:

$$\frac{p}{\rho} + \frac{\partial \varphi}{\partial t} + \frac{1}{2}[\nabla_0 \varphi]^2 + gz = 0 \tag{2.16}$$

which relates the pressure and the velocity potential. Note that these equations are not depth-averaged and are exact to the extent that irrotationality holds.

We are primarily interested in determining the movement of the free surface $\zeta(\mathbf{x},t)$ for the case of long water waves. (Of course, we also hope to obtain information on the other physical variables in the process.) Our approach will be to use the Laplace and Bernoulli equations, which involve φ and p, along with the boundary conditions involving φ, ζ, and p, to introduce an appropriate expansion for φ and obtain a relationship between $\overline{\nabla\varphi}$, ζ and $\overline{\nabla p}$. Once we have this relationship we can substitute it into Eq. 2.9 and proceed to solve the approximated layer-averaged pair of transport equations, (2.8) and (2.9), for ζ.

It is convenient at this time to nondimensionalize the equations, so that all variables (except for those specifically noted later) are of order unity and their relative magnitudes are revealed by the accompanying order parameters. The dimensionless variables are given by:

$$\begin{aligned}
&\mathbf{x} = \frac{\mathbf{x}_D}{\lambda}, && z = \frac{z_D}{h_0}, && t = \left(\frac{c}{\lambda}\right)t_D, \\
&\zeta = \frac{\zeta_D}{A}, && h = \frac{h_D}{h_0}, && \eta = \frac{\eta_D}{h_0}, \\
&\varphi = \left(\frac{h_0}{\lambda A c}\right)\varphi_D, && p = \frac{p_D}{\rho g h_0},
\end{aligned} \tag{2.17a}$$

where

- the subscript D denotes a dimensional variable,
- λ is a characteristic wavelength,
- h_0 is the maximum water depth,
- c is the typical wave speed: $c = \sqrt{gh_0}$,
- A is a representative wave amplitude, and
- ρ is the density.

In addition, we can deduce from (2.17a) that

$$\mathbf{u} \equiv \nabla \varphi = (\frac{h_0}{Ac})\mathbf{u}_d = (\frac{h_0}{Ac})\nabla_D\varphi_D, \text{ and} \tag{2.17b}$$

$$w \equiv \frac{\partial\varphi}{\partial z} = (\frac{h_0^2}{\lambda Ac})w_D = (\frac{h_0^2}{\lambda Ac})\frac{\partial\varphi_D}{\partial z_D}. \tag{2.17c}$$

Unless otherwise specifically stated, all variables will henceforth be taken to be dimensionless. We will presently discuss the two dimensionless parameters

$$\alpha = \frac{A}{h_0} \quad \text{and} \quad \varepsilon = \frac{h_0}{\lambda} \tag{2.17d}$$

which emerge when (2.17) is substituted into the set of basic equations. For convenience, the first two transport equations (Eqs. 2.8 and 2.9) are rewritten below, after substituting the nondimensional variables from 2.17 and replacing $\overline{\mathbf{u}}$ by $\overline{\nabla\varphi}$:

$$\frac{\partial\eta}{\partial t} + \alpha\nabla\cdot[\eta\overline{\nabla\varphi}] = 0, \tag{2.18}$$

$$\alpha\frac{\partial}{\partial t}(\eta\overline{\nabla\varphi}) + \alpha^2\nabla\cdot[\eta\overline{\nabla\varphi\nabla\varphi}] = -\eta\overline{\nabla p} \tag{2.19}$$

where $\eta = (\alpha\zeta + h)$, and $\overline{\nabla\varphi}$ and the other similarly denoted layer-averaged quantities are described by the non-dimensionalized version of (2.7a). The Laplace (2.15) and Bernoulli (2.16) equations can also be non-dimensionalized using (2.17):

$$\varepsilon^2\nabla^2\varphi = -\frac{\partial^2\varphi}{\partial z^2}, \tag{2.20}$$

$$p + z = -\alpha\frac{\partial\varphi}{\partial t} - \frac{\alpha^2}{2}\left\{(\nabla\varphi)^2 + \frac{1}{\varepsilon^2}(\frac{\partial\varphi}{\partial z})^2\right\}. \tag{2.21}$$

Finally, we nondimensionalize the kinematic boundary condition on the bottom (Eq. 2.3):

$$\alpha w = -\varepsilon^2 \frac{\partial h}{\partial t} - \alpha\varepsilon^2(\mathbf{u}\cdot\nabla h) \qquad \text{on } z = -h(\mathbf{x},t). \tag{2.22}$$

The dimensionless parameter, α, provides a measure of the nonlinearity. This nonlinearity is physically manifested as the tendency of the front of the wave to steepen during propagation. ε is the dispersion parameter and it gauges the tendency of a single wave to disperse into a train of oscillatory waves. As stated at the outset of this thesis, we are considering only long waves and ε therefore must be a small parameter by definition. Additionally, we assume that the wave amplitude remains small compared to the water depth, thus α is also a small parameter.

It is the relative magnitudes of these two parameters that determine which phenomenon (nonlinearity or dispersion) dominates during the propagation of these long waves. Ursell (1953) elucidated the following classification:

$$\alpha \begin{cases} << \varepsilon^2 \ \ldots\ \text{linear wave class} & \text{(dispersion dominates)}, \\ \approx \varepsilon^2 \ \ldots\ \text{Boussinesq-class,} & \text{(nonlinearity balances dispersion)}, \\ >> \varepsilon^2 \ \ldots\ \text{Airy-class,} & \text{(nonlinearity dominates)}. \end{cases}$$

The Ursell number, $\mathrm{Ur}=\frac{\alpha}{\varepsilon^2}$, is often used to succinctly indicate the class of long waves under consideration. Naturally, these classes are not completely exclusive -- there can be some overlap between the linear and Boussinesq classes and between the Boussinesq and Airy classes. The widest variety of phenomena can be described by assuming the waves to be of the Boussinesq-class, which will allow for some encroachment onto the other two classes. Accordingly, we will take $\alpha \approx \varepsilon^2$.

Since $\zeta \leq O(1)$ and $\eta \leq O(1)$, we infer from Eq. 2.18 that $\overline{\nabla\varphi} \leq O(1)$ and $\bar{u} \leq O(1)$. Subsequent inspection of Eq. 2.20 implies that $w \leq O(\varepsilon^2)$ and

consequently, from (2.22), we must have $\frac{\partial h}{\partial t} \leq O(\alpha)$ and $\nabla h \leq O(1)$ in order to ensure self-consistency. Based on the form of the nondimensional Laplace equation, we assume the following expansion for φ:

$$\varphi = \sum_{n=0}^{\infty} \varepsilon^{2n} \Phi_{2n}(\mathbf{X},t). \tag{2.22}$$

Substituting (2.22) into (2.20) we obtain the recursion relations for Φ_{2n} as

$$\begin{aligned} \Phi_0 &= \varphi_0(\mathbf{x},t), \\ \Phi_2 &= \varphi_2(\mathbf{x},t) + z\varphi_3(\mathbf{x},t) - \frac{z^2}{2}\nabla^2\varphi_0, \\ \Phi_{2n} &= \varphi_{2n}(\mathbf{x},t) + z\varphi_{2n+1}(\mathbf{x},t) - \nabla^2 \int^{z} dz_1 \int^{z_1} \Phi_{2(n-1)}(\mathbf{x},\xi,t)d\xi, \end{aligned} \tag{2.24}$$

for n=1,2,3,....., where φ_0, φ_1, ... represent unknown functions of $\mathbf{x}$ and t only. A possible additive term $z\varphi_1(\mathbf{x},t)$ for Φ_0 has been discarded in order to satisfy the order estimate for w.

We now define the expansions

$$\begin{aligned} \mathbf{u} = \nabla\varphi &= \nabla\varphi_0 + \varepsilon^2\nabla\Phi_2 + \varepsilon^4\nabla\Phi_4 + \cdots \\ &= \mathbf{u}_0 + \varepsilon^2\mathbf{u}_1 + \varepsilon^4\mathbf{u}_2 + \cdots \end{aligned} \tag{2.25}$$

and

$$\begin{aligned} w = \frac{\partial}{\partial z}\varphi &= \varepsilon^2\left[\frac{\partial}{\partial z}\Phi_2 + \varepsilon^2\frac{\partial}{\partial z}\Phi_4 + \cdots\right] \\ &= \varepsilon^2[w_1 + \varepsilon^2 w_2 + \cdots]. \end{aligned} \tag{2.26}$$

Note that $\mathbf{u}_0 = \nabla\varphi_0(\mathbf{x},t)$ is independent of z, however, all other terms in the expansions of $\mathbf{u}$ and w can vary with z.

2.3 Generalized Form of the Classical Boussinesq Equations.

Since the first order expansion terms for $\mathbf{u}$ are independent of z, we can show from the expansion (2.25) that

$$\overline{\nabla\varphi\nabla\varphi} = \overline{\nabla\varphi}\;\overline{\nabla\varphi} + \varepsilon^4[\overline{\nabla\Phi_2\nabla\Phi_2} - \overline{\nabla\Phi_2}\;\overline{\nabla\Phi_2}] + O(\varepsilon^6).$$

This permits Eq. 2.19 to be simplified to

$$\alpha\frac{\partial}{\partial t}\overline{\nabla\varphi} + \alpha^2\overline{\nabla\varphi}\cdot\nabla[\overline{\nabla\varphi}] = -\overline{\nabla p} + O(\varepsilon^6). \tag{2.27}$$

We now turn to the Bernoulli equation (2.21) to determine $\overline{\nabla p}$. Substituting the expansion for φ, we have

$$p + z = -\alpha[\dot{\varphi}_0 + \varepsilon^2\dot{\Phi}_2 + \frac{\alpha}{2}\mathbf{u}_0^2] + O(\alpha\varepsilon^4,\alpha^2\varepsilon^2) \tag{2.28}$$

where the dot $\dot{}$ indicates a partial derivative with respect to t. If we evaluate (2.28) at the free surface, using the boundary condition (2.4) we have

$$p_0 + \alpha\zeta = -\alpha[\dot{\varphi}_0 + \varepsilon^2\dot{\varphi}_2 + \frac{\alpha}{2}\mathbf{u}_0^2] + O(\alpha\varepsilon^4,\alpha^2\varepsilon^2). \tag{2.29}$$

If we layer-average the horizontal gradient of Eq. 2.28 and subtract the horizontal gradient of Eq. 2.29 we find

$$\begin{aligned}\overline{\nabla p} &= \alpha\nabla\zeta + \nabla p_0 - \alpha\varepsilon^2[\overline{\nabla\dot{\Phi}_2} - \nabla\dot{\varphi}_2] + O(\alpha\varepsilon^4,\alpha^2\varepsilon^2)\\ &= \alpha\nabla\zeta + \nabla p_0 + \alpha\varepsilon^2[\frac{h}{2}\overline{\nabla\dot{\varphi}_3} + \frac{h^2}{6}\nabla^2\nabla\dot{\varphi}_0] + O(\alpha\varepsilon^4,\alpha^2\varepsilon^2)\end{aligned} \tag{2.30}$$

Further utilizing the expansions for φ, $\mathbf{u}$, and w, we find through substitution that (2.22) determines φ_3 to be:

$$\varphi_3 = -\left[\frac{1}{\alpha}\frac{\partial h}{\partial t} + \nabla\cdot(h\mathbf{u}_0)\right] + O(\varepsilon^2). \tag{2.31}$$

Combining (2.30) and (2.31), we obtain an expansion for $\overline{\nabla p}$ as

$$\overline{\nabla p} = \alpha\nabla\zeta + \nabla p_0 - \alpha\varepsilon^2\left[\frac{h}{2}\frac{\partial}{\partial t}\nabla\left\{\frac{1}{\alpha}\frac{\partial h}{\partial t} + \nabla\cdot(h\mathbf{u}_0)\right\} - \frac{h^2}{6}\frac{\partial}{\partial t}\nabla^2\mathbf{u}_0\right] + O(\alpha\varepsilon^4,\alpha^2\varepsilon^2) \tag{2.32}$$

Rewriting (2.18) and substituting (2.32) into (2.27), we obtain the following two equations:

$$\alpha\frac{\partial\zeta}{\partial t} + \alpha\nabla\cdot\left[(h + \alpha\zeta)\overline{\nabla\varphi}\right] = -\frac{\partial h}{\partial t}, \tag{2.33}$$

$$\begin{aligned}\alpha\frac{\partial\overline{\nabla\varphi}}{\partial t} + \alpha^2\overline{\nabla\varphi}\cdot\nabla[\overline{\nabla\varphi}] + \alpha\nabla\zeta = &-\nabla p_0 + \alpha\varepsilon^2\left[\frac{h}{2}\frac{\partial}{\partial t}\nabla\left\{\frac{1}{\alpha}\frac{\partial h}{\partial t} + \nabla\cdot(h\overline{\nabla\varphi})\right\}\right.\\ &\left. - \frac{h^2}{6}\frac{\partial}{\partial t}\nabla^2\overline{\nabla\varphi}\right] + O(\alpha\varepsilon^4,\alpha^2\varepsilon^2)\end{aligned} \tag{2.34}$$

where we have substituted $\mathbf{u}_0 = \bar{\mathbf{u}} + O(\varepsilon^2)$ and $\bar{\mathbf{u}} = \overline{\nabla\varphi}$ in the highest order terms retained, i.e., in the terms on the right-hand side of (2.34). This operation has no effect on the error estimate. This set of equations for ζ and $\overline{\nabla\varphi}$ governs the propagation of weakly nonlinear* long waves in water of variable depth. The depth variation may be prescribed to vary with both space and time variables. These equations constitute a generalization of the Boussinesq equations.† Note that the first equation (2.33) is an exact statement of mass conservation for an incompressible fluid; Eq. 2.34 is correct to $O(\alpha\varepsilon^4, \alpha^2\varepsilon^2)$. D

2.4 Introduction of the Irrotational Layer-Mean Velocity.

It is important to note that although $\mathbf{u}=\nabla\varphi$ is irrotational, the layer-averaged quantity $\bar{\mathbf{u}}=\overline{\nabla\varphi}$ is a rotational vector field whenever $\nabla h \neq 0$. (See (2.36) below.) Consequently, we cannot successfully integrate the layer-averaged momentum equations (2.34) to obtain a single Bernoulli-like equation relating the potential φ to the surface height ζ. The vorticity $\nabla\times\bar{\mathbf{u}}$ in this layer-averaged flow is generally small ($O(\varepsilon^2)$, as shown below) and is fed by the last two terms on the right-hand side of Eq. 2.34. Wu (1981) has identified these terms as frequency diffusion effects due to the depth variation.

We now define a new irrotational velocity ‡ for the layer-averaged flow as:

$$\mathbf{u}' \equiv \nabla\overline{\varphi}\,, \quad \text{such that} \quad \nabla\times\mathbf{u}' = 0. \tag{2.35}$$

We are able then to relate $\bar{\mathbf{u}}$ to $\mathbf{u}'$ by using the expansion for φ in Eq. 2.22:

---

* Weak nonlinearity is taken to mean $\alpha \approx \varepsilon^2$

† The original Boussinesq (1872) equations were derived for the two-dimensional propagation of weakly nonlinear long waves in a rectangular channel of constant water depth. Transcribed into *our* notation, and taking h_0 as the water depth, these equations are (in dimensional form):

$$\int_x^\infty \frac{\partial}{\partial t} u_{-h}\, dx = g\,\zeta + \frac{g}{2}\left[\frac{\zeta^2}{h_0} + h_0^2 \frac{\partial^2\zeta}{\partial x^2}\right],$$

$$\frac{\partial\zeta}{\partial t} = -h_0 \frac{\partial}{\partial x} u_{-h} - \sqrt{g h_0}\frac{\partial}{\partial x}\left[\frac{\zeta^2}{h_0} - \frac{h_0^2}{6}\frac{\partial^2\zeta}{\partial x^2}\right].$$

Goring (1978) has shown that these two equations are equivalent to the layer-averaged formulation which we present in Eq. 2.33 and 2.34 above.

‡ Lepelletier (1981) refers to this new velocity as the pseudo-velocity.

$$\bar{\mathbf{u}} = \mathbf{u}' + \varepsilon^2\left\{\frac{1}{2}\varphi_3 + \frac{h}{3}\nabla^2\varphi_0\right\}\nabla h + O(\varepsilon^4). \tag{2.36}$$

Clearly, $\bar{\mathbf{u}} = \mathbf{u}' + O(\varepsilon^4)$ when $\nabla h \equiv 0$. Substitution of (2.36) into (2.33) yields:

$$\alpha\frac{\partial\zeta}{\partial t} + \alpha\nabla\cdot\left[(h + \alpha\zeta)\nabla\bar{\varphi}\right] = -\frac{\partial h}{\partial t} - \alpha\varepsilon^2\nabla\cdot\left[\left\{\frac{h}{2}\varphi_3 + \frac{h^2}{3}\nabla^2\varphi_0\right\}\nabla h\right] + O(\alpha\varepsilon^4, \alpha^2\varepsilon^2) \tag{2.37}$$

Furthermore, using (2.35) we can express a Bernoulli-type equation in terms of $\nabla\bar{\varphi}$, ζ and $\mathbf{u}'$ as:

$$\alpha\frac{\partial\bar{\varphi}}{\partial t} + \frac{\alpha^2}{2}(\mathbf{u}')^2 + \alpha\zeta + p_0 = \alpha\frac{\partial\bar{\varphi}}{\partial t} + \frac{\alpha^2}{2}(\mathbf{u}')^2 - \alpha[\dot{\varphi}_0 + \varepsilon^2\dot{\varphi}_2 + \frac{\alpha}{2}\mathbf{u}_0^2] + O(\alpha\varepsilon^4, \alpha^2\varepsilon^2)$$

$$= \alpha\varepsilon^2\left\{-\frac{h}{2}\frac{\partial}{\partial t}\varphi_3 - \frac{h^2}{6}\frac{\partial}{\partial t}\nabla^2\varphi_0\right\} + O(\alpha\varepsilon^4, \alpha^2\varepsilon^2), \tag{2.38}$$

where we have substituted from (2.29) for $(\alpha\zeta + p_0)$ on the left side. Rewriting (2.37) and (2.38) after substituting for φ_3 from (2.31), we have, respectively,

$$\alpha\frac{\partial\zeta}{\partial t} + \alpha\nabla\cdot\left[(h + \alpha\zeta)\nabla\bar{\varphi}\right] = -\frac{\partial h}{\partial t} + \alpha\varepsilon^2\nabla\cdot\left[\left\{\frac{h}{2}\left[\frac{1}{\alpha}\frac{\partial h}{\partial t} + \nabla\cdot(h\nabla\bar{\varphi})\right]\right.\right. \tag{2.39}$$

$$\left.\left. - \frac{h^2}{3}\nabla^2\bar{\varphi}\right\}\nabla h\right] + O(\alpha\varepsilon^4, \alpha^2\varepsilon^2)$$

$$\alpha\frac{\partial\bar{\varphi}}{\partial t} + \frac{\alpha^2}{2}(\nabla\bar{\varphi})^2 + \alpha\zeta = -p_0 + \alpha\varepsilon^2\left\{\frac{h}{2}\frac{\partial}{\partial t}\left[\frac{1}{\alpha}\frac{\partial h}{\partial t} + \nabla\cdot(h\nabla\bar{\varphi})\right]\right. \tag{2.40}$$

$$\left. - \frac{h^2}{6}\frac{\partial}{\partial t}\nabla^2\bar{\varphi}\right\} + O(\alpha\varepsilon^4, \alpha^2\varepsilon^2),$$

where we have substituted $\varphi_0 = \bar{\varphi} + O(\varepsilon^2)$ in the highest order terms retained. This pair of equations for ζ and $\bar{\varphi}$ forms the theoretical basis for the present study. This system belongs to the same class of weakly nonlinear long wave equations as the system formed by (2.33) and (2.34) since the error remains at the same order. Equations 2.39 and 2.40 are thus entirely equivalent to the typical set of extended* Boussinesq equations. The new formulation is superior, however, since it reduces the number of dependent variables from

*The depth may have space and time variations; wave propagation is allowed in two horizontal dimensions.

three scalar unknowns (namely, $\bar{u}$ and ζ) to two ($\bar{\varphi}$ and ζ). In addition, equation (2.40) is one order less as a partial differential equation than (2.34). Furthermore, ζ may be eliminated by substituting ζ from (2.40) into (2.39), leaving only one equation and one scalar unknown, $\bar{\varphi}$. Once $\bar{\varphi}$ has been determined, ζ and $\bar{u}$ may be readily deduced from Eqs. 2.40 and 2.36 respectively.

This is the first time that it has been possible to combine a full Boussinesq-class set of equations without the loss of bidirectional propagation. Through limiting the propagation to one-direction only, previous investigators had obtained a one equation description of weakly non-linear wave propagation. Aside from the combination of the two equations and subsequent elimination of one dependent variable, there appears to be no significant advantage in limiting propagation to one direction only. When reflection becomes important, this limitation is a serious disadvantage. Some rather elaborate "switch-on/switch-off" schemes have been developed to compensate for the limitations of unidirectional propagation in situations involving reflection. Our approach, however, finds the limitation to unidirectional propagation unnecessary, since it is possible to directly combine the two governing equations into a single equation for $\bar{\varphi}$.

2.5 The Relationship of the Governing Equations to Other Long Wave Models.

Since the clarification by Ursell in 1953 and the subsequent introduction of the Ursell number, it is clear that the Boussinesq equations provide an appropriate and accurate model for long waves of small amplitude. The explicit governing equations for other classes of long waves actually emerge as sub-classes of the full equations (2.39) and (2.40). By assuming appropriate relationships between the order parameters α and ε, these models may be

separated under the following headings:

- **Linear Nondispersive Model.** In the simplest long wave model all the nonlinear and dispersive effects are neglected. The relevant Ursell number is $Ur << O(1)$, with $\alpha << 1$ and $\varepsilon^2 << 1$ in addition. Physically, this system is one in which the wave amplitude is extremely small compared to the depth and the wavelength is extremely long compared to the depth. For this case the full equations reduce to:

$$\alpha\frac{\partial\zeta}{\partial t} + \alpha\nabla\cdot[h\nabla\bar{\varphi}] = -\frac{\partial h}{\partial t}, \tag{2.41}$$

$$\alpha\frac{\partial\bar{\varphi}}{\partial t} + \alpha\zeta + p_0 = 0. \tag{2.42}$$

For constant depth, $h=h_0$ and no forcing from the prescribed free-surface pressure, $p_0=0$ both $\bar{\varphi}$ and ζ satisfy the well-known wave equation:

$$\bar{\varphi}_{tt} = h\nabla^2\bar{\varphi}, \quad \zeta_{tt} = h\nabla^2\zeta.$$

- **Nonlinear Nondispersive Model.** This model was originally thought to constitute the fundamental equations for long water waves of finite amplitude. Now, however, it can be seen that the nonlinear nondispersive model equations -- often called the Airy equations -- can be extracted from the full equations. The Ursell number for this system is $Ur >> O(1)$; α is small but finite, $\alpha< 1$; and $\varepsilon^2<< 1$.† The full equations reduce to:

$$\alpha\frac{\partial\zeta}{\partial t} + \alpha\nabla\cdot\left[(h + \alpha\zeta)\nabla\bar{\varphi}\right] = -\frac{\partial h}{\partial t}, \tag{2.43}$$

$$\alpha\frac{\partial\bar{\varphi}}{\partial t} + \frac{\alpha^2}{2}(\nabla\bar{\varphi})^2 + \alpha\zeta = -p_0. \tag{2.44}$$

This system predicts that all waves steepen and eventually break.

- **Linear Dispersive Model.** Finally we consider a system, not discussed by Ursell, which has approximately the same Ursell number as the Linear

† Actually this case must have $\alpha\approx\varepsilon$. If α is taken to be larger in relation to ε, say, $\alpha\approx\sqrt{\varepsilon}$ then terms of order α^3 should have been retained instead of $\alpha\varepsilon^2$.

Nondispersive Model presented above. This case, however, models the physical situation of extremely small amplitude waves, $\alpha << 1$, with only *moderately* long wavelength, $\varepsilon^2 < 1$.‡

$$\alpha\frac{\partial\zeta}{\partial t} + \alpha\nabla\cdot\left[h\nabla\bar{\varphi}\right] = -\frac{\partial h}{\partial t} + \alpha\varepsilon^2\nabla\cdot\left[\left\{\frac{h}{2}\left[\frac{1}{\alpha}\frac{\partial h}{\partial t} + \nabla\cdot(h\nabla\bar{\varphi})\right] - \frac{h^2}{3}\nabla^2\bar{\varphi}\right\}\nabla h\right], \tag{2.45}$$

$$\alpha\frac{\partial}{\partial t}\bar{\varphi} + \alpha\zeta = -p_0 + \alpha\varepsilon^2\left\{\frac{h}{2}\frac{\partial}{\partial t}\left[\frac{1}{\alpha}\frac{\partial h}{\partial t} + \nabla\cdot(h\nabla\bar{\varphi})\right] - \frac{h^2}{6}\frac{\partial}{\partial t}\nabla^2\bar{\varphi}\right\}. \tag{2.46}$$

Each of these models displayed above is embedded in the full (Boussinesq-class) equations, (2.39) and (2.40), and need not be invoked explicitly. This means that the full equations may be used when the class of long waves is indeterminate, or when the class may change either across the physical region of interest or during propagation (as long as breaking does not occur). This feature is especially useful in numerical work which may be required since the full equations generally cannot be solved in closed form. In some cases, theoretical solutions are available for the three sub-classes described above. These solutions, however, may become quite tedious or even impossible when the bottom topography is three-dimensional or when the wave is passing from one long-wave class to another.

2.6 Permanent Form Solutions for Constant Depth

We are interested in determining if the governing equations, (2.39) and (2.40), will support solutions of permanent form. While such solutions are of theoretical interest, they also provide initial conditions and stringent checks on the accuracy of the numerical scheme. The lack of an exact permanent form solution to the classical Boussinesq equations, has caused some confusion in previous numerical studies. In the past, investigators have prescribed initial

‡ Again we must have $\alpha \approx \varepsilon^4$. If α is smaller than this, some of the higher order dispersive terms which were neglected should have been retained.

conditions based on the permanent-form solution to the Korteweg-deVries* (KdV) Equation. This equation, which is valid only for uni-directional waves, is an approximation of the full Boussinesq set. The exact permanent-form solution to the KdV equation, however, is not an exact solution to the parent Boussinesq equations. This discrepancy in initial conditions has been used to explain some propagational anomalies (such as the appearance of an oscillatory tail -- see the discussion in Section 3.3) which appear in the numerical solution of the classical Boussinesq pair of equations. Our new exact solution to the actual equation which is solved numerically provides a rigorous and clear test on the numerical scheme, since the computed solution must approach the exact theoretical solution as the numerical errors induced by finite stepsize and convergence tolerance are reduced.

If we restrict our attention to the case of one-dimensional long waves propagating in water of constant depth, $h = h_0$, the full equations reduce to:

$$\zeta_t + \alpha[\zeta\varphi_x]_x + h_0\varphi_{xx} = O(\varepsilon^4,\alpha\varepsilon^2), \tag{2.47}$$

$$\varphi_t + \frac{\alpha}{2}[\varphi_x]^2 + \zeta - \varepsilon^2\frac{h_0^2}{3}\varphi_{xxt} = O(\varepsilon^4,\alpha\varepsilon^2), \tag{2.48}$$

where, to simplify notation, we have dropped the bar from φ and used subscripts to denote partial derivatives: $\varphi_{tt} = \frac{\partial^2\varphi}{\partial t^2}$, $\varphi_x = \frac{\partial\varphi}{\partial x}$, and so on.

If we follow the KdV-model route at this early point in the analysis, then the resulting equation is limited to one directional propagation only. As already mentioned in Section 2.5, we can directly combine the two governing equations into a single equation for $\bar{\varphi}$, without restricting wave motion to one direction.

---

* In addition to the original description in the Korteweg and deVries paper (1895), a large number of papers and texts describe the derivation of the permanent form solution to the KdV equations, see for example Whitham (1974). For reference, the KdV Equation is given below in dimensional form:

$$\zeta_t + c\,\zeta_x[1 + \frac{3}{2h_0}\zeta] + \frac{ch_0^2}{6}\zeta_{xxt} = 0$$

where $c = \sqrt{gh_0}$.

Our next step, therefore, will be to combine the equations (2.47) and (2.48), still permitting motion in both directions. In order to permit comparisons to other permanent form solutions of the Boussinesq-class, we will revert to dimensional equations for the remainder of this section. The combined, constant-depth equations, in dimensional form, are:

$$- \varphi_{tt} - 2\varphi_x\varphi_{xt} - \varphi_t\varphi_{xx} + \frac{h_0^2}{3}\varphi_{xxtt} + c^2\varphi_{xx} = O(\alpha\varepsilon^4,\alpha^2\varepsilon^2), \qquad (2.49)$$

where c is the wave speed, $c = \sqrt{gh_0}$. We assume a permanent form for the solution as:

$$\varphi(x,t) = F(\chi) \quad \text{where} \quad \chi = x - U\cdot t.$$

U is an unknown phase velocity of the wave, to be determined later. Substitution of the permanent form expression into Eq. 2.49 for φ yields

$$(c^2 - U^2)F'' + 3UF'F'' + \frac{U^2h_0^2}{3}F'''' = 0 \qquad (2.50)$$

where the prime ' indicates an ordinary derivative with respect to χ: $F' = \frac{dF}{d\chi}$.

We can obtain a first integral of (2.50) as

$$(c^2 - U^2)F' + \frac{3}{2}U(F')^2 + \frac{U^2h_0^2}{3}F''' + G_1 = 0 \qquad (2.51)$$

where G_1 is a constant of integration. Another integration is possible after multiplying (2.51) by F'' and this step yields

$$(c^2 - U^2)(F')^2 + U(F')^3 + \frac{U^2h_0^2}{3}(F'')^2 + G_1F' + G_2 = 0 \qquad (2.52)$$

where G_2 is a constant of integration. If we assume that F' and its derivatives tend to zero at infinity, then we must take $G_1 = G_2 = 0$. Furthermore, we can write (2.52) as:

$$\frac{Uh_0^2}{3}(F'')^2 = (F')^2\left[A_u - F'\right] \qquad (2.53a)$$

where

$$A_u = U(1 - \frac{c^2}{U^2}). \tag{2.53b}$$

A_u is the amplitude of F', the permanent form solution to (2.53a). Specifically, this permanent form solution is found to be:

$$F' = A_u \operatorname{sech}^2(\beta \chi) \tag{2.54}$$

where $\beta^2 = \frac{3A_u}{4Uh_0^2}$. Returning to Eq. 2.48 and substituting this solution for φ, we obtain a permanent form solution for the surface height ζ:

$$\zeta(x,t) = \frac{h_0}{c^2}\left\{ A_u(U - A_u)\operatorname{sech}^2[\beta(x-Ut)] + A_u^2\operatorname{sech}^4[\beta(x-Ut)]\right\} \tag{2.55}$$

Setting the arguments to zero in (2.55) will reveal the amplitude ζ_0 of ζ which we write as

$$\alpha \equiv \frac{\zeta_0}{h_0} = \frac{A_u}{c^2} U$$

Substituting for A_u from (2.53b), we obtain a relationship between the phase velocity U of the permanent wave form and the nondimensional wave height α as

$$\alpha = \frac{U^2}{c^2} - 1. \tag{2.56}$$

Solving for U yields the following two-directional formula:

$$U = \pm c[1 + \alpha]^{\frac{1}{2}} = \pm c\left\{1 + \frac{\alpha}{2} - \frac{\alpha^2}{8} + \ldots .\right\} \tag{2.57}$$

In order to compare the form of our permanent surface wave to that from the KdV equation, we put the surface height in terms of ζ_0, the peak amplitude, to yield:

$$\zeta = \frac{\zeta_0}{(1+\alpha)}\left\{\operatorname{sech}^2[\beta(x-Ut)] + \alpha \operatorname{sech}^4[\beta(x-Ut)]\right\} \tag{2.58}$$

where we may write β in terms of α

$$\beta = \left[\frac{3\alpha}{4h_0^2(1+\alpha)}\right]^{\frac{1}{2}} \tag{2.59}$$

The solution for the KdV soliton is given in Whitham (1974) as:

$$\eta = \eta_0 \mathrm{sech}^2\left\{\left[\frac{3\alpha}{4h_0^2}\right]^{\frac{1}{2}}(x-U_k t)\right\} \tag{2.60}$$

where $U_k = 1 + \frac{\alpha}{2}$. These two solutions are compared in Fig 2.2 and 2.3 for two amplitudes (0.1 and 0.7) with h_0 taken to be 1.0. The new solution has a somewhat smaller wave number and falls slightly to the outside of the KdV solitary wave solution.

Our solution has the advantage over the classical formulation in that it clearly permits propagation in both directions. Furthermore, the present result for phase velocity U is in better agreement than the KdV model with higher order solutions to the nonlinear dispersive equations which give

$$\frac{U}{c} = 1 + \frac{\alpha}{2} - \frac{3}{20}\alpha^2 + \ldots.$$

(See Fenton [1972].) The permanent surface wave form is only slightly different from the KdV solution, our solution having a somewhat wider shape for the same amplitude. The differences however, may be fortuitous since they are all consistent with the order of the approximations.

The permanent form solution derived in this section will be used extensively as the basic reference case in Chapter 4 to investigate the response of the numerical scheme to variation of the computational parameters.

2.7 Combination of the Governing Equations

For reference, the combination of the governing equations (2.39) and (2.40) discussed in Section 2.4 is presented below:

$$\varphi_{tt} = h\nabla^2\varphi + \nabla h\cdot\nabla\varphi + \frac{1}{\alpha}(h-p_0)_t + \varepsilon^2\left\{\frac{h}{2}H_t - \frac{h^2}{6}\nabla^2\varphi_t\right\}_t \tag{2.58}$$

$$- \varepsilon^2\nabla\cdot\left[\left\{\frac{h}{2}H - \frac{h^2}{3}\nabla^2\varphi\right\}\nabla h\right] - \alpha[2\nabla\varphi_t\cdot\nabla\varphi - \varphi_t\nabla^2\varphi] + O(\varepsilon^4,\alpha\varepsilon^2)$$

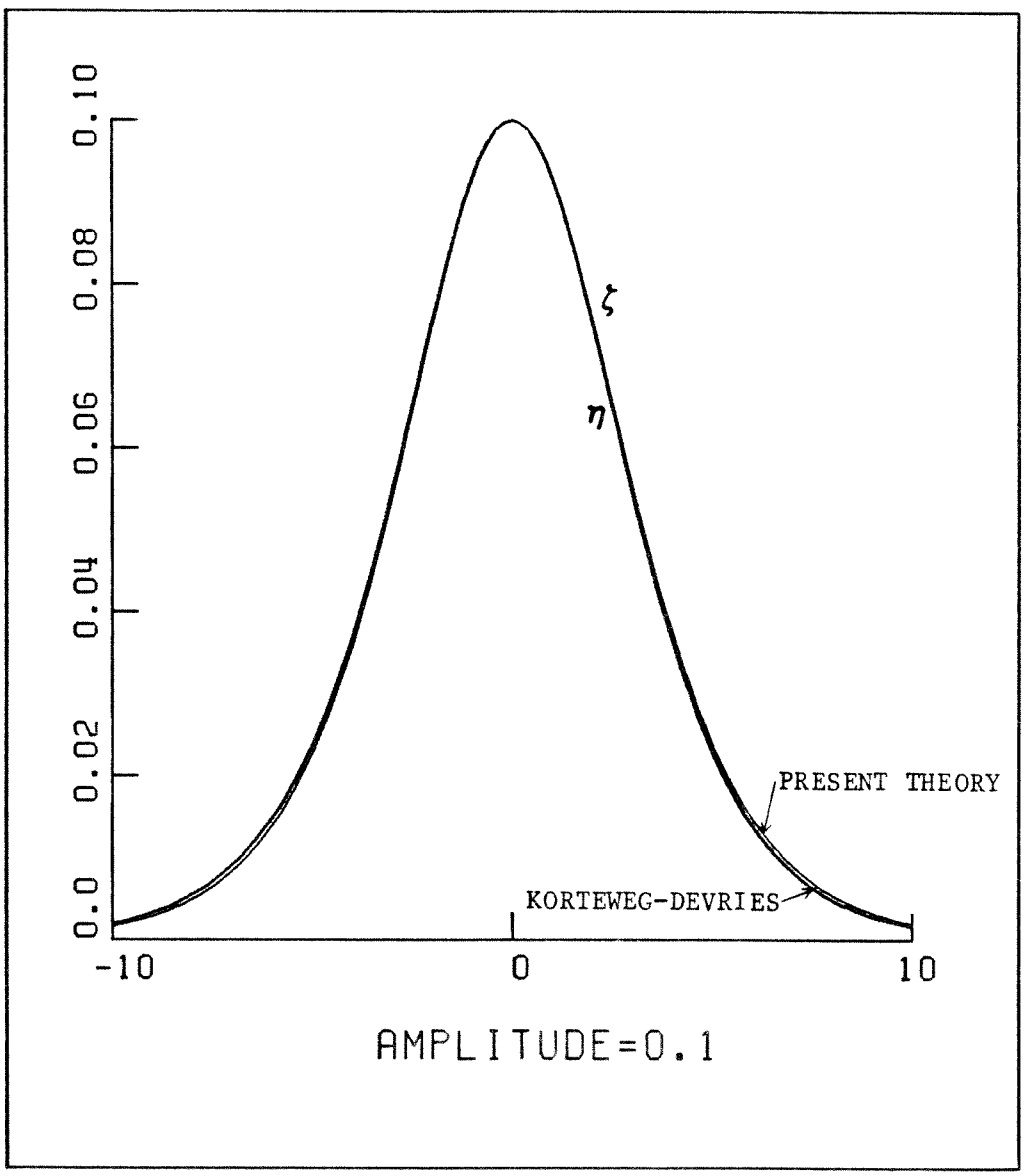

Figure 2.2 Comparison of solitary wave shapes for amplitude of 0.1. Korteweg-deVries curve is calculated from Eq. 2.60. Present theory surface height is taken from Eq. 2.58. Water depth is taken to be 1.0.

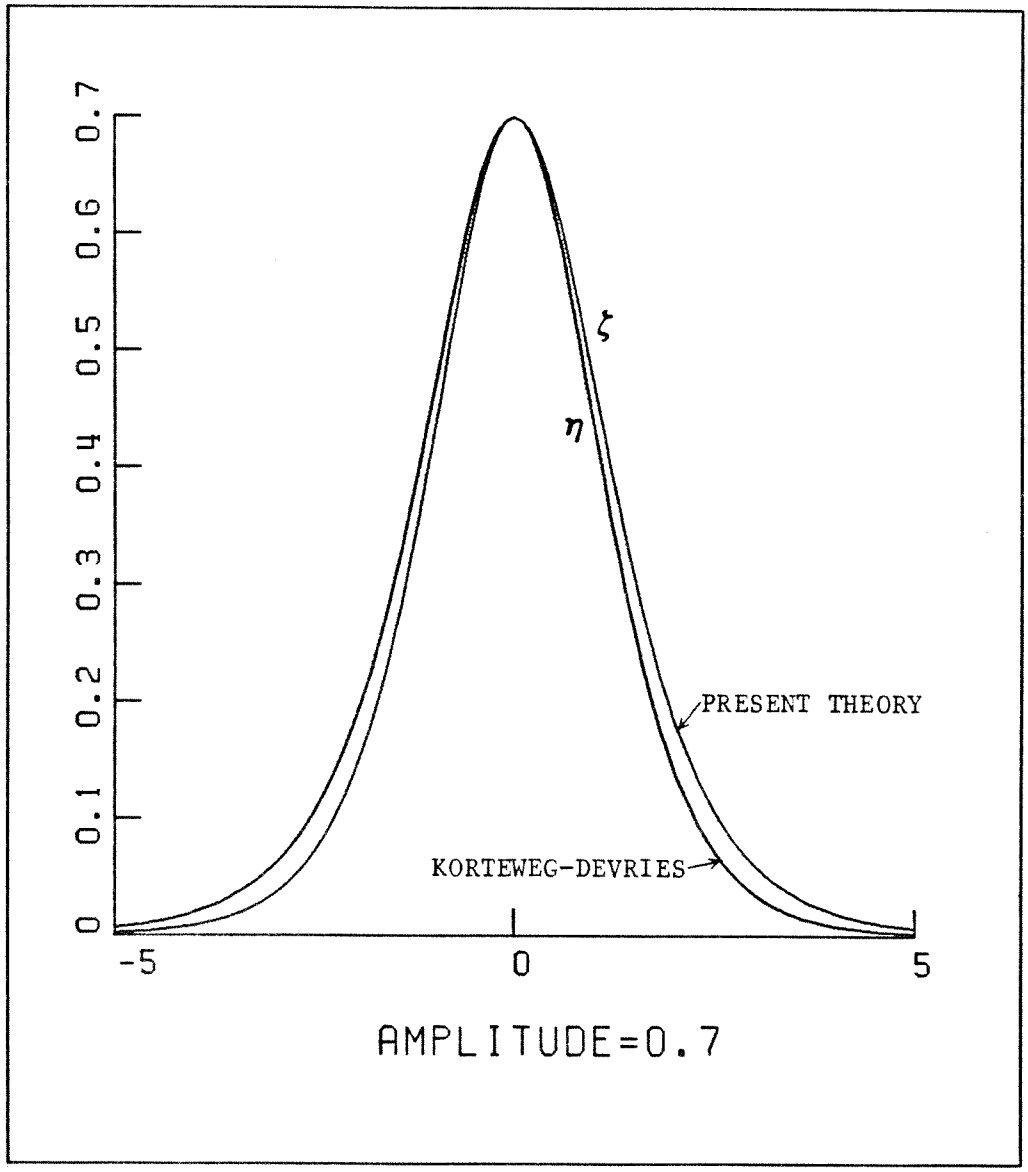

Figure 2.3 Comparison of solitary wave shapes for amplitude of 0.7. Korteweg-deVries curve is calculated from Eq. 2.60. Present theory surface height is taken from Eq. 2.58. Water depth is taken to be 1.0.

where H is given by

$$H = \frac{h_t}{\alpha} + \nabla\cdot(h\nabla\varphi)$$

and to simplify notation we have dropped the bar from φ and used subscripts to denote partial derivatives as in Section 2.6. Higher order terms have been dropped in a manner consistent with the derivation leading to Eqs. 2.39 and 2.40.

The specific cases discussed in this thesis do not include floor motion or variaton in free-suface pressure, therefore, the combined equation for $h\equiv 0$ and $p_0\equiv 0$ is shown below:

$$\varphi_{tt} = h\nabla^2\varphi + \nabla h\cdot\nabla\varphi - \alpha[2\nabla\varphi_t\cdot\nabla\varphi - \varphi_t\nabla^2\varphi] + \varepsilon^2\left\{\frac{h}{2}\nabla h\cdot\nabla\varphi_t + \frac{h^2}{3}\nabla^2\varphi_t\right\}_t \qquad (2.59)$$

$$- \varepsilon^2\nabla\cdot\left[\left\{\frac{h}{2}\nabla h\cdot\nabla\varphi + \frac{h^2}{6}\nabla^2\varphi\right\}\nabla h\right] + O(\varepsilon^4,\alpha\varepsilon^2)$$

In the following chapter, futher simplifcations of the combined equations will be presented for the special cases computed numerically.

CHAPTER 3

The Numerical Procedure

The numerical procedure described in this chapter is used throughout the rest of this thesis to solve the governing partial differential equation (3.59) for selected bottom topographies. In order to efficiently perform a variety of numerical experiments, two numerical programs were developed: One for solving the governing equation in the reduced case of one horizontal dimension (1HD), and another for solving this equation in two horizontal dimensions (2HD). Both programs have their foundation in classic finite-difference methods, and both follow similar paths toward the solution of Equation 3.59, with a single exception involving matrix inversion (discussed in Section 3.2). We will first examine the solution method for the 1HD case; the 2HD case will follow in Section 3.2 as a natural extension of the techniques described for the 1HD case. The permanent form solution, described in the previous chapter, provides a stringent test of the accuracy of our scheme. In order to provide convincing evidence of the reliability of our numerical procedure, we present in Section 3.3 the results of exhaustive testing based on comparison with the permanent form solution. We use the information from these tests to select our numerical parameters and present an estimation of the errors for a number of key quantities.

3.1 The Numerical Method for the Case Involving One Horizontal Dimension.

In this section, we consider motion in one horizontal dimension (1HD) only. For reference, the equation for $\varphi(x,t)$, the depth averaged potential in 1HD is:

$$\varphi_{tt} = (h\varphi_x)_x - 2\varphi_x\varphi_{xt} - \varphi_t\varphi_{xx} + \frac{h^2}{3}\varphi_{xxtt} + \frac{hh_x}{2}\varphi_{xtt} - \frac{h^2}{6}[h_x\varphi_{xx}]_x \qquad (3.1)$$

Here t represent time and subscripts denote partial derivatives; h=h(x) is the water depth. For simplicity we have taken h to be slowly varying in space and fixed in time, specifically, $h_x, h_{xx}, \cdots \leq O(\alpha)$ and $h_t \equiv 0$. Higher order terms involving φ and derivatives of h have been dropped in a manner consistent with the derivation in Chapter 3. In addition, the order parameters α and ε * have been absorbed into the accompanying variables in equation (3.1), so that the appropriate relative magnitudes of the quantities are restored. The quantities to the immediate left and right of the equal sign in (3.1) constitute the well-known wave equation in nonuniform media. The next two terms are nonlinear contributions, while the last three terms represent the effects of dispersion. Of the dispersive constituents of (3.1) only the first term contributes in regions where the depth is constant, as in the classical Boussinesq model. Once φ has been obtained, we determine the surface height ζ by using Equation (3.40) in 1HD, which is

$$\zeta(x,t) = -\varphi_t - \frac{1}{2}(\varphi_x)^2 + \frac{h^2}{3}\varphi_{xxt} + \frac{h}{2}h_x\varphi_{xt}. \qquad (3.2)$$

We will now discuss the numerical aspects of solving (3.1). As an initial, heuristic indicator of numerical stability, we examine the linearized version of Equation 3.1 for constant depth, $h = h_0$:

$$\varphi_{tt} = h_0\varphi_{xx} + \frac{h_0^2}{3}\varphi_{xxtt}. \qquad (3.3)$$

We assume that, given some suitable initial conditions, we may make a Fourier expansion of the solution to (3.3). We consider the effects of a single term of this expansion, $\varphi(x,t) = Be^{i(\kappa x - \omega t)}$, where B is a constant, κ ($= \frac{2\pi}{\lambda}$) is the

* As discussed in Section 3.2, $\alpha = \frac{A}{h_0}$, where A is a representative wave amplitude and h_0 is a typical water depth; $\varepsilon = \frac{A}{\lambda}$, where λ is a typical wavelength; $\alpha \approx \varepsilon^2$.

wavenumber, and ω is the frequency. Substitution into (3.3) yields a relationship between the wavenumber and the frequency as:

$$\omega^2 = \frac{h_0\kappa^2}{1 + \frac{1}{3}h_0^2\kappa^2} \tag{3.3a}$$

This equation, known as the dispersion relation, may be taken to imply stability with respect to the introduction of small short wavelength errors due to numerical approximation -- unlike in some linearized forms of the Korteweg deVries (KdV) Equation. Such small errors, having large κ will not cause the frequency to become imaginary and thus destroy the hyperbolic nature of the problem.

We approximate the partial differential equation (3.1) in the continuous variable φ by an appropriately chosen difference equation in the difference variable Φ, assuming $\varphi(x_j,t_n) \approx \Phi(j,n)$, where the arguments of φ and Φ are related through the stepsizes of the difference scheme chosen. We examine the difference equation in a limited spatial domain: $X_L \leq x \leq X_R$, where X_L and X_R are the left and right boundary values, respectively. We choose uniformly spaced mesh points along the restricted x-axis; Δx denotes the spacing between each point. N_x, the number of points along the restricted x-domain, satisfies

$$(N_x - 1)\cdot\Delta x = X_R - X_L.$$

The time interval is the constant Δt, and our objective is to obtain Φ (and thus deduce ζ) on the given x-domain mesh at times $(n\cdot\Delta t)$, for $n=1,2,3,\ldots$. We have noted before that the basic form of the governing equations is the wave equation, $\varphi_{tt} = h\varphi_{xx}$, plus nonlinear and dispersive terms. Our selected finite-difference representation of Eq. 3.1 is based on those finite difference methods which are known to be successful with the wave equation.† We use a three time

† Many texts and papers discuss finite-difference solutions to the wave equation. Our approach loosely follows the averaging scheme described in Greenspan (1974), which was first developed in a more general form by Von Neumann (see O'Brien [1951] for a discussion of the generalized scheme).

level scheme which averages Φ_{xx} over the top and bottom time levels. We implicitly solve for the full range of space values at each time step, based on information from the previous two time steps, which are assumed known through either initial conditions or previous time-step solutions. Correction is made for the nonlinear terms which involve time derivatives through an iterative process, described more fully below. Nonlinear factors which do not include time derivatives require no iteration since the solution at the middle time level is known. A flowchart of the numerical method for the 1HD case appears in Figure 3.1

We begin by solving the linearized version of (3.1), which is

$$\varphi_{tt} = (h\varphi_x)_x + \frac{h^2}{3}\varphi_{xxtt} + \frac{h}{2}h_x\varphi_{xtt} - \frac{h^2}{6}[h_x\varphi_{xx}]_x \tag{3.4}$$

to obtain a first approximation $\Phi^{(0)}$ to φ. We represent the finite difference form of this equation as

$$\{B\}\cdot\{\Phi^{(0)}(j,n+1)\} = \{r[\Phi(j,n),\Phi(j,n-1)]\} \tag{3.5}$$

where:

- $\{B\}$ represents a tridiagonal matrix in which the lower diagonal, diagonal and upper diagonal entries in the j^{th} row are, respectively:

$$\{B\}_{j-1,j} = -\left[\frac{h}{2}\frac{\Delta t^2}{\Delta x^2} + \frac{h^2}{3\Delta x^2} - \frac{hh_x}{4\Delta x}\right]$$

$$\{B\}_{j,j} = \left[1 + h\frac{\Delta t^2}{\Delta x^2} + \frac{2h^2}{3\Delta x^2}\right] \tag{3.5a}$$

$$\{B\}_{j+1,j} = -\left[\frac{h}{2}\frac{\Delta t^2}{\Delta x^2} + \frac{h^2}{3\Delta x^2} + \frac{hh_x}{4\Delta x}\right]$$

and $j=2,3,\ldots,(N_x-1)$. Boundary conditions ($j=1$ and $j=N_x$) will be discussed later.

- The superscript following Φ denotes the iteration number within the particular time step; if no superscript appears, Φ is a converged solution from a previous time step or an initial condition.

- $\{\Phi^{(0)}(j,n+1)\}$ is the column vector of N_x values (unknown) of Φ at the new

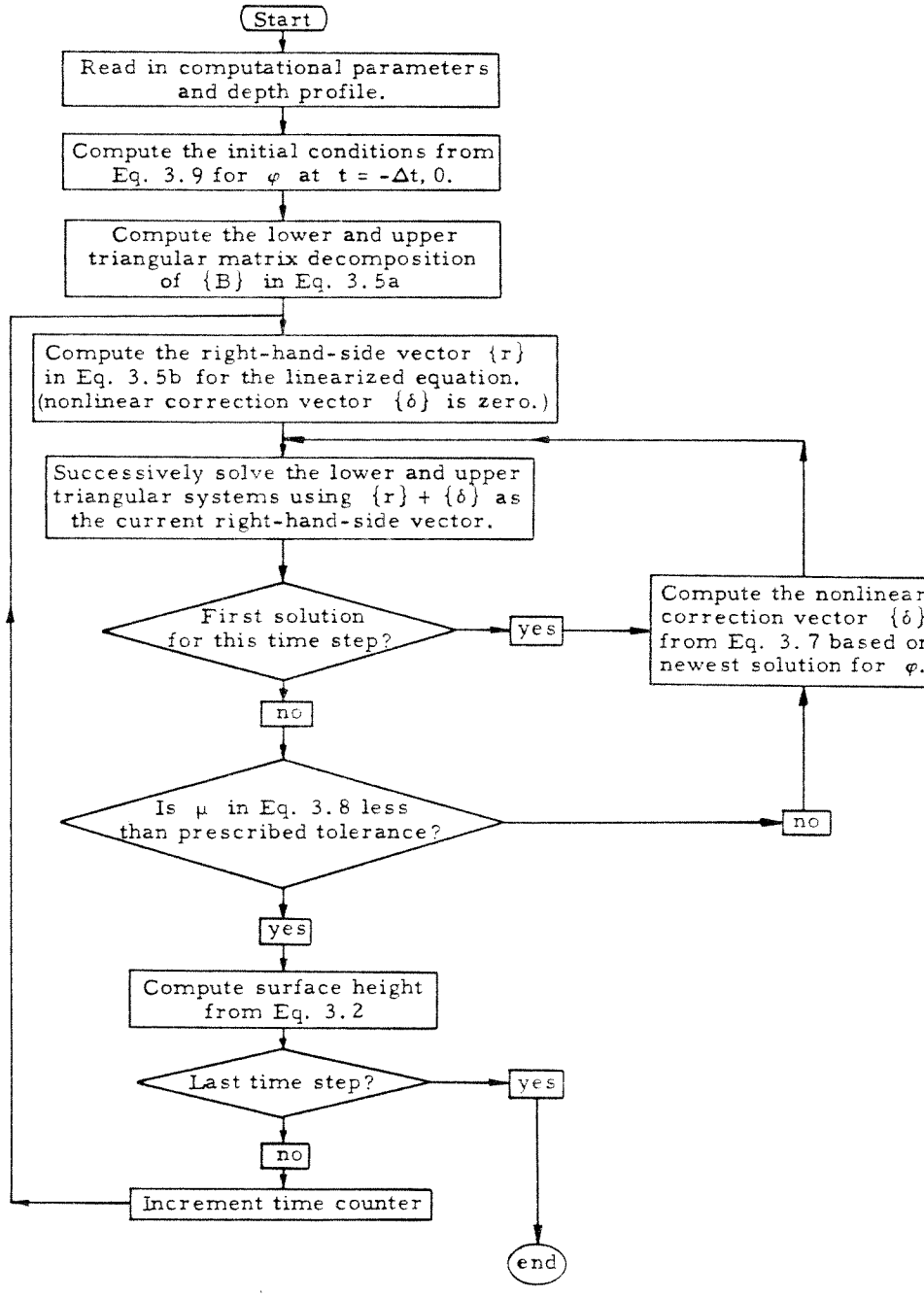

Figure 3.1. Flow Chart for IHD Case.

time step.

- $\{r[\Phi(j,n),\Phi(j,n-1)]\}$ is the right-hand-side column vector based on known values of Φ at the middle and lower time levels. Specifically, the j^{th} component of r is given as

$$\{r\}_j = 2\Phi(j,n) - \Phi(j,n-1) + C_1\Phi_x(j,n) + C_2\Phi_x(j,n-1) \qquad (3.5b)$$
$$+ C_3\Phi_{xx}(j,n) + C_4\Phi_{xx}(j,n-1) + C_5\Phi_{xxx}(j,n)$$

for $j=2,3,\ldots,(N_x-1)$, where

$$C_1 = \Delta t^2 h_x(1-h), \qquad C_2 = \frac{\Delta t^2 h h_x}{2},$$

$$C_3 = -\frac{2h^2}{3} - \frac{\Delta t^2 h^2 h_{xx}}{6}, \qquad C_4 = \frac{h\Delta t^2}{2} + \frac{h^2}{3}, \qquad C_5 = -\frac{\Delta t^2 h^2 h_x}{6},$$

and the finite differences for the x-derivatives used above are taken to be the standard central difference formulas:

$$\Phi_x(j,n) = \frac{1}{2\Delta x}\left[\Phi(j+1,n) - \Phi(j-1,n)\right]. \qquad (3.5c)$$

$$\Phi_{xx}(j,n) = \frac{1}{\Delta x^2}\left[\Phi(j+1,n) - 2\Phi(j,n) + \Phi(j-1,n)\right], \qquad (3.5d)$$

$$\Phi_{xxx}(j,n) = \frac{1}{2\Delta x^3}\left[\Phi(j+2,n) - 2\Phi(j+1,n) + 2\Phi(j-1,n) + \Phi(j-2,n)\right]. \qquad (3.5e)$$

- The arguments of Φ indicate the node numbers for space and time grids respectively.

- The scheme (excluding boundaries) uses centered difference quotients and (in the standard numerical nomenclature) is consistent‡ with the linearized equation (3.4). Also, we can show (for the linearized equation) that the scheme is unconditionally stable* for all Δx and Δt. The truncation error is

‡ Consistency means that as the stepsizes (Δt, Δx) tend to zero *in any manner* the truncation error (from truncating the Taylor expansions used to generate the finite differences) tends to zero.

* The term stable here is intended in the standard numerical sense which may be loosely characterized to mean that there is an upper limit (as Δt goes to zero) to the amplification of a perturbation arising from any sort of error in the calculation. Unconditional stability indicates that the scheme is stable without regard to the ratio of the stepsizes in the x or t direction

$O[(\Delta x)^3] + O[(\Delta t)^3]$.

Equation 3.5 represents a system of N_x equations for the N_x unknowns $\Phi^{(0)}(j,n+1)$. This system of equations can be easily and efficiently solved by decomposing B into upper and lower triangular matrices and solving the resultant triangular systems successively. The upper and lower matrices need only to be calculated once and can be used throughout the computation.

In order to solve the full equation (3.1) we must employ an iterative technique. The i^{th} approximation to $\Phi(j,n+1)$ can be represented as

$$\{B\}\cdot\{\Phi^{(i)}(j,n+1)\} = \{r[\Phi(j,n),\Phi(j,n-1)]\} + \{\delta^{(i)}[\Phi^{(i-1)}(j,n),\Phi(j,n),\Phi(j,n-1)]\} \tag{3.6}$$

where $\{\delta^{(i)}\}$ represents the column vector of corrections to the known vector $\{r\}$ due to the nonlinear terms. Specifically, we calculate the j^{th} row entry of $\{\delta^{(i)}\}$ by

$$\{\delta^{(i)}\}_j = -\Delta t\cdot\Phi_x(j,n)[\Phi_x^{(i-1)}(j,n+1) - \Phi_x(j,n-1)] - \Delta t\cdot\frac{\Phi_{xx}(j,n)}{2}[\Phi^{(i-1)}(j,n+1) - \Phi(j,n-1)], \tag{3.7}$$

for $j=2,3,\ldots,(N_x-1)$, where Φ_x, Φ_{xx} are as given in Eq. 3.5c, 3.5d.

We use a type of uniform convergence test to examine each iteration for convergence, taking as successful an iteration which has μ less than some prescribed tolerence where μ is given by

$$\mu = \frac{\left\{\sum_{j=1}^{N_x}\left[\Phi^{(i)}(j,n+1) - \Phi^{(i-1)}(j,n+1)\right]^2\right\}^{\frac{1}{2}}}{\left\{\sum_{j=1}^{N_x}\left[\Phi^{(i)}(j,n+1) - \Phi(j,n)\right]^2\right\}^{\frac{1}{2}}}. \tag{3.8}$$

This tolerance test compares the iteration differences to the time step differences.

We assume that no wave of significant amplitude approaches near to either

boundary. Consequently, conditions at the boundaries are taken to be especially simple. We assume that the second space derivative of the potential is zero at the boundaries, that is,

$$\Phi_{xx}(1,n) = 0, \quad \text{and} \quad \Phi_{xx}(N_x,n) = 0.$$

Physically , this condition implies that the layer-mean velocity is constant at the boundaries, an assumption which is good for our situation in which the wave is kept in the middle region of the computational domain, and little change is observed at the boundaries. Calculations indicate that any leakage of mass into or out of the computational domain due to these boundary assumptions is negligibly small for situations such as those permitted in this study.

As initial conditions we use the permanent form, constant-depth solution which was derived in the Section 3.6. The permanent form solution may be integrated to give φ directly at the two initial time-steps as

$$\Phi(j,n) = \frac{4\alpha}{3}\tanh\left\{\beta[(j\cdot\Delta x) - U(n\cdot\Delta t)]\right\} \qquad j=1,2,\ldots,N_x; \quad n=-1,0 \qquad (3.9)$$

where

- U is the phase speed given by $U = (1 + \alpha)^{\frac{1}{2}}$,
- and the constant β equals $[\frac{3\alpha}{4U^2}]^{\frac{1}{2}}$.

A copy of the FORTRAN program developed from the description presented here for 1HD propagation resides in Appendix B. Results for a number of cases using this 1HD program will be presented in Section 3.3, along with a discussion of specific values for step size, tolerance, wave height and other key quantities.

3.2 The Numerical Method for the Case Involving Two Horizontal Dimensions

The numerical method for the two horizontal dimension (2HD) case follows the 1HD case quite closely. The equation for $\varphi(x,y,t)$ is taken from (2.59)

assuming, as in Section 3.1, that h = h(x,y) is slowly-varying in space and fixed in time:

$$\varphi_{tt} = \nabla\cdot(h\nabla\varphi) - 2\nabla\varphi\cdot\nabla\varphi_t - \varphi_t\nabla^2\varphi + \frac{h^2}{3}\nabla^2\varphi_{tt} + \frac{h}{2}\nabla h\cdot\nabla\varphi_{tt} - \frac{h^2}{6}\nabla\cdot[(\nabla^2\varphi)\nabla h] \qquad (3.10)$$

Higher order terms involving derivatives of h have been dropped in a manner consistent with the derivation in Chapter 3 and the order parameters α and ε have been absorbed into the accompanying variables. The terms in (3.10) correspond to those discussed for (3.1). The surface height $\zeta(x,y,t)$ is computed from (2.40) for this model situation:

$$\zeta(x,y,t) = -\varphi_t - \frac{1}{2}(\nabla\varphi)^2\frac{h^2}{3}\nabla^2\varphi_t + \frac{h}{2}\nabla h\cdot\nabla\varphi_t$$

As in Section 3.1 we assume that the continuous varible $\varphi(x_j,y_k,t_n)$ can be approximated by the discrete variable $\Phi(j,k,n)$ through an appropriate difference representation of Eq. 3.10. The computational domain is defined by $X_L \le x \le X_R$ and $Y_L \le y \le Y_R$. The mesh points are uniformly spaced along the restricted axes; Δx, Δy, Δt represent the stepsizes in the x, y and t directions. N_x and N_y denote the number of points along the x and y axes. N_T (the total number of grid points) is defined as:

$$N_T = N_x\cdot N_y \qquad (3.11)$$

A flowchart of the numerical method for the 2HD case appears in Figure 3.3. For a basic description of the solution method, see Section 3.1, paragraph 3. The specific changes implemented on the 1HD method for the 2HD case are discussed below.

We introduce a numbering convention which will sequentially number the mesh in the (x,y) plane. The new index m runs from 1 to N_T and is defined by

$$m = j + (k - 1)\cdot N_x \qquad \text{for } j = 1,\ldots,N_x;\quad k = 1,\ldots,N_y. \qquad (3.12)$$

All the discrete (x_j,y_k) points may now be referenced by a a single subscript m.

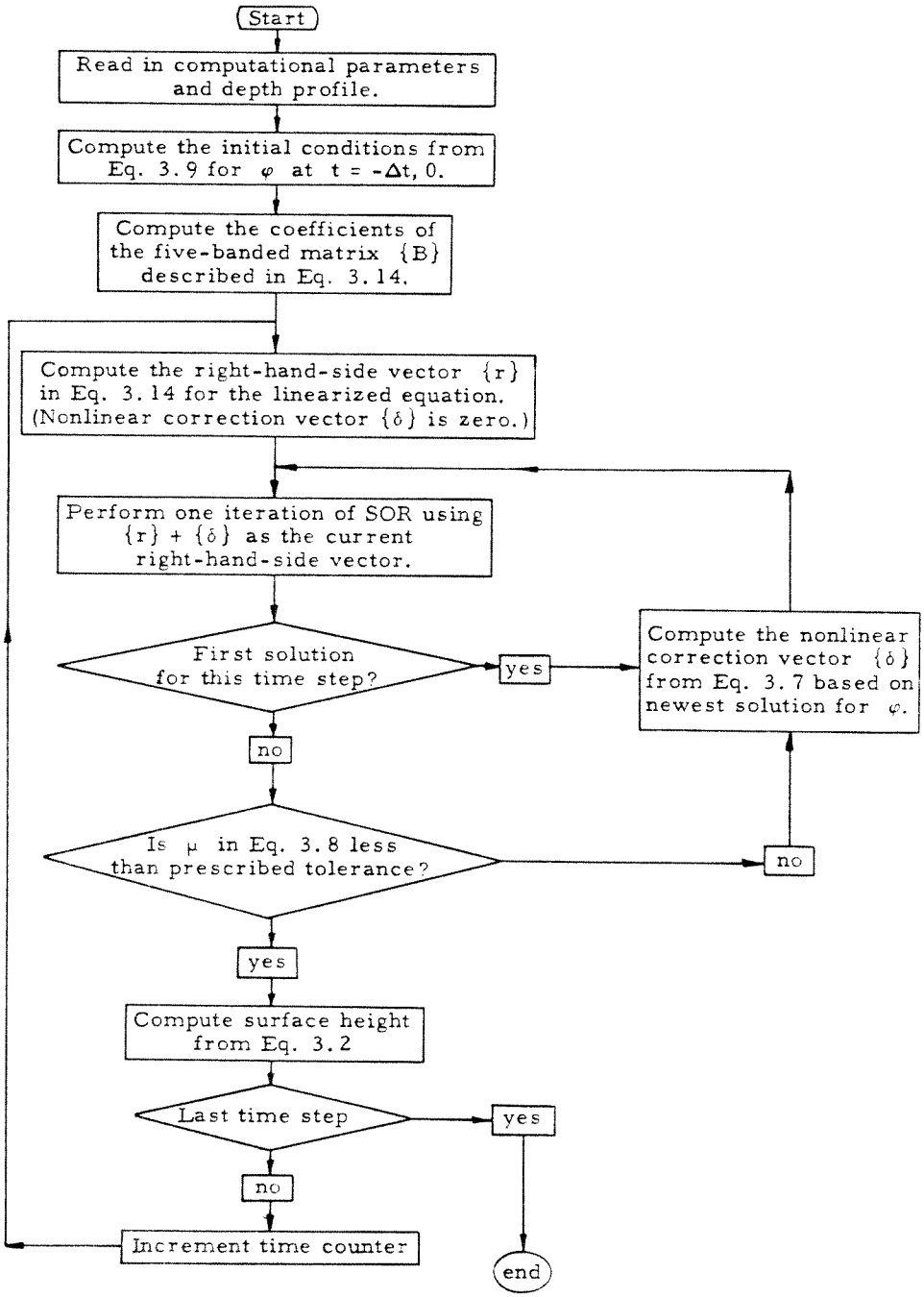

Figure 3.3. Flow Chart for 2HD Case.

The linearized version of (3.10) is

$$\varphi_{tt} = \nabla\cdot(h\nabla\varphi) + \frac{h^2}{3}\nabla^2\varphi_{tt} + \frac{h}{2}\nabla h\cdot\nabla\varphi_{tt} - \frac{h^2}{6}\nabla\cdot[(\nabla^2\varphi)\nabla h] \tag{3.13}$$

and we represent the finite-difference form of this equation as in Equation 3.5 of Section 3.1:

$$\{B\}\cdot\{\Phi^{(0)}(m,n+1)\} = \{r[\Phi(m,n),\Phi(m,n-1)]\} \tag{3.14}$$

however the quantities listed above are now defined as follows:

- $\{B\}$ represents a banded matrix of rank $N_T \times N_T$ whose nonzero elements lie on the five diagonal lines pictured in Figure 3.4. These five entries are given on the m^{th} row as:

$$\{B\}_{m-N_x,m} = -\left[\frac{h}{2}\frac{\Delta t^2}{\Delta y^2} + \frac{h^2}{3\Delta y^2} - \frac{hh_y}{4\Delta y}\right]$$

$$\{B\}_{m-1,m} = -\left[\frac{h}{2}\frac{\Delta t^2}{\Delta x^2} + \frac{h^2}{3\Delta x^2} - \frac{hh_x}{4\Delta x}\right]$$

$$\{B\}_{m,m} = 1 + \left(h\Delta t^2 + \frac{2h^2}{3}\right)\cdot\left\{\frac{1}{\Delta x^2} + \frac{1}{\Delta y^2}\right\} \tag{3.14a}$$

$$\{B\}_{m+1,m} = -\left[\frac{h}{2}\frac{\Delta t^2}{\Delta x^2} + \frac{h^2}{3\Delta x^2} + \frac{hh_x}{4\Delta x}\right]$$

$$\{B\}_{m+N_x,m} = -\left[\frac{h}{2}\frac{\Delta t^2}{\Delta y^2} + \frac{h^2}{3\Delta y^2} + \frac{hh_y}{4\Delta y}\right]$$

for m: j=2,3,...,(N_x-1) and k=2,3,...,(N_y-1) where m is defined by (3.12). Boundary conditions will be discussed later.

- The superscript following Φ denotes the iteration number within the particular time step; if no superscript appears, Φ is a converged solution from a previous time step or an initial condition.

- $\{\Phi^{(0)}(m,n+1)\}$ is the column vector of N_T values (unknown) of Φ at the new time step.

- $\{r[\Phi(m,n),\Phi(m,n-1)]\}$ is the right-hand-side column vector based on known values of Φ at the middle and lower time levels. Specifically, the m^{th} (excluding those points which lie on either an x or y boundary) component of r

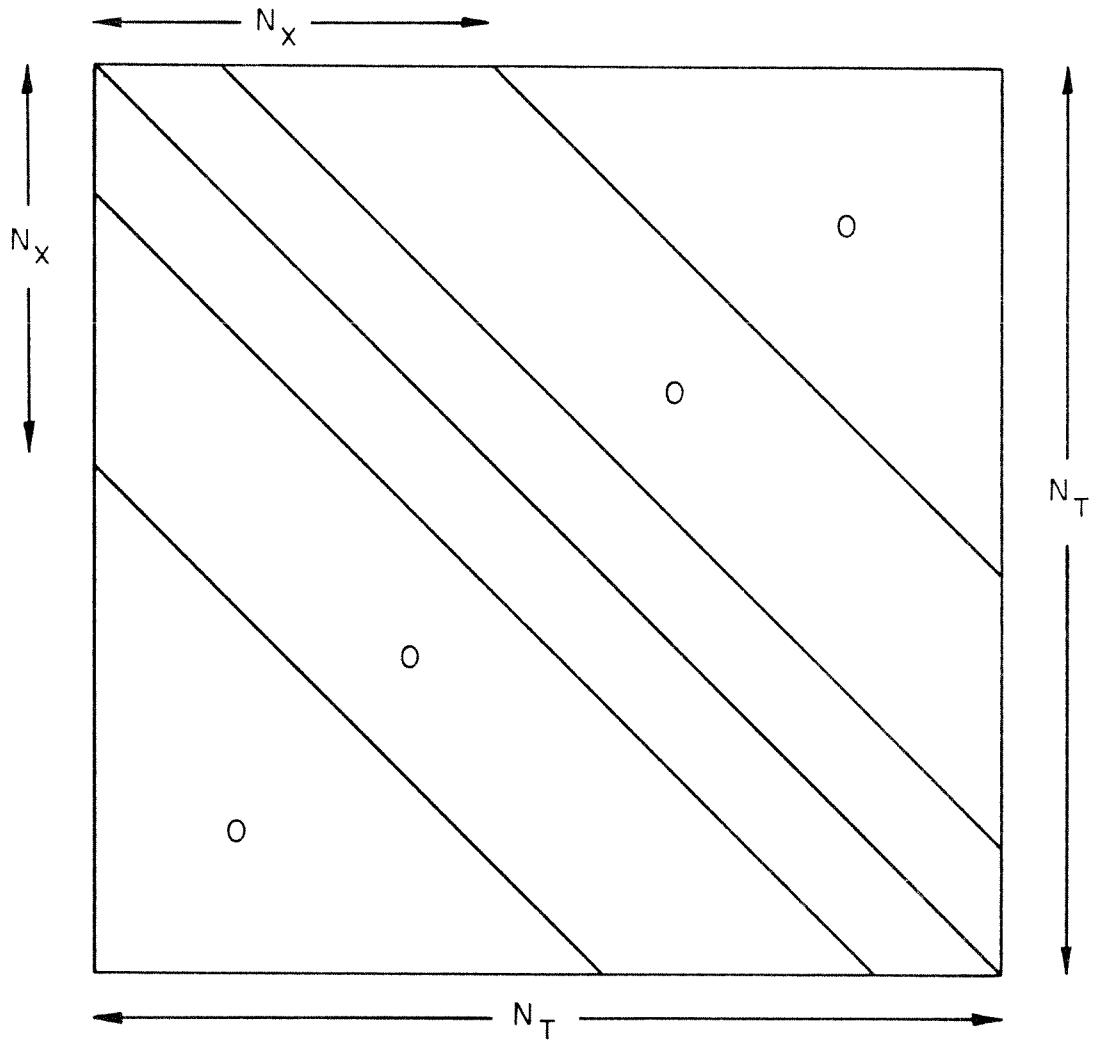

Figure 3.4 Schematic representaion of the nonzero elements of the banded matrix $\{B\}$. The five diagonal lines show the location of the nonzero elements.

is given as

$$\{r\}_m = 2\Phi(m,n) - \Phi(m,n-1)C_1\nabla h\cdot\nabla\Phi(m,n)C_2\nabla h\cdot\nabla\Phi(m,n-1) \qquad (3.14b)$$
$$C_3\nabla^2\Phi(m,n) + C_4\nabla^2\Phi(m,n-1) + C_5\nabla h\cdot\nabla[\nabla^2\Phi(m,n)]$$

for m: j=2,3,...,(N_x -1); k=2,3,...(N_y−1), where

$$C_1 = \Delta t^2 - h, \qquad C_2 = \frac{h}{2}$$

$$C_3 = -\frac{h^2\nabla^2 h\Delta t^2}{6} - \frac{2h^2}{3}, \qquad C_4 = \frac{h^2}{3}, \qquad C_5 = -\frac{h^2\Delta t^2}{6},$$

and the finite differences for the derivatives above are taken as the appropriate centered difference quotients.

- The scheme described here is consistent with equation 3.13 and is unconditionally stable. The truncation error is $O[(\Delta t)^3] + O[(\Delta x)^3] + O[(\Delta y)^3]$.

Equation (3.14) represents a system of N_T equations in N_T unknowns $\Phi^{(0)}(m,n+1)$. This system of equations is rather large and is not efficiently solved by direct matrix methods which destroy the five-banded structure. Instead, we solve the system using the Successive Over-Relaxation (SOR) method which is an iterative inversion scheme that exploits the banded nature of the matrix.

In order to solve the full equation (3.10) we must also iterate on the nonlinear correction terms. We represent the i^{th} approximation to $\Phi(m,n+1)$ as:

$$\{B\}\cdot\{\Phi^{(i)}(m,n+1)\} = \{r[\Phi(m,n),\Phi(m,n-1)]\} \qquad (3.15)$$
$$+ \{\delta^{(i)}[\Phi^{(i-1)}(m,n),\Phi(m,n),\Phi(m,n-1)]\}$$

where $\{\delta^{(i)}\}$ represents the column vector of corrections to the known vector $\{r\}$ due to the nonlinear terms. Specifically, we calculate the m^{th} row entry of $\{\delta^{(i)}\}$ by

$$\{\delta^{(i)}\}_m = -\Delta t\cdot\Big\{\ \Phi_x(m,n)[\Phi_x^{(i-1)}(m,n+1) - \Phi_x(m,n-1)] \tag{3.16}$$

$$- \Phi_y(m,n)[\Phi_y^{(i-1)}(m,n+1) - \Phi_y(m,n-1)]$$

$$- \frac{\Phi_{xx}(m,n)}{2}[\Phi^{(i-1)}(m,n+1) - \Phi(m,n-1)]\Big\},$$

for m: j=2,3,...,(N_x -1); k=2,3,...N_y, where the indicated derivatives are composed of standard centered finite-difference quotients. Since we must already use SOR to iterate for the solution at each iteration, we streamline the process and minimize the iteration count by combining the SOR iteration with the iteration on the nonlinear correction. (See the flowchart Fig 3.3 for the specific procedure)

Our convergence test is essentially the same as that given in Eq. 3.8. The summation for the 2HD case runs from 1 to N_T in both the numerator and denominator.

The initial conditions consist of placing the permanent form solution specified in Eq. 3.9 along each row of points in the x-direction. This initializes a planar permanent-form wave moving in the x-direction, with no variation in the y-direction.

The specific situation we wish to model for the 2HD case is that of a wave propagating down an infinite channel. For the restricted computational domain, we have four boundaries consisting of a total of [2(N_x + N_y−1)] points to consider instead of just 2 boundary points for the 1HD situation. Figure 3.5 shows the boundary points and the naming convention for the boundaries. We retain the simple features of the 1HD case at the entrance and exit boundaries, where we take

$$\Phi_{xx}(M_{en},n) = 0 \quad \text{and} \quad \Phi_{xx}(M_{ex},n) = 0 \tag{3.17}$$

where

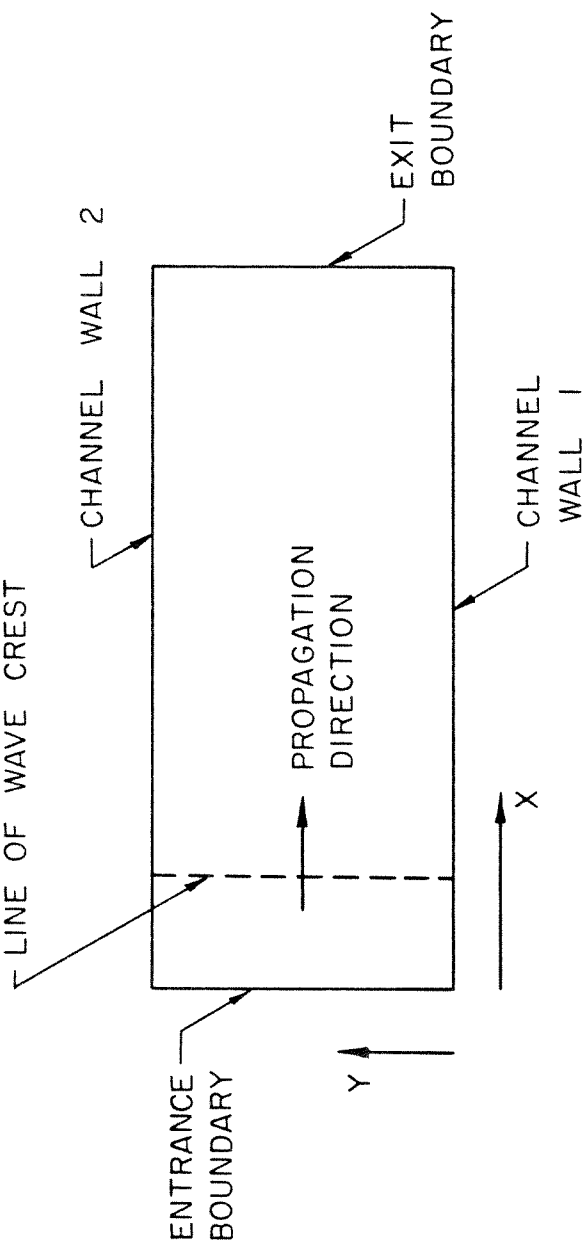

Figure 3.5 Nomenclature for the four boundaries. Cross-channel direction is *y*; x-axis coincides with the direction of propagation.

$$M_{en} = 1 + (k-1)\cdot N_x, \qquad M_{ex} = k\cdot N_x \qquad \text{for } k=1,2,\ldots,N_y.$$

The other two boundaries are the channel walls, which affords the obvious condition that the velocity perpendicular to the wall is zero, i.e.,

$$\Phi_y(M_{w1},n) = 0 \quad \text{and} \quad \Phi_y(M_{w2},n) = 0 \tag{3.18}$$

where

$$M_{w1} = 1,2,\ldots,N_x, \qquad M_{w2} = [(N_y-1)N_x+1],[(N_y-1)N_x+2],\ldots,N_T.$$

For bottom topographies which are symmetric about the channel center-line we need only to consider half of the region of interest. The boundary conditions for this symmetric situation are identical to (3.18) since there is no flow across a line of symmetry.

A copy of the FORTRAN program described in this section may be found in Appendix C. The following section will discuss specific tests performed with the 2HD program.

3.3 The Numerical Checks

The numerical scheme described in the previous two sections can be shown to be consistent with the appropriate linearized equation and unconditionally stable (also in reference to the linearized equation). The iteration scheme used to include the nonlinear terms is standard, and these nonlinear terms can be shown to be small relative to the dominant terms which have previously been identified as the well-known wave equation in a nonuniform medium. Any errors, then, are assumed to be associated with (1) the finite grid spacing, (2) the convergence tolerance parameter, or (3) round-off errors due to inadequate precision. We refer to (1) and (2) as the numerical parameters. In this section, we show that our numerical scheme when given the exact permanent form solution (derived in Section 2.6) as an initial condition does, in fact, converge to the exact permanent form solution. We show that the errors in key quantities,

such as peak amplitude, excess mass and wave speed, behave in a regular fashion with respect to the the numerical parameters. We discuss the effects of the finite grid spacing and select the stepsize and the tolerance to be used in later numerical experiments. Finally we give the expected range of validity for the numerical experiments (to be discussed Chapter 5) for the chosen numerical parameters.

The permanent form solution derived in Section 2.6 is of crucial importance in this section. Without this solution, we would have no way to insure that the stepsize, tolerence and precision used in the numerical program were adequate for the model problems. However, in order to know what numerical checks to perform, we must know what type of numerical experiments are planned. As we have discussed in Chapter 1, our primary aim is to study three-dimensional propagation effects through the use of some basic curving bottom topographies. All of the topographies mentioned in Chapter 1 share the feature of a deep flat section joined by some sort of curving ramp to a shallower flat section. We therefore perform our series of tests with wave parameters designed to simulate propagation in the two extreme cases -- (1) the deep flat section and (2) the shallow flat section. Since no permanent-form or other exact theoretical solutions are available for regions with variable bottom topography, we do not consider these cases in this chapter. However, a number of investigators have numerically solved the 1HD case for variable depth and, in Chapter 5, we discuss the results for some comparable cases.

The parameters which govern the initial conditions that we have chosen to use in this series of tests are summarized by the order parameter α. Specifically, we examine two cases: $\alpha = 0.1$ and $\alpha = 0.4$, which we expect to cover the range of this parameter in the 2HD numerical experiments described in the upcoming chapter. We arbitrarily take the depth to be unity and scale all other

quantities from this length. A range for possible stepsizes can be chosen by inspection of the initial conditions plots. From these graphs we can see that the wavelength of the waves plotted is roughly 20 units, however the region of swiftest change is only about a quarter of this distance. Therefore, in order to represent this important region adequately, we establish the range of stepsize values to be investigated as $0.2 \leq \Delta t, \Delta x, \Delta y \leq 0.8$.

We wish to examine the numerical scheme for the stepsize range above in the absence of errors induced by incomplete convergence and round-off. Initial computation indicates that if μ in Eq. 3.8 is required to be less than 10^{-5} there is no appreciable change in the results; therefore, we assume that there is complete convergence for the 1HD case if $\mu \leq 10^{-5}$. This tolerance requires from 3 to 5 iterations per time step for the 1HD case, depending on the amplitude and stepsize. In addition, we introduce the use of double-precision which dramatically reduces the effects of round-off error. In order to simplify the process of stepsize examination, we take the stepsizes in the three directions x,y,and t to be equal in length, i.e.,

$$\Delta t = \Delta x = \Delta y = \Delta \qquad \text{for } 0.2 \leq \Delta \leq 0.8.$$

Figures 3.6 and 3.7 show the results of stepsize variation using the 1HD program for the cases $\alpha = 0.1$ and $\alpha = 0.4$ respectively. The initial wave peak was located at x=0 and the wave was propagated for 100 time units (or as close to that value as the stepsize permitted). The number of actual time steps (of size Δ) taken varied from 126 (for Δ=0.8) to 501 (for Δ=0.2). It is clear from the figures that the scheme converges to the exact solution as the mesh spacing is refined. The solutions for the larger grid spacings display an oscillatory tail which deviates from the exact solution. This undular tail was also apparent in similar calculations by Goring (1978) who used a finite-element formulation to solve the Boussinesq equations. Goring attributed the formation of an

Figure 3.6 The surface height after propagation for 100 time units for an initial solitary wave amplitude of 0.1. The upper seven curves depict surface heights computed for various stepsizes using the 1HD program. From top to bottom the stepsizes used are $\Delta t = \Delta x = 0.8$, 0.7, 0.6, 0.5, 0.4, 0.3 and 0.2. The last curve shows the surface height computed for t=100 from the permanent-form solution Eq. 2.58.

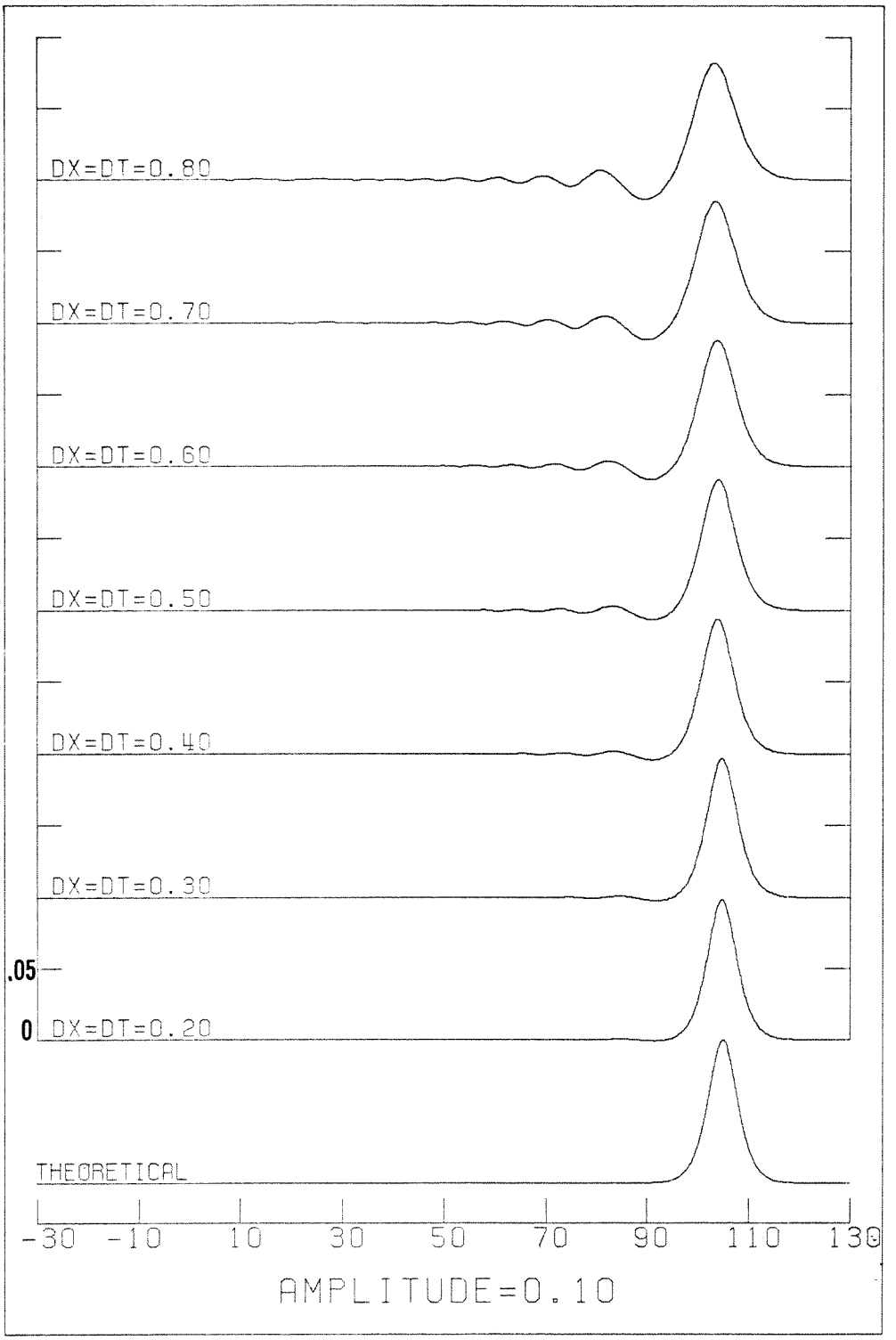
DX=DT=0.80
DX=DT=0.70
DX=DT=0.60
DX=DT=0.50
DX=DT=0.40
DX=DT=0.30
.05
0
DX=DT=0.20
THEORETICAL
-30
-10
10
30
50
70
90
110
130
AMPLITUDE=0.10

Figure 3.6

Figure 3.7 The surface height after propagation for 100 time units for an initial solitary wave amplitude of 0.4. The upper seven curves depict surface heights computed for various stepsizes using the 1HD program. From top to bottom the stepsizes used are $\Delta t = \Delta x = 0.8$, 0.7, 0.6, 0.5, 0.4, 0.3 and 0.2. The last curve shows the surface height computed for t=100 from the permanent-form solution Eq. 2.58.

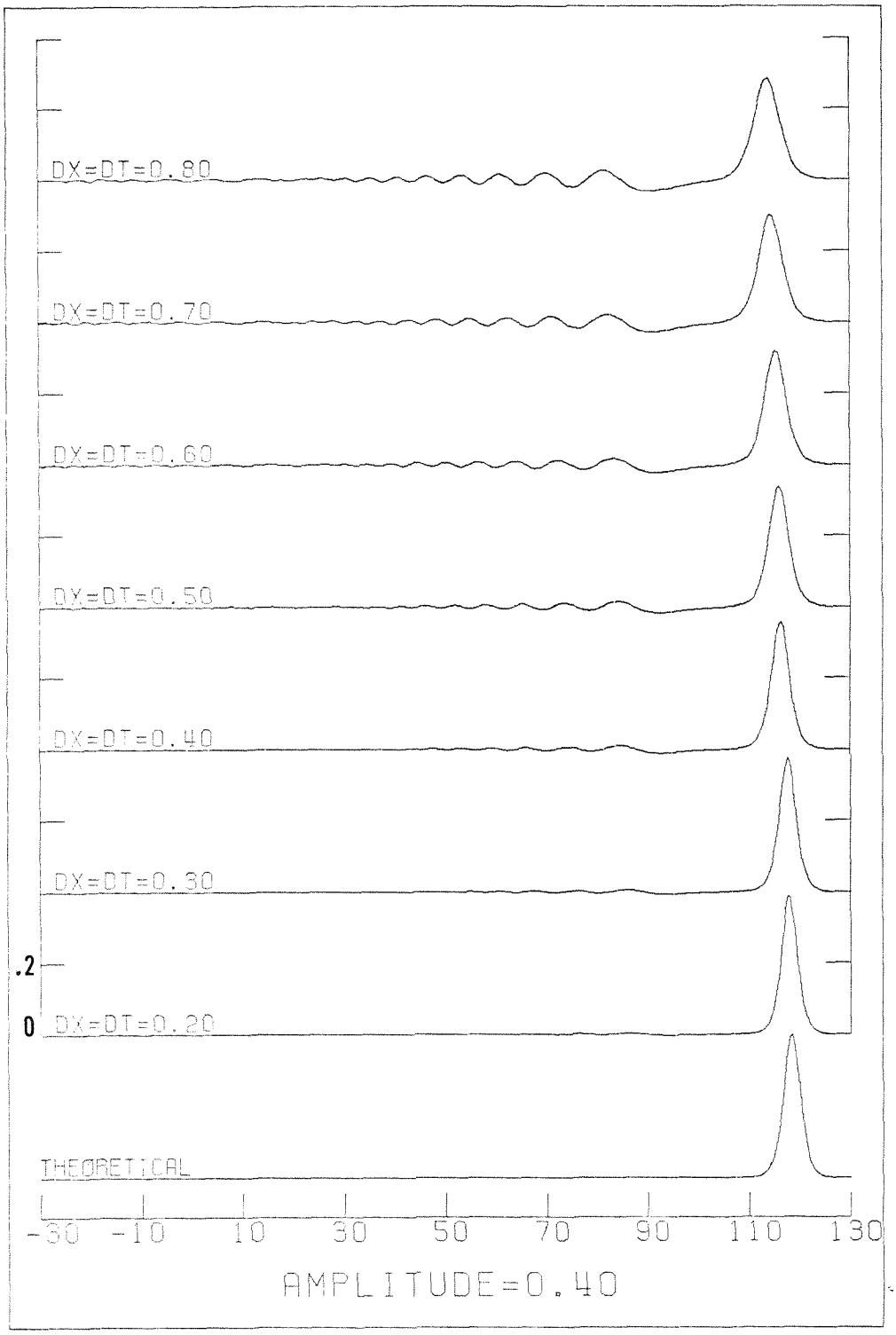
DX=DT=0.80
DX=DT=0.70
DX=DT=0.60
DX=DT=0.50
DX=DT=0.40
DX=DT=0.30
.2
0
DX=DT=0.20
THEORETICAL
-30
-10
10
30
50
70
90
110
130
AMPLITUDE=0.40

Figure 3.7

oscillatory tail to his use of inexact† initial conditions. However, the results illustrated in Figs. 3.6 and 3.7 indicate that, at least for our formulation, this oscillatory tail is a spurious result generated by insufficient mesh refinement.‡

We may examine the results from the stepsize variation in more detail through Tables 3.1 and 3.2. These tables show that the errors in excess mass (a conserved quantity), peak amplitude, wave shape and wave speed are reduced as the stepsize is refined for the two different amplitudes. Under excess mass we have established two separate categories: "Range/Theo. Excess" and "Final/Theo. Excess." The first entry is meant as an indicator of the extent to which the excess mass anomalously varies as a function of time (normalized by the theoretical excess mass value). The theoretical excess mass can be shown to be constant for the range of motion considered in the computational domain. By inspecting the value of the excess mass at each time step, it was discovered that, as the oscillatory tail develops, the excess mass also undergoes an oscillation. As the wave continues to propagate, the oscillations become smaller until they approach a straight line. The "Final/Theo. Excess" entry indicates the ratio of this final excess mass to the theoretically predicted value. The final values are usually quite close to the predicted theoretical value. The next column entry in the tables indicates the degradation in the peak amplitude resulting from the stepsize choice. The quantity listed in the table is the peak value after propagation for 100 time units normalized by the initial wave height. This quantity is also seen to respond favorably to the mesh refinement. The next column marked "Trough/Initial Amp." is intended to act as a measure of the shape distortion of the permanent form wave due to the spacing. The entries

† As previously discussed in Section 2.6, the KdV permanent-form solution, which Goring used as an initial condition, is not an exact solution to the Boussinesq equations. In this study, the initial condition used is an exact permanent-form solution to the equation which we solve numerically.

‡ For comparison, Goring used stepsizes of $\Delta x = 0.7$ and $\Delta t = 0.7575$, about equivalent to the stepsizes we used to obtain the second curve from the top in Figs. 3.6 and 3.7.

TABLE 3.1

AMPLITUDE = 0.10

Step Size	-- EXCESS MASS --- Range/ Theo.Excess	Final/ Theo.Excess	Peak/ Initial Amp	Trough/ Initial Amp	Wave Speed/ Th. Wave Speed
0.80	0.0068797	0.999679	0.838518	-0.137809	0.979870
0.70	0.0054652	0.999733	0.864645	-0.114860	0.984710
0.60	0.0041470	0.999772	0.891544	-0.091421	0.987408
0.50	0.0029646	0.999841	0.918232	-0.067307	0.990812
0.40	0.0019489	0.999889	0.943632	-0.044252	0.993845
0.30	0.0011198	0.999933	0.966309	-0.024150	0.996418
0.20	0.0005048	0.999971	0.984166	-0.008851	0.998363

TABLE 3.2

AMPLITUDE = 0.40

Step Size	-- EXCESS MASS --- Range/ Theo.Excess	Final/ Theo.Excess	Peak/ Initial Amp	Trough/ Initial Amp	Wave Speed/ Th.Wave Speed
0.80	0.0173026	0.996818	0.776089	-0.090037	0.958665
0.70	0.0139315	0.997847	0.809006	-0.076454	0.966002
0.60	0.0106851	0.998010	0.843432	-0.062138	0.973252
0.50	0.0077080	0.998427	0.879125	-0.047622	0.980215
0.40	0.0051216	0.998535	0.914262	-0.033454	0.986584
0.30	0.0029701	0.999175	0.947358	-0.020343	0.992064
0.20	0.0013482	0.999592	0.974863	-0.009637	0.996335

listed were obtained by dividing the maximum trough depth by the initial peak amplitude. Values for the larger stepsizes show a comparatively large degree of distortion from the theoretical shape, which is confirmed in Figures 3.6 and 3.7. The final column in Tables 3.1 and 3.2 gauges the accuracy of the position of the wave after 100 time units by computing the wave speed and comparing it to the value theoretically determined in Section 2.6. (Both the peak height used in column 3 and the peak amplitude position used to determine the average wave speed have been interpolated from the grid points for more accurate results.) The wave speed comparison indicates that the wave invariably travels slower on larger grid spacings for our numerical scheme. Some simple computations indicate that this slower speed may be primarily attributed to the degradation in peak height.

The tables and figures discussed above were made using the 1HD program. Ideally, similar tables and plots should be made using the 2HD program as well, however such a project is prohibitively time-consuming and expensive for a reasonably sized grid. (The core region required goes up as the square of the space step and the time requirements go up by a factor larger than the cube of the stepsize because the combined nonlinear and Successive Over-Relaxation iteration scheme dictated by the larger sized grid requires from 10 to 15 more iterations.) Instead, a small group of well-chosen tests were performed using the 2HD program and these results were then compared to those from the 1HD program. These tests indicate that, for a tolerance of 10^{-7}, the results from the 2HD cases are identical to the 1HD. Because we are able to show that, for high enough tolerances, the 2HD case results converge to those from the 1HD case, we may apply the results from the 1HD stepsize variation to the 2HD case.

It is clear that smaller stepsizes yield superior results. For the 2HD program this is a unpleasant (although certainly not unexpected) conclusion

because the stepsize so greatly influences the time, cost and region storage requirements. Therefore, we must balance the time, cost and space disadvantages against accuracy in our computed results, keeping in mind the types of phenomena we want to examine in the numerical experiments. This balancing resulted in a choice of 0.4 as the selected stepsize for 2HD calculations. This parameter is large enough to keep the disadvantages from becoming prohibitive, yet small enough to allow us to observe important features in the propagation with confidence. However, since the 1HD program does not have the soaring costs and time requirements of the 2HD program, and since we may be interested in some more subtle features in the 1HD case, we will take the 1HD stepsize to be as small as appropriate for the numerical experiments discussed in Chapter 5.

With regard to the tolerance parameter, we are primarily interested in determining what is the largest possible value that will allow us to reduce the following two effects:

- Cross-channel drift recognizable as the generation of spurious y-derivatives, and
- Systematic changes in the values of key quantities such as excess mass, peak height, and wave speed from the 1HD results for the same stepsize (Δ = 0.4).

Our chosen tolerance of 10^{-4} is found to permit a maximum drift of 0.2% in amplitude values across the channel after propagation for 100 time units. Table 3.3 compares the differences in the key quantities mentioned above for the 1HD case with a tolerance of 10^{-5} and the 2HD case at the same stepsize (Δ = 0.4) with a tolerance of 10^{-4}.

An attempt was made to revert to single-precision from the double-precision used in the test cases; however, it was discovered that single precision

TABLE 3.3

Initial Peak Amplitude	Case	---- EXCESS MASS ----- Range/ Theo.Excess	Final/ Theo.Excess	Peak/ Initial Amp	Trough/ Initial Amp	Wave Speed/ Th.Wave Speed
0.1	1HD	0.0019489	0.999889	0.943632	-0.044252	0.993845
0.1	2HD	0.0086074	1.000050	0.943454	-0.045677	0.993284
0.4	1HD	0.0051216	0.998535	0.914262	-0.033454	0.986584
0.4	2HD	0.0056127	0.989639	0.914111	-0.032280	0.986189

is not adequate for the calculations we wish to perform. Thus we have insisted on double-precision for all our calculations. All computations presented in this thesis were performed on the IBM 370/3023 digital computer in the Booth Computing Center of the California Institute of Technology. The programs required approximately 350 kilobytes of core storage for the 1HD cases and 1.6 megabytes of core storage for the 2HD cases. A typical 1HD case, running for 100 time units, used about 120 seconds of CPU time while the equivalent typical 2HD case used about 1800 seconds.

We are now prepared to state the expected maximum errors for the special cases we will consider in the upcoming chapter. These errors are listed in Table 3.4 for a typical 1HD stepsize and for the selected 2HD step size of 0.4 with tolerances of 10^{-5} and 10^{-4} respectively. We have chosen the numerical parameters such that the ranges given are more than adequate for model problems discussed in Chapter 1.

TABLE 3.4

MAXIMUM ESTIMATED ERRORS

CASE	SELECTED PARAMETERS		Peak Amplitude Degradation	Oscillatory Tail Amplitude	Wave Speed	Cross-Channel Amplitude Variation
	Step Size	Tolerance				
1HD	0.2	10^{-5}	3%	1.1%	0.2%	not applicable
2HD	0.4	10^{-4}	10%	5.0%	2.0%	.2%

CHAPTER 4

Results and Discussion

The results presented in this chapter were obtained using the numerical methods described in Chapter 3. The first set of results concerns the propagation in one horizontal dimension (1HD) of a solitary wave from a constant depth, up a gradual ramp, into a shallower flat region. The wave is seen to steepen and gain amplitude as it passes over the ramp and eventually to separate (or fission) into two or more solitary waves (solitons). We show that, for the cases which we consider, at least 80% of the initial excess mass moves onto the shelf, the remainder being reflected back from the ramp. We make some comparisons of our results with other theoretical and numerical predictions of the primary shelf soliton amplitude and find good agreement for all the cases considered. As might be expected, the second soliton amplitude is found to be lower than that predicted by a model which assumes no wave reflection from the shelf. Comparison with experiment confirms the basic form of the solution on the shelf.

We continue our investigation of wave propagation into shallower water by use of the 2HD program with a plane solitary wave initial condition, similar to the 1HD case above. We examine propagation under the influence of four related bottom topographies. These depth profiles share the features of a uniform depth region joined by a gradual, curving ramp to another, shallower uniform depth region. Once the wave has propagated over the submerged ramp and onto the shelf, the effects of focussing, or defocussing, due to the 2HD depth variation are clearly apparent. We examine the cross-channel variation in amplification of the primary soliton height. We find that the peak amplitude

may vary considerably across the channel since the bottom topography sets up a kind of rocking motion in the fliud. The delayed formation of the secondary solitons is apparent at some channel points, and the line of fully-formed primary and secondary soliton crests deviates noticeably from the straight line crests of the uniform cases. Linear nondispersive theory is used to recompute one of the cases and the results are significantly different from those computed through nonlinear dispersive theory

4.1 Results for Propagation in One Horizontal Dimemsion: Variable Depth

In this section we use the 1HD program developed in Chapter 3 to investigate the propagation of a solitary wave from a region of constant depth, over a gradual ramp, and onto a shelf. Figure 4.1 is a sketch of the bottom topography for the series of cases considered in this section. We present these 1HD results for two reasons: first, to introduce the phenomenon of a wave climbing up a ramp, keeping in mind the model problems for 2HD discussed in Chapter 1, and second, to provide a baseline for comparison with the upcoming 2HD results.

As an initial condition we take a solitary wave moving to the right with peak located at x=0. The specific form of this initial condition is given by Equation 3.9 with α taken to be 0.12. For convenience, we take the water depth h_0 in the deeper region to be unity and the ramp length L_R to be 10. Other parameters are in Figure 4.1 are: $X_L = -30$, $X_S = 6$, and $X_R = 90$. The shelf depths which we consider are h_1=0.451, 0.5, and 0.614. The first and last of these values are chosen for special reasons, which we will discuss next.

We have previously mentioned the KdV equation in the discussion of permanent form solutions (see Section 2.6) for constant depth. A variable-coefficient KdV equation (which we will refer to as the VKdV equation), which

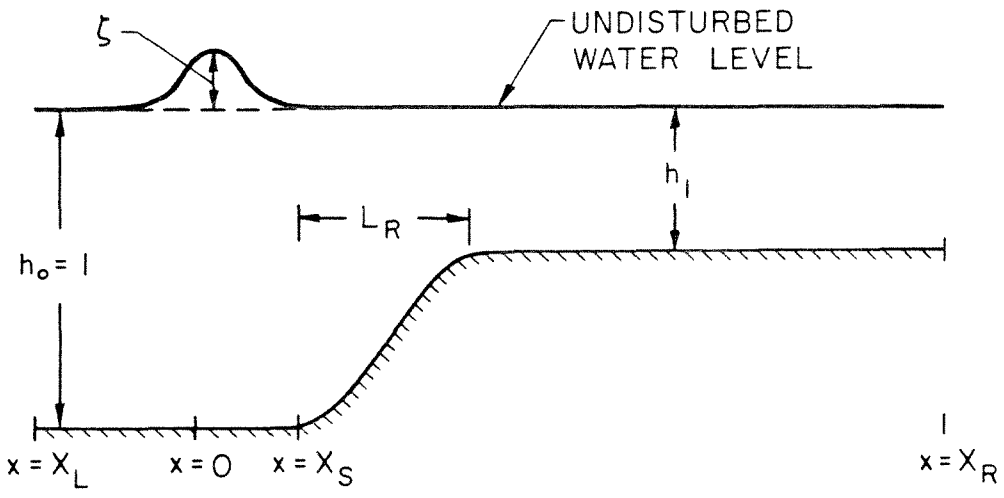

Figure 4.1 Definition sketch for the bottom topography.

describes a solitary wave moving onto a shelf, has been derived by Johnson (1972) and separately by Kakutani (1971) in a similar form. This equation predicts that a solitary wave† moving into a region of decreased depth will break up into a finite number of solitons plus (possibly) an oscillatory tail. This conclusion is in agreement with the experimental and numerical work of Madsen and Mei (1969). The depth of the shelf relative to the initial depth influences the number of solitons which emerge from a solitary wave initial input. For some special depths (eigendepths), only solitons and no oscillatory tail will be produced. These eigendepths h_e are given by:

$$h_e = h_0[\tfrac{1}{2}N(N+1)]^{-\frac{4}{9}} \tag{4.1}$$

where N gives the number of solitons on the shelf. In particular, since we have taken h_0 to be unity, the eigendepth for two solitons is $h_e = 0.614$ and for three solitons is $h_e=0.451$. These depths correspond to two values of h_1 in our numerical experiments.

For the more general case where the shelf depth h_1 is not an eigendepth, Johnson shows (for initial solitary wave input) that N solitons (of nonzero amplitude) will emerge where N is the largest integer which satisfies $N \leq p$ and p is defined as:

$$p = -\frac{1}{2} + \frac{1}{2}\left\{1 + 8[h_1]^{-\frac{9}{4}}\right\}^{\frac{1}{2}} \tag{4.2}$$

Furthermore, the amplitude A_n of the n^{th} soliton on the shelf relative to the initial solitary wave amplitude A_0 is:

$$\frac{A_n}{A_0} = h_1^{-\frac{1}{4}}\left\{\frac{2(p-n)^2}{p(p+1)}\right\} \tag{4.3}$$

where n=1,2,...,N. Tappert and Zabusky (1971) also derived these relationships

† The solitary wave discussed in reference to the KdV and VKdV equations is defined by Equation 2.60 in Section 2.6.

by a different method. Johnson has found good agreement with these predictions through a numerical finite-difference solution to the VKdV equation. For a shelf depth of 0.5 (4.2) predicts the production of three solitons. Equation 4.3 gives the relative amplitudes of these solitons as 1.71, 0.66, and 0.11 for the first, second and third solitons respectively.

We are interested in comparing the results from our governing equation (2.62) for an initial input from (3.9) with the theoretical and numerical results discussed above. Figures 4.2 through 4.4 show the results of our 1HD numerical experiments taking h_1 to be 0.614, 0.5, and 0.451 respectively. Our formulation of the 1HD ramp problem yields results similar to those described for the VKdV equation by Johnson(1972) and also to those of Madsen and Mei(1969). As the wave approaches the ramp, the front side steepens and the peak amplitude (measured from the still water level) grows. Once the wave is on the shelf, two or three solitons are formed and these waves gradually separate due to differences in their velocity (since the velocity is a function of amplitude). Examination of the computed solution indicates that two solitons are formed for $h_1 = 0.614$, while three solitons emerge for $h_1 = 0.5$ and 0.415, in agreement with the prediction of (4.2). The low-amplitude reflected wave can be seen travelling toward the left in Figs. 4.2 through 4.4 at times t=20 and t=40. At time t=60 and t=80 this reflected wave interacts with the left boundary. Since our boundary conditions are not adequate to allow the wave to simply pass out of the computational region, there is some reflection off the left boundary. However, the wave reflected by the left boundary is sufficiently far away from the shelf solitons so that it does not affect this region of primary interest.

Table 4.1 shows some specific results for the 1HD cases. All the results for the shelf solitons have been normalized by the initial amplitude of the solitary wave. The figures for soliton heights and excess mass on shelf are taken from

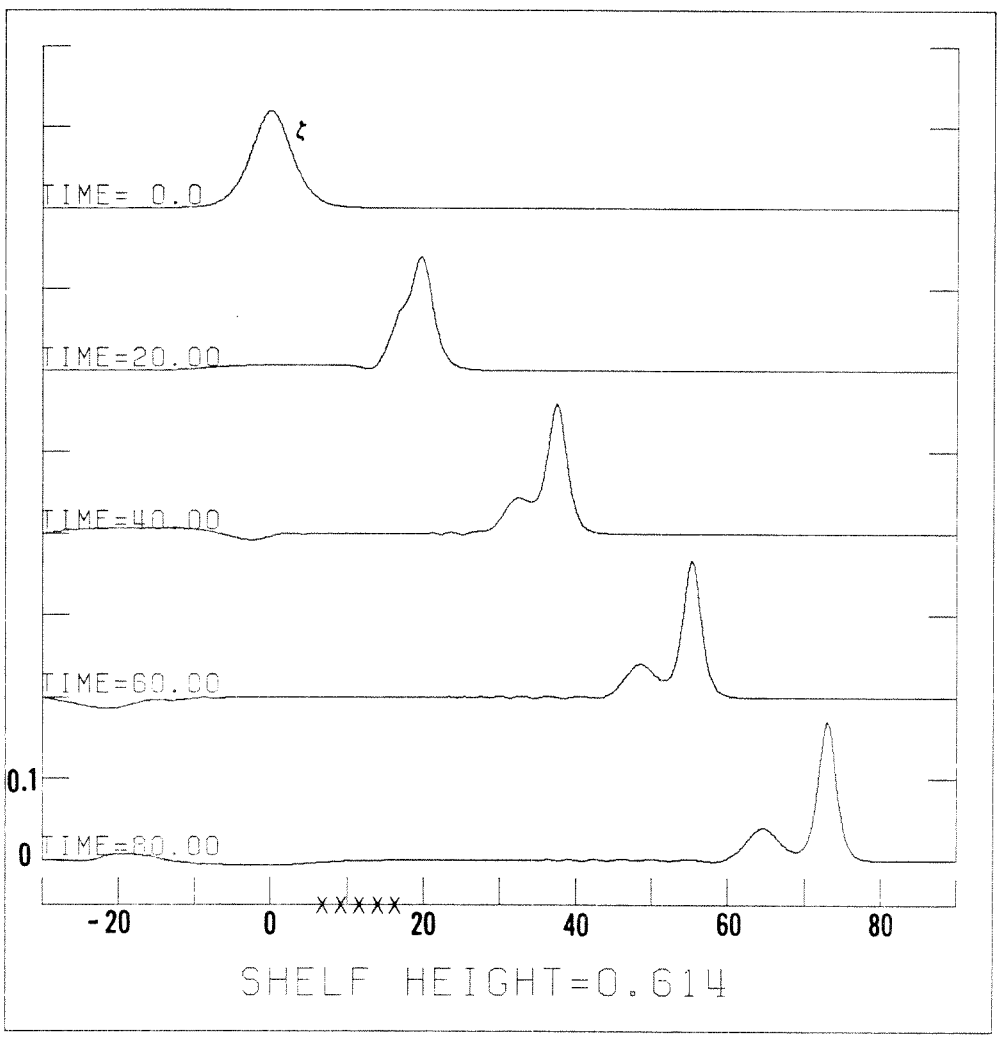

Figure 4.2 Computed surface heights for various times. Initial solitary wave amplitude is 0.12, depth on the shelf is 0.614. The X's on the x-axis denote the position of the ramp.

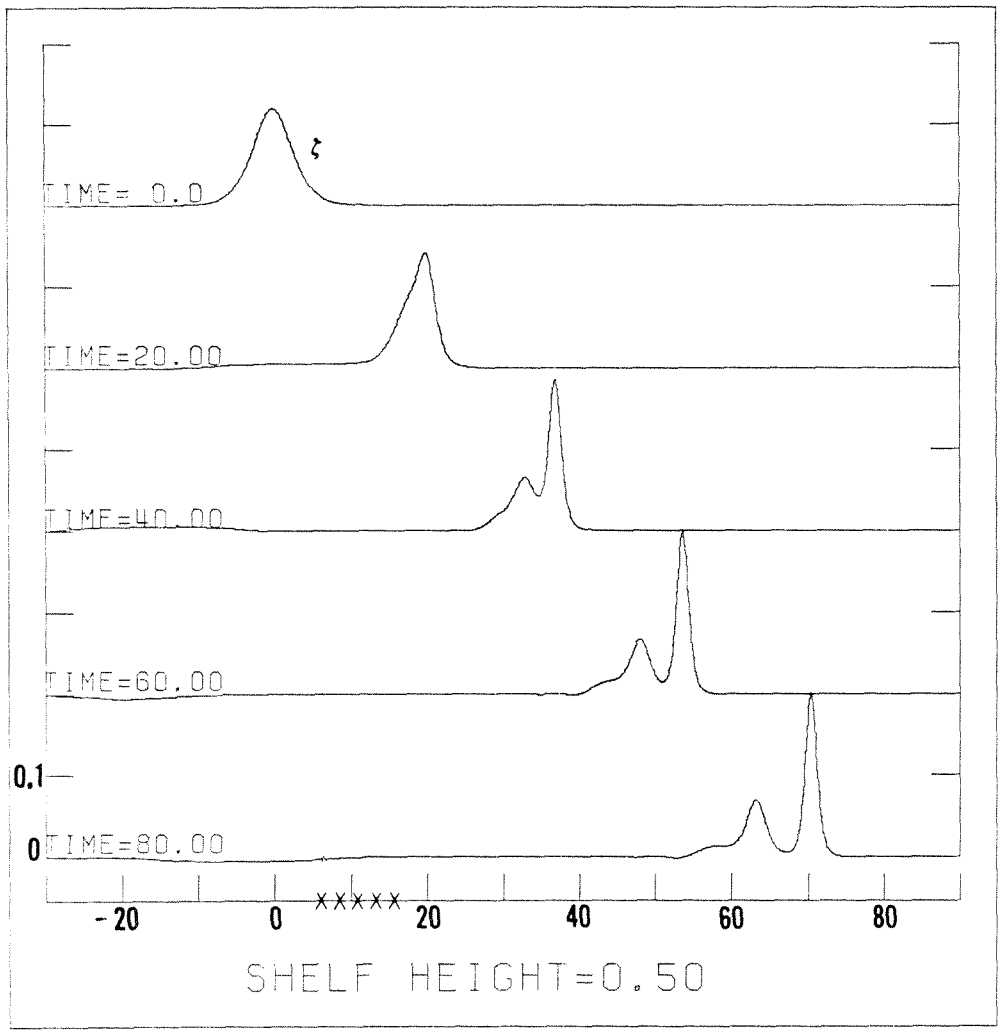

Figure 4.3 Computed surface heights for various times. Initial solitary wave amplitude is 0.12, depth on the shelf is 0.5. The X's on the x-axis denote the position of the ramp.

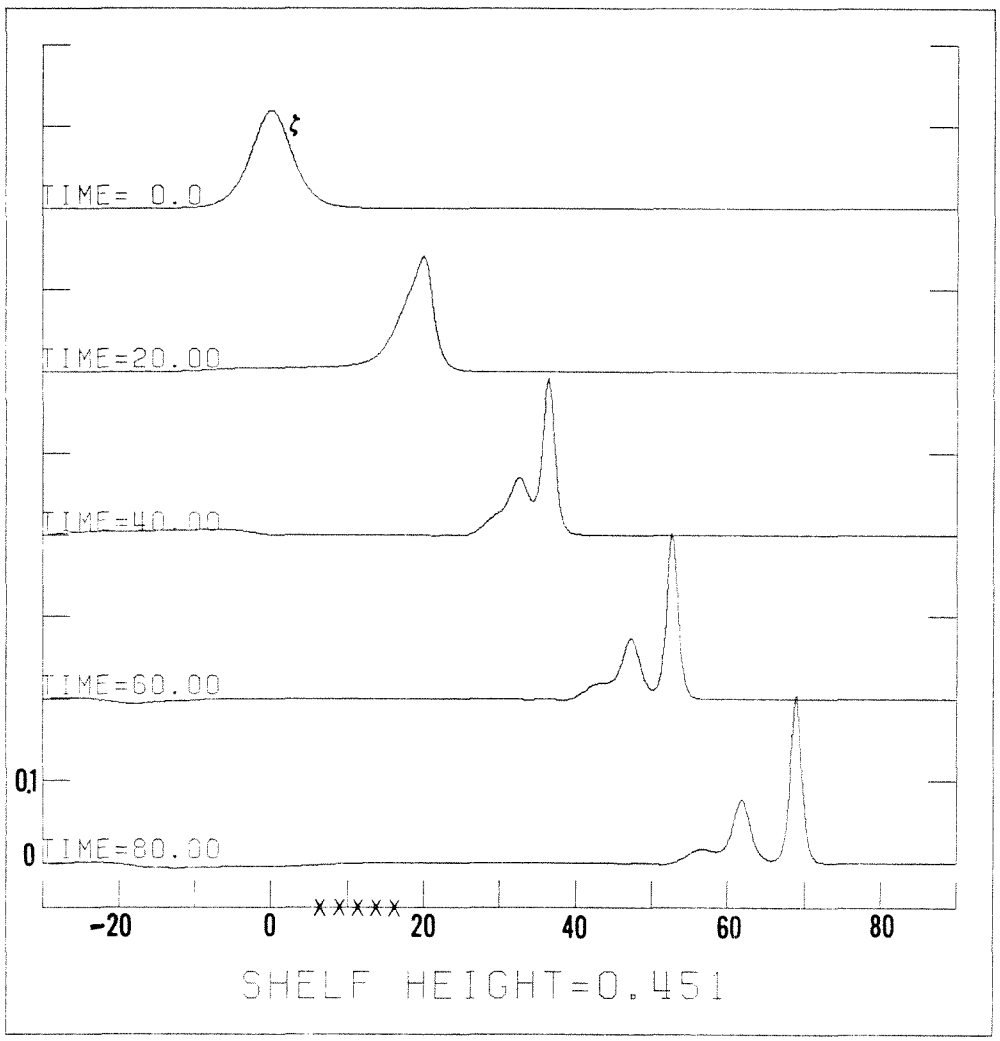

Figure 4.4 Computed surface heights for various times. Initial solitary wave amplitude is 0.12, depth on the shelf is 0.451. The X's on the x-axis denote the position of the ramp.

TABLE 4.1

Comparison of Results for 1HD Cases

		Shelf Depth, h_1	Grid Size	Shelf Soliton Heights†			% Excess Mass on Shelf
				first	second	third	
Present results		0.451	0.2	1.71	0.64	0.14	82%
Johnson (1972)	numerical	0.451	*	1.8	0.8	0.2	100%
	theoretical		-	1.83	0.81	0.20	
Present results		0.5	0.2	1.62	0.52	‡	84%
			0.1	1.68	0.58	0.1	
			0.05	1.69	0.59	0.12	
Johnson (1972)	numerical	0.5	*	1.73	0.65	0.10	100%
	theoretical		-	1.71	0.66	0.11	
Madsen and Mei (1969)	numerical	0.5	vari-able	1.66	0.75	0.2	85%
	experimental		-	1.2	0.4	#	
Present results		0.614	0.2	1.42	0.33	none	89%
Johnson (1972)	numerical	0.614	*	1.5	0.4	none	100%
	theoretical		-	1.51	0.38		

† Soliton heights are normalized by the initial solitary wave height.
* Johnson uses a different coordinate system; stepsizes may not be comparable.
‡ At this mesh size, the third soliton was not resolved.
# A third soliton was not apparent from the experimental results.

results after the wave front has travelled the equivalent of approximately 80 units, where distances are normalized by the relavant h_0 for each case. From this table we can see that our results are in fairly good agreement with those of Johnson as well as Madsen and Mei. However, our results for all three depths are somewhat lower than the corresponding results given by Johnson. This is expected, since our formulation includes reflection, an effect which is discarded in the KdV and VKdV derivations. In fact, our results indicate that up to 18% of the excess mass may be reflected by the gradual slopes selected for our numerical experiments, and this is in agreement with Madsen and Mei's figure of 15% reflection for depth 0.5. Due to this reflection, it is reasonable to expect smaller soliton amplitudes on the shelf and, in accordance with this hypothesis, we find that the normalized differences in amplitude between our results and Johnson's become larger as the reflected mass becomes larger. We must be conservative about these conclusions, however, since results for a range of stepsizes for shelf depth of 0.5 indicate that larger stepsizes also yield lower results.

Our results for the first soliton amplitude and excess mass on the shelf agree quite well with those shown in Table 4.1 from Madsen and Mei's numerical integration of a variant of the Boussinesq equations. The second and third soliton heights, however, show some disagreement. Our results for the second and third soliton amplitudes are lower than the corresponding amplitudes presented by Johnson. Madsen and Mei, however, report computed second and third soliton amplitudes which are *larger* than Johnson's corresponding results. As mentioned in the previous paragraph, it is physically reasonable that the soliton amplitudes would be *lower* (than amplitudes computed by a model like Johnson's which neglects wave reflection) since the Boussinesq formulation which we use includes reflection. Madsen and Mei, however, also rely on the

Boussinesq equations (i.e., reflection is included) and yet the amplitudes which they report for the second and third solitons are actually larger than those given by Johnson's theoretical predictions and numerical calculations as well as by our computations. We attribute the discrepancy between our result and that of Madsen and Mei to their extensive replacement of the original terms of the Boussinesq equations by other terms within the same order of approximation. Their error terms, therefore, may be quite different from ours and over the course of the numerical integration, these differences may accumulate. Note that on the shelf, where α has increased to approximately 0.4, the size of the error terms relative to the dominant terms can be as large as $O(\alpha^2)$ or about 16%. Such an error probably accounts for the differences between our results and those of Madsen and Mei.

Finally, in reference to Table 4.1, note that the theoretical and numerical results presented are in qualitative agreement with the experimental results regarding the shelf soliton heights. Madsen and Mei attribute the lack of quantitative agreement to the use of a rather crude wave generation technique and to the effects of viscous damping.

4.2 Results for Propagation in Two Horizontal Dimemsion: Variable Depth

Using the results from Section 4.1 as a guide, we have identified a series of cases with 2HD variations in bottom topography. These model problems are extensions of the 1HD ramp cases. Here we consider waves propagating in a long channel containing a submerged ramp which connects two constant depth areas. This is similar to the 1HD problem except that now the ramp may vary across the channel. The cross-channel variable is y while the x-axis corresponds to the longitudinal axis of the channel. The y-origin lies on the center longitudinal line of the channel; as before, the x-origin is taken directly

under the wave peak at t=0. Four test topographies are selected: two of which have convex curvature in relation to the initial planar solitary wave, while the other two are concave with respect to the initial wave. All of these cases have the y=0 axis as a line of symmetry. Figures 4.5a through 4.5d show the four curving ramp configurations chosen for study. For convenience in dealing with this group of cases we will refer to these topographies as in the following table:

Table 4.2

Key to 2HD Bottom Topographies

Case	Acronym	Figure Number
Concave, Narrow	(IN)	4.5a
Concave, Wide	(IW)	4.5b
Convex,Narrow	(ON)	4.5c
Convex,Wide	(OW)	4.5d

(I and O above stand for curving *in* and curving *out*.) The front edges of these curving ramp sections all lie at the point correspnding to $x=X_S$ in Figure 4.1. As in the previous section, h_0 is taken to be unity and the ramp length is 10. The channel length for our computation is taken to be 120. The specific values defining the width of the cross-channel features for the separate cases may be read from Figure 4.5. Ramp profiles are obtained by curving a straight ramp of slope 1:20 along the line f(y) defined by

$$f(y) = 10\cos^2\left[\frac{2\pi y}{y_c}\right] \qquad y \leq y_c \tag{4.4}$$

y_c is the width of the curving section of the ramp and it may be read from Figures 4.5a through d. The ramp is taken to be straight in the cross-channel direction for $y \geq y_c$. The shelf depth has been taken to be 0.5 and the channel width is 32. The spacing in x,y and t is 0.4. The initial conditions consist of a planar solitary wave defined by Eq. 3.9 with α = 0.12. For comparison, we also solve the degenerate case of a straight ramp for the same initial conditions. We will refer to this case as (S). Since these cases are symmetric about the

Figure 4.5a,b,c,d The four curving ramp bottom topographies. The front of the ramp is placed in the channel at position $x=X_s$ shown in Fig. 4.1. The cases are denoted:

(a) Narrow concave. (IN)

(b) Wide concave. (IW)

(c) Narrow convex. (ON)

(d) Wide convex. (OW)

CASE (IN)

NARROW CONCAVE RAMP

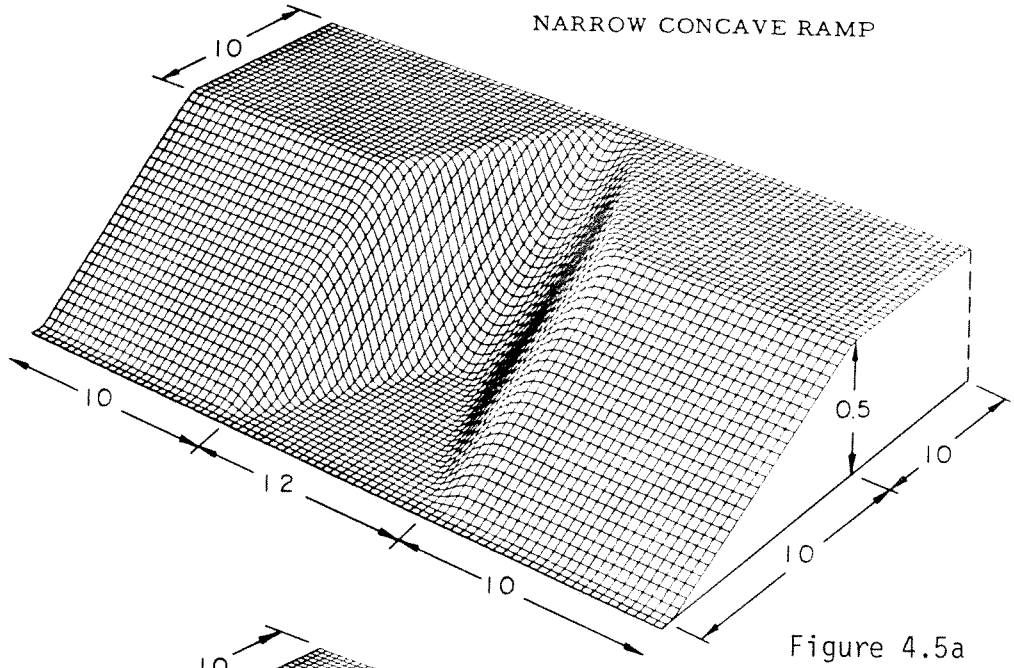

Figure 4.5a

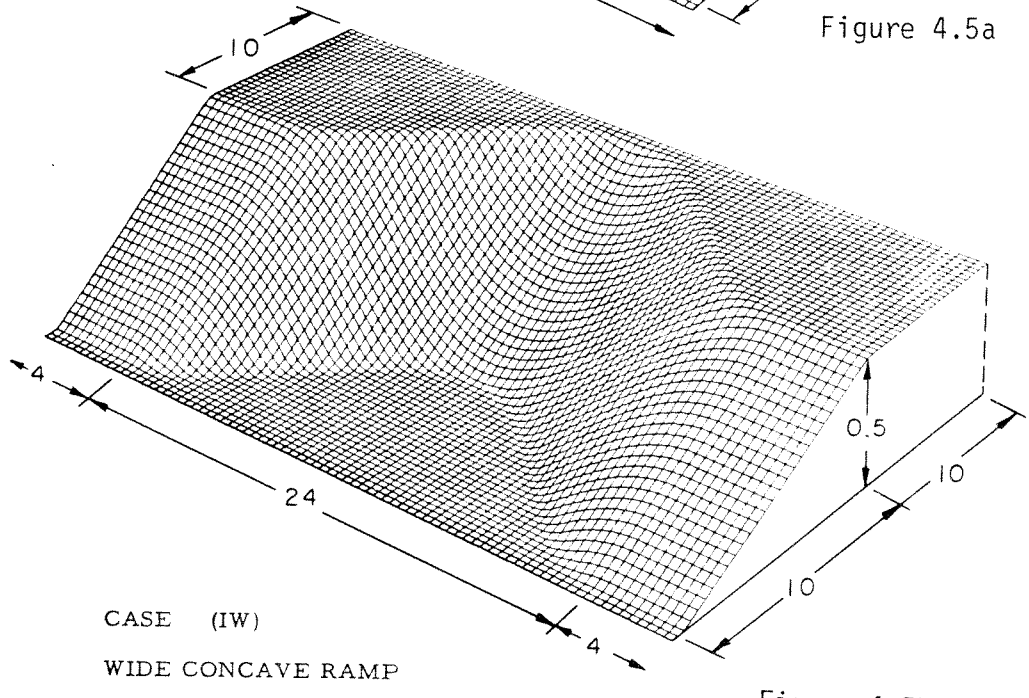

CASE (IW)

WIDE CONCAVE RAMP

Figure 4.5b

CASE (ON)

NARROW CONVEX RAMP

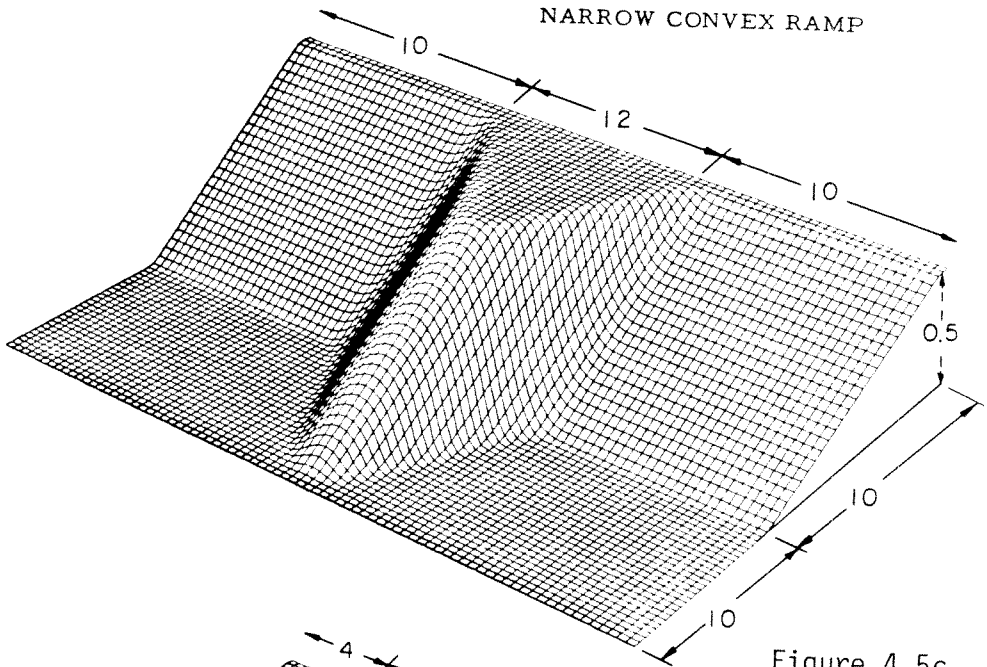

Figure 4.5c

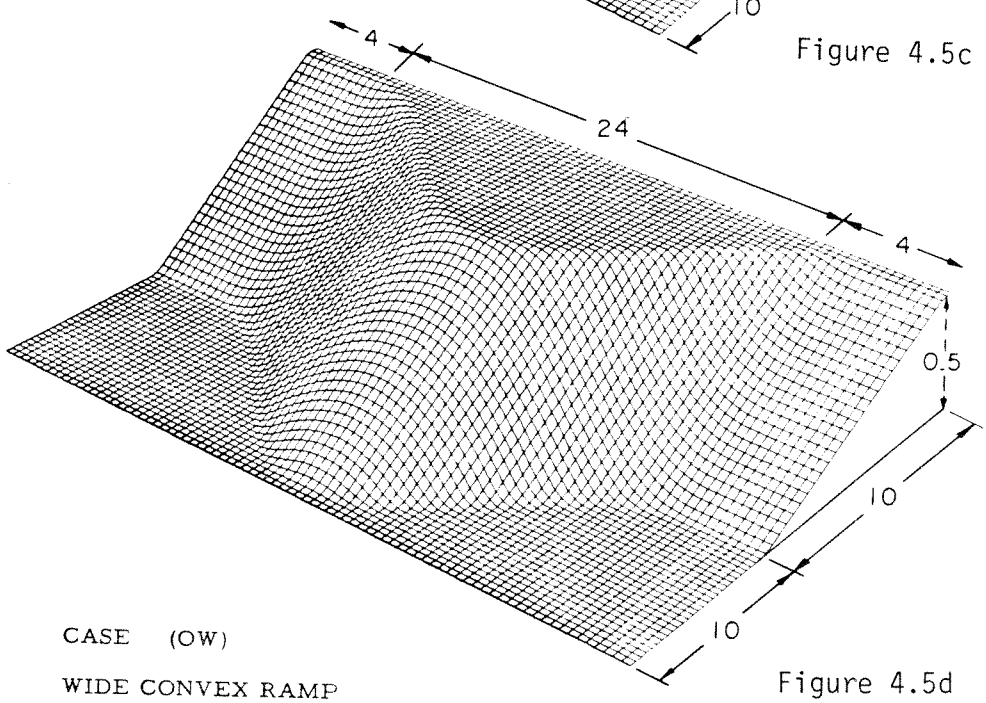

CASE (OW)

WIDE CONVEX RAMP

Figure 4.5d

centerline, we need only to compute for half the width of the channel.

Figures 4.6a through 4.6d present three-dimensional perspective views of the waveforms at selected times as computed by the 2HD program using topographies (IN), (IW), (ON), and (OW) respectively. It is clear from inspection of these figures that the waveform has been strongly affected by the passage over the curving ramp. We can immediately separate the concave from convex topographies: In the concave ramp cases, (IN) and (IW), the primary wave crest is amplified along the wall, while for the convex cases, (ON) and (OW), the peak is amplified along the centerline. This effect can be explained by recalling that a line of wave crests obliquely approaching a straight ramp will turn in their propagation in such a way as to make the angle between the crestline and the depth contours smaller. Figure 4.7 presents a sketch of this phenomena for a concave topography. The ray lines -- lines which are perpendicular to the crests -- turn toward shallower water as the wave passes over the curved ramp. In general then, any outcropping will tend to focus the wave amplitudes along the central line of the protrusion and this phenomena is clearly present in our computed solutions.

Figures 4.6a through 4.6d also show that a second and in some cases a third soliton forms behind the main wave. In fact, as we would expect, many of the features present in the 1HD solutions are also seen in the 2HD cases. However, the features vary dramatically across the channel. In order to show the cross-channel differences more quantitatively, we present Figures 4.8a through 4.8d. These figures display the surface height along cuts made longitudinally at the centerline and the wall. The concave cases (IN) and (IW) show the similar features (at the final timestep) of strong, well-defined first and second soliton peaks along the wall, while the centerline cuts show smaller peak amplitudes and the second soliton definition is poor, though discernible. The

Figure 4.6a,b,c,d Three-dimensional perspective views of the computed surface height at verious times for the cases : (a) narrow, concave ramp, (b) wide, concave ramp, (c) narrow, convex ramp and (d) wide, convex ramp.

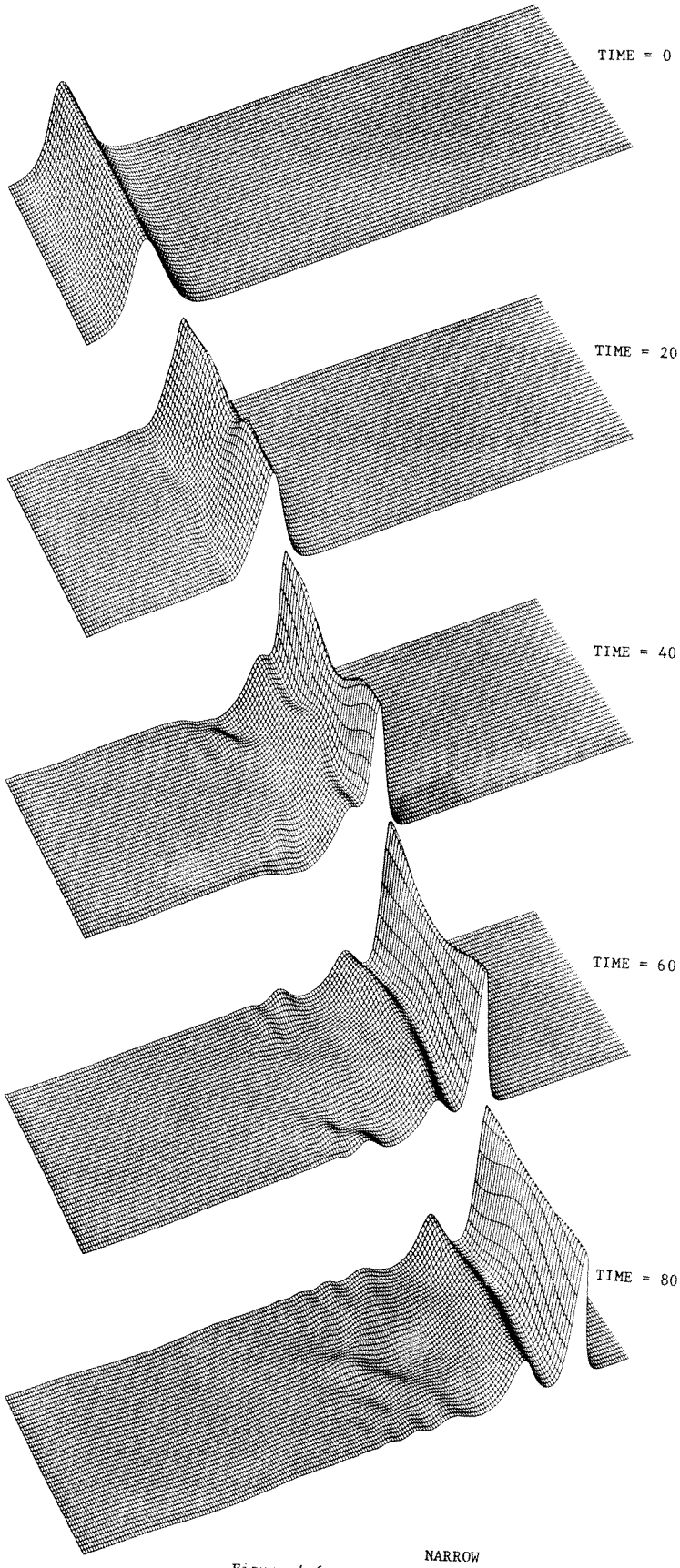

Figure 4.6a NARROW CONCAVE RAMP

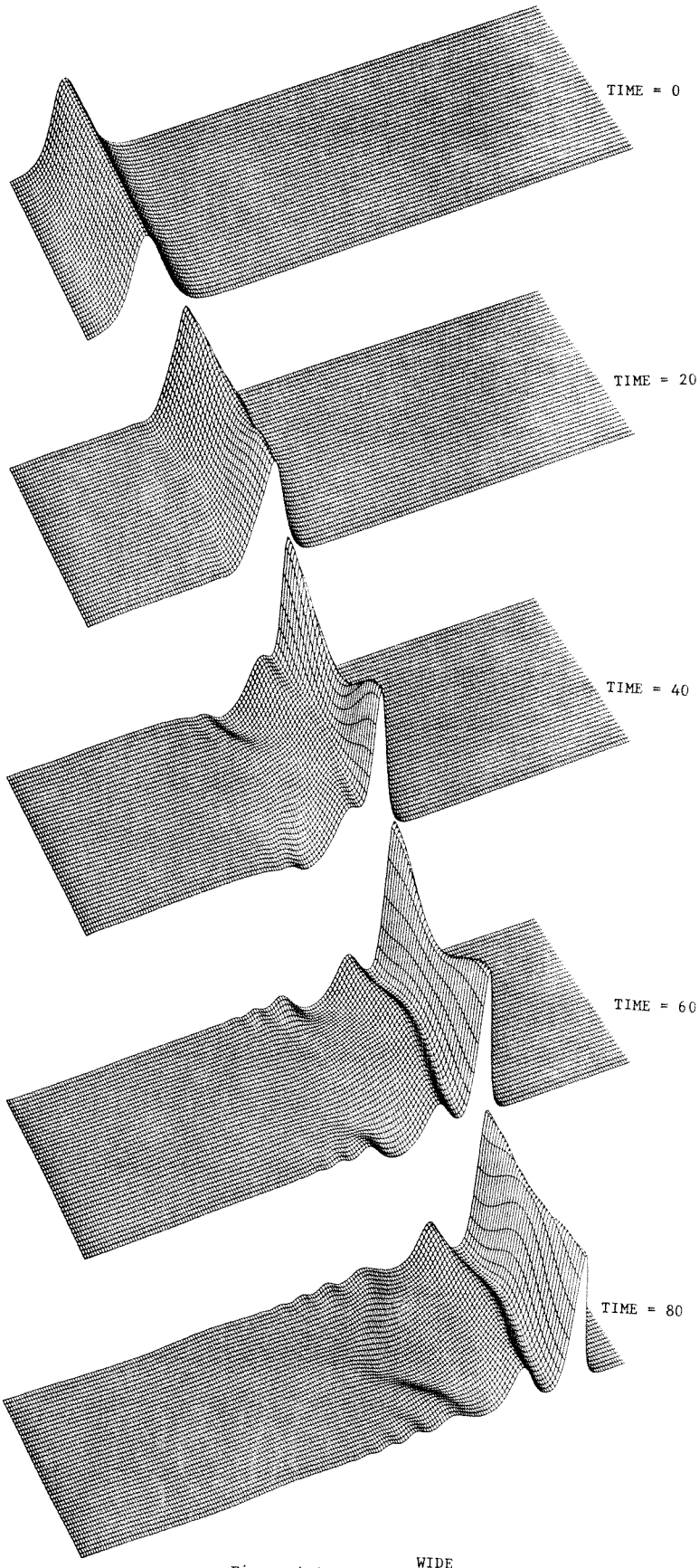

Figure 4.6b WIDE CONCAVE RAMP

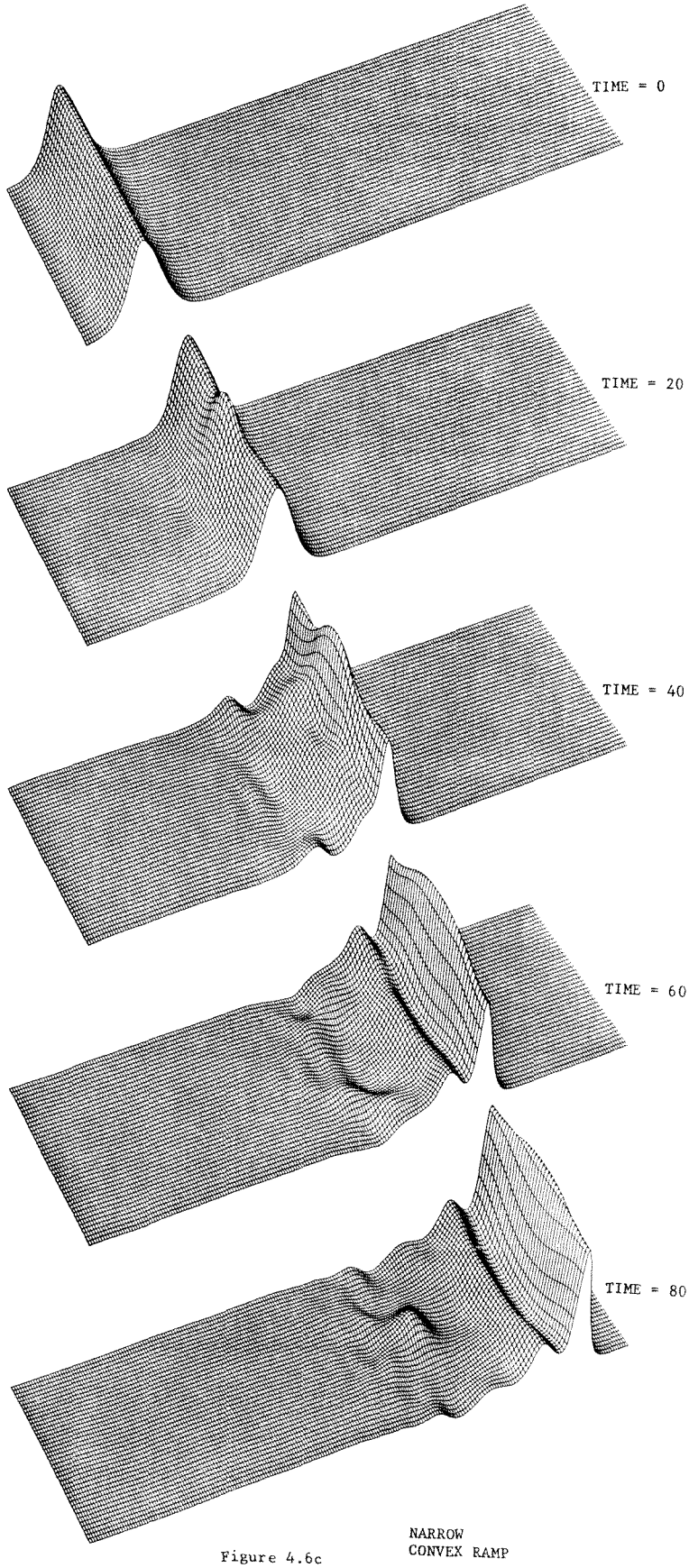

Figure 4.6c

NARROW
CONVEX RAMP

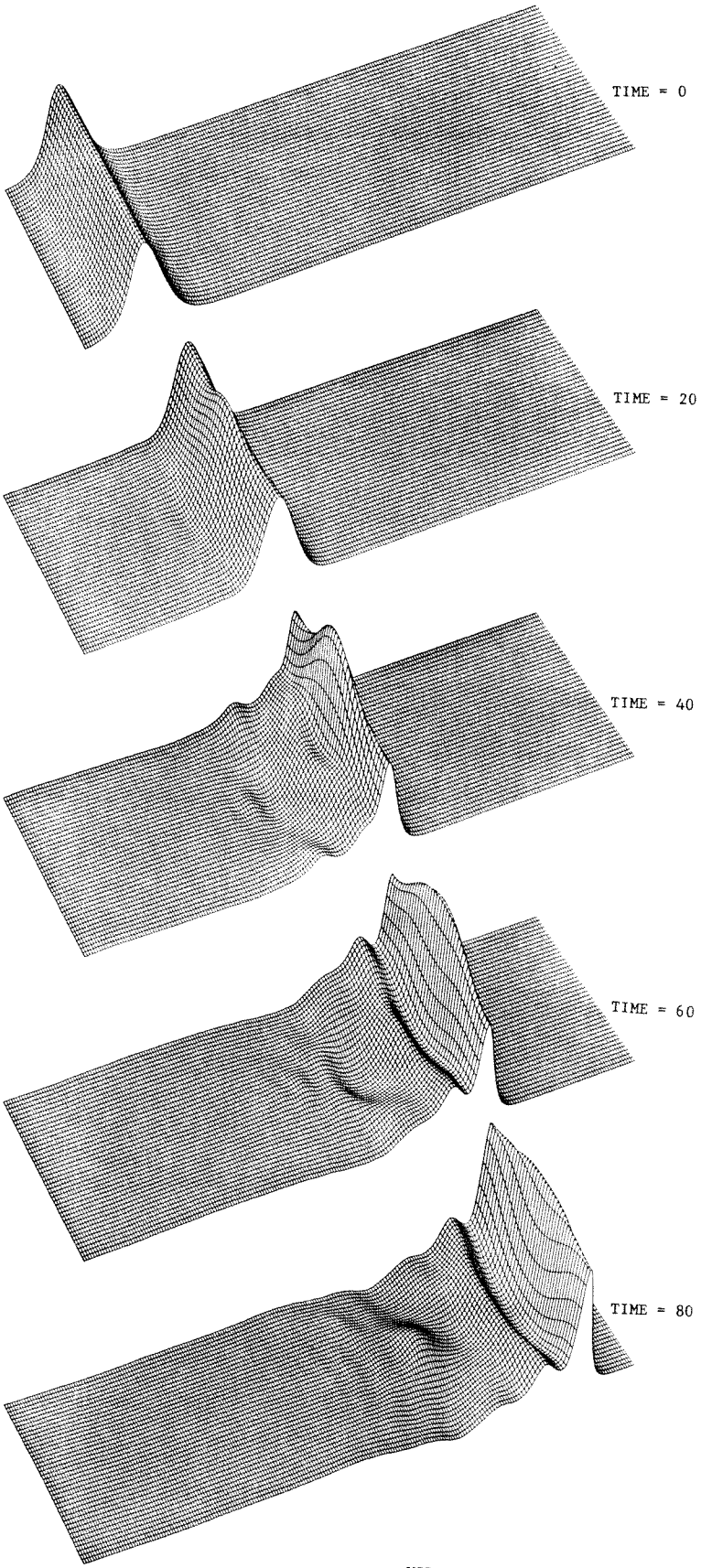

Figure 4.6d WIDE CONVEX RAMP

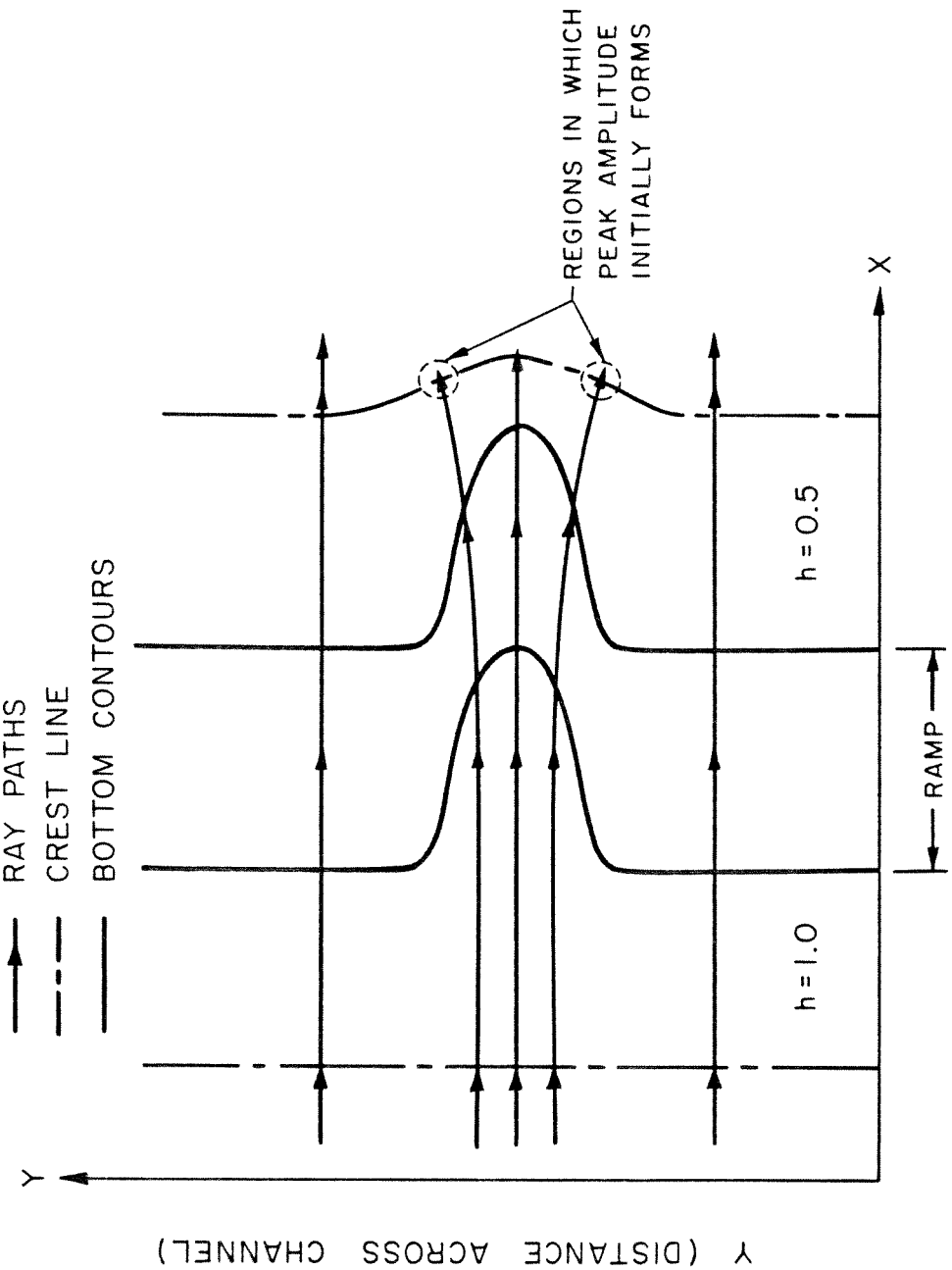

Figure 4.7 Sketch showing the bending of ray lines as a straight crest approaches a concave ramp.

Figure 4.8a,b,c,d Profiles of the computed surface height at the centerline and the wall for the (a) narrow, concave ramp, (b) wide, concave ramp, (c) narrow, convex ramp and (d) wide, convex ramp.

For the two concave cases:

- Along the centerline, the ramp begins at 16 and ends at 26.
- Along the wall, the ramp begins at 6 and ends at 16.

For the two convex cases:

- Along the centerline, the ramp begins at 6 and ends at 16.
- Along the wall, the ramp begins at 16 and ends at 26.

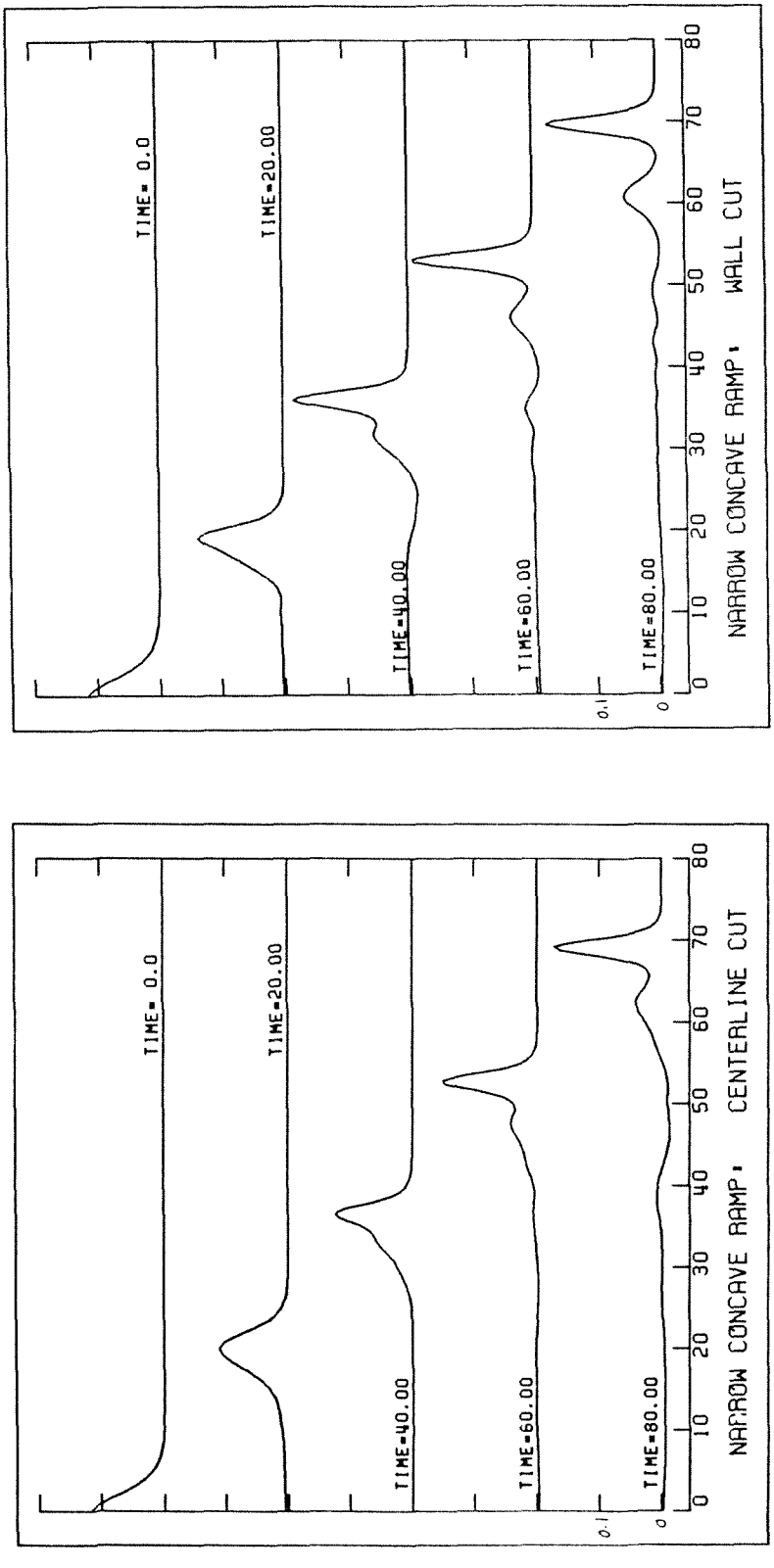
TIME= 0.0
TIME=20.00
TIME=40.00
TIME=60.00
TIME=80.00
NARROW CONCAVE RAMP, CENTERLINE CUT
TIME= 0.0
TIME=20.00
TIME=40.00
TIME=60.00
TIME=80.00
NARROW CONCAVE RAMP, WALL CUT

Figure 4.8a

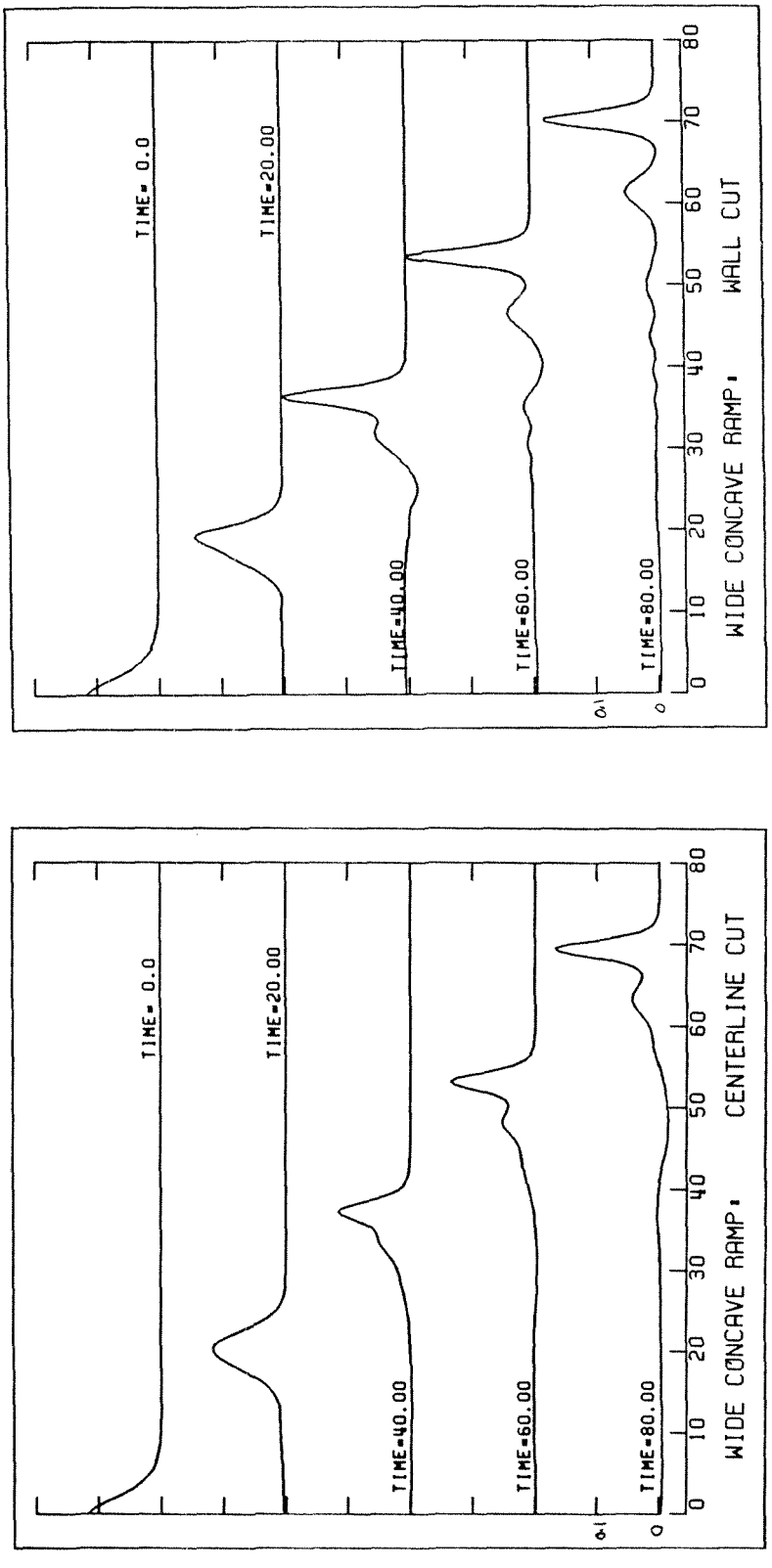
TIME= 0.0
TIME=20.00
TIME=40.00
TIME=60.00
TIME=80.00
WIDE CONCAVE RAMP: CENTERLINE CUT
WIDE CONCAVE RAMP: WALL CUT
0
10
20
30
40
50
60
70
80
-1
0

Figure 4.8b

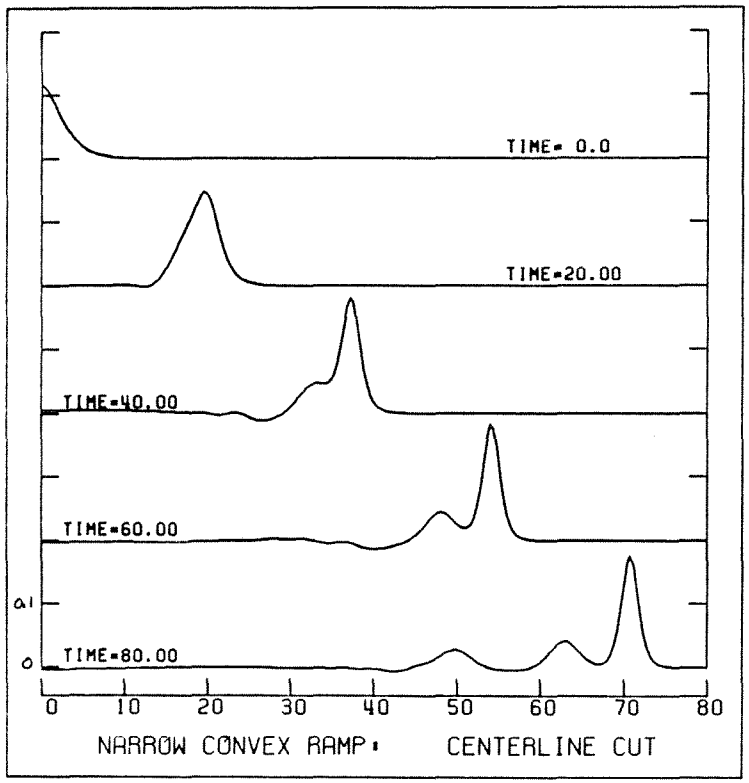
TIME= 0.0
TIME=20.00
TIME=40.00
TIME=60.00
TIME=80.00
0.1
0
0 10 20 30 40 50 60 70 80
NARROW CONVEX RAMP: CENTERLINE CUT

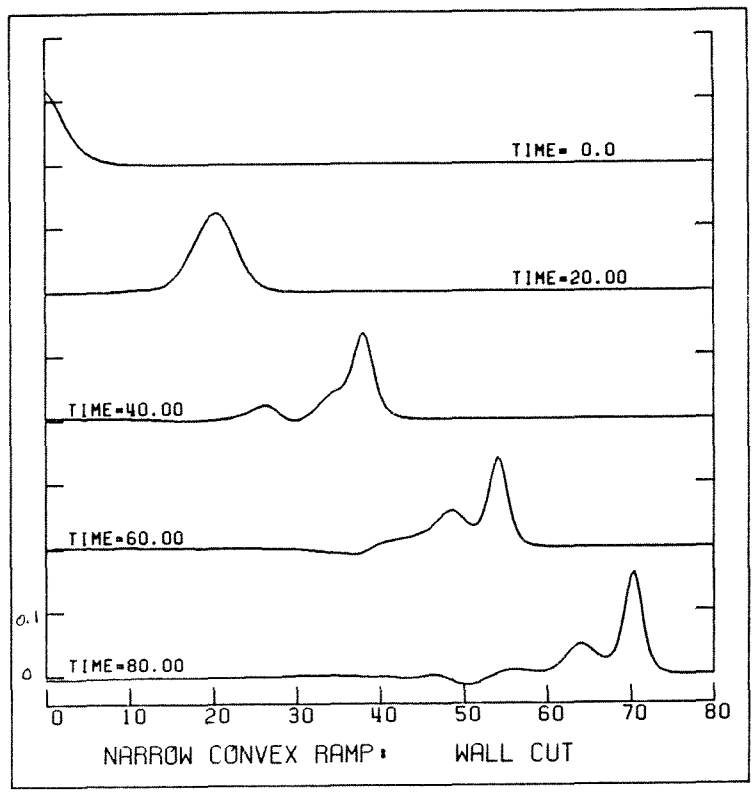
TIME= 0.0
TIME=20.00
TIME=40.00
TIME=60.00
TIME=80.00
0.1
0
0 10 20 30 40 50 60 70 80
NARROW CONVEX RAMP: WALL CUT

Figure 4.8c

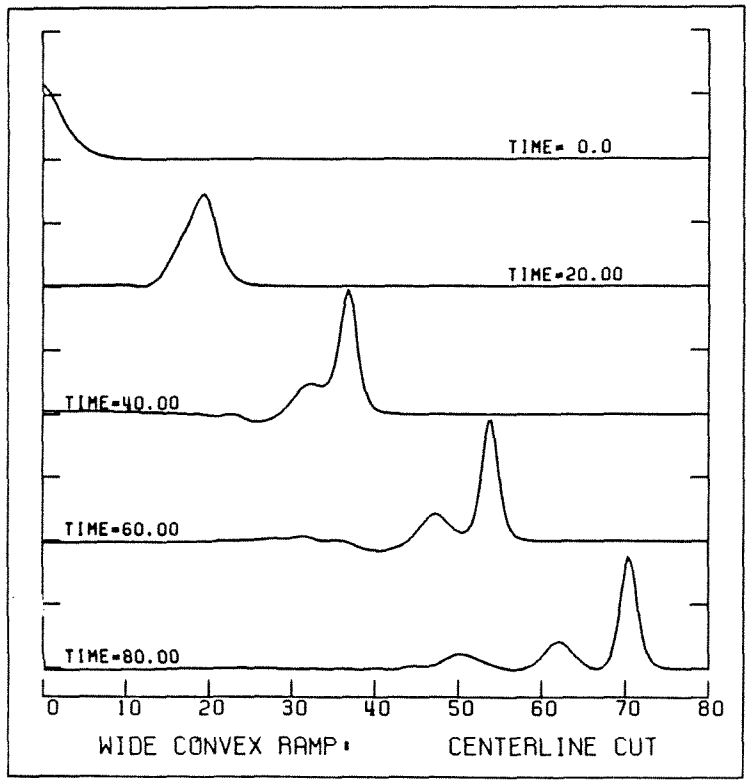
TIME= 0.0
TIME=20.00
TIME=40.00
TIME=60.00
TIME=80.00
0 10 20 30 40 50 60 70 80
WIDE CONVEX RAMP: CENTERLINE CUT

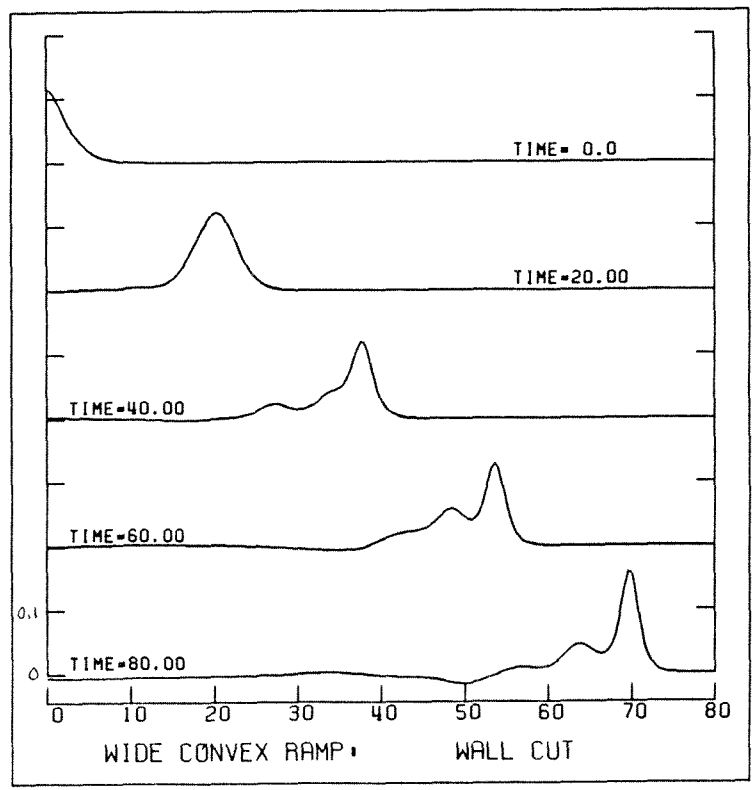
TIME= 0.0
TIME=20.00
TIME=40.00
TIME=60.00
0.1
0
TIME=80.00
0 10 20 30 40 50 60 70 80
WIDE CONVEX RAMP: WALL CUT

Figure 4.8d

undular tail apparent at time=80 may result from dispersion of the large negative trough which forms at the back of the wave at time=40. More investigation is necessary to determine if this tail is a real effect or simply a result of the stepsize used. (See the discussion of numerical dispersion due to stepsize in Chapter 3.) Along the centerline cuts for the (ON) and (OW) cases, the solitons are seen to quickly become separated and well defined. Trailing behind the second soliton at time=80, both cases exhibit another low wide peak which may be a third soliton. Recall that the KdV theory predicts three solitons (and an oscillatory tail) for the depths chosen for these experiments. However, even at a stepsize which is half of what is used here the 1HD program was unable to resolve the third soliton. In addition, the amplitude is too large for a predicted third soliton and its position is too far behind the second crest. Returning to the plots 4.6c and 4.6d it appears that the third hump which appears is the result of a cross channel oscillatory mode with node points at the one-quarter and three quarter lines of the channel. This oscillation appears to be gradually separating from the primary and secondary wave crests. Inspection of the wall cuts for cases (ON) and (OW) show a gradual transition of waveforms with the final timestep displaying a still unseparated second soliton.

Figures 4.9a through 4.9d give the peak soliton amplitude as a function of time for 3 longitudinal cuts down the channel: wall, centerline and quarterline. These graphs again make clear that the centerline of the convex cases and the wall line of the concave cases are the primary regions of focussing during the wave's progression over the ramp. What these plots also indicate is that an initial depletion occurs in the region away from the focussing. Loosely speaking, the quarterline amplitude remains between the two extrema located at the center and wall lines, with the quarterline position functioning as a kind of node for oscillation across the channel width. The curves for the wall and centerline

Figure 4.9a,b,c,d The peak amplitude along three longitudinal lines as a function of time for the cases: (a) narrow, concave ramp, (b) wide, concave ramp, (c) narrow, convex ramp and (d) wide, convex ramp.

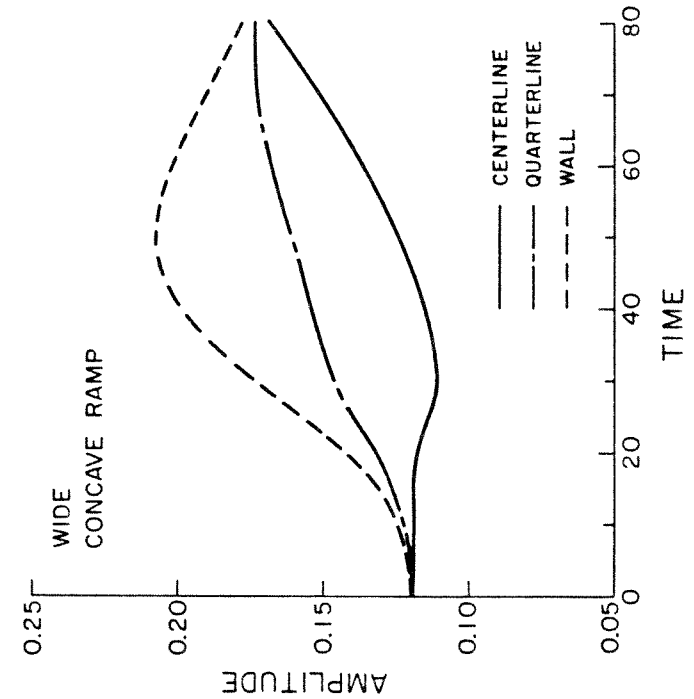

Figure 4.9b

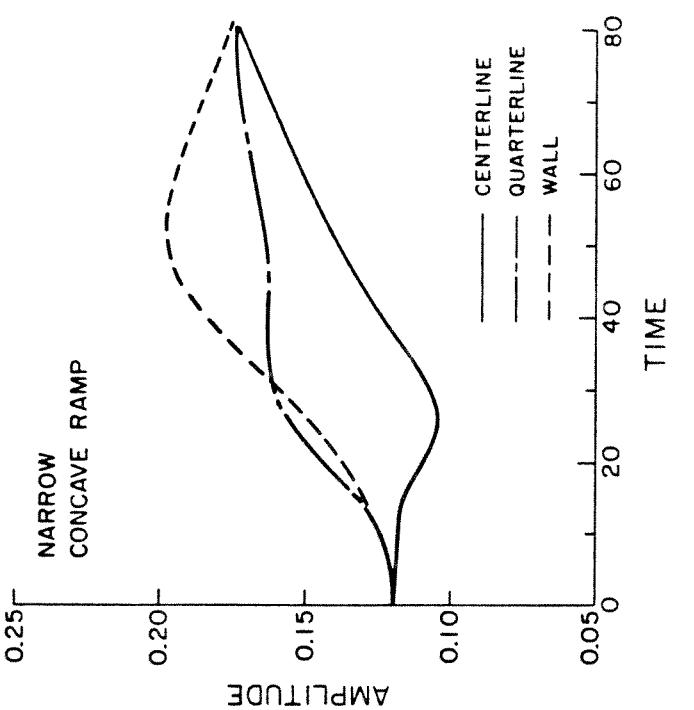

Figure 4.9a

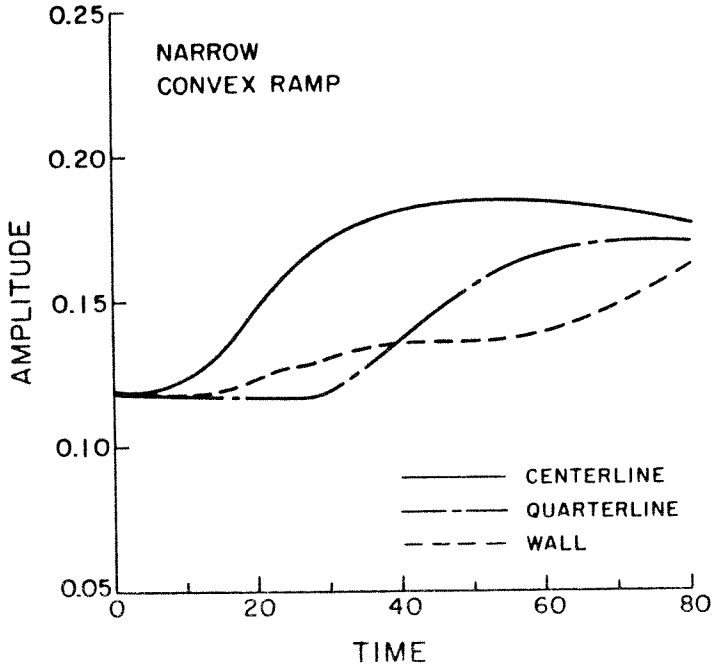

Figure 4.9c

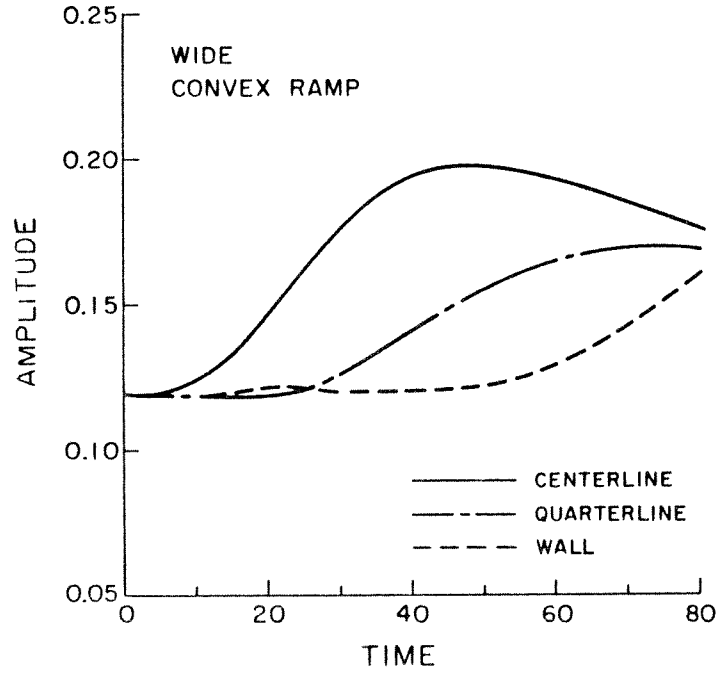

Figure 4.9d

amplitudes move apart rapidly as the wave passes over the ramp, then approach each other again and appear to cross near the end of the computation. Preliminary computation for larger stepsizes and longer times showed that the amplitude curves actually do cross at time $\approx$ 80. Computation was terminated before it was apparent if another crossing would take place. Additional computation would be necessary to determine if a long-time ringing has been initiated, or if the wall effects are strong enough to quickly return the wave to a planar form. (These computations must be done cautiously, since peak amplitude degradation due to insufficient mesh refinement may mask long-time ringing.)

Figures 4.10a through 4.10d are contour plots of the surface height at various times for all four cases. The first few plots have been truncated in order to fit the entire sequence on a single page. In these plots we can see that the line of crests is bent as the wave passes over the submerged curved ramps. This happens because part of the wave is in deeper water and, since the wave speed may be estimated as the square root of the depth,† the part of wave in deeper water travels faster than the part which is passing over the decreasing depth region. If we examine the plots for time=20, it appears that the contour lines are pinched at the centerline in the convex ramp cases and at the walls in the concave cases. This pinching also occurs because the effects of decreasing depth are not felt at the same time across the channel. As the wave moves into shallower water, the front face of the wave steepens and the peak amplitude grows. These changes are reflected by an increase in the order parameter α. We can see from the figures in section 2.6 which show the form of solitary waves for different α that as α increases the wave length decreases. The α for the primary soliton on the shelf is roughly three times larger than that for the wave in the

† The actual speed c of the shallow water wave is, of course, $c = \sqrt{gh}$ however, we have normalized our coordinates so that c is unity when the depth is 1.

Figure 4.10a,b,c,d Contour plots of the surface height at various times for the cases: (a) narrow, concave ramp, (b) wide, concave ramp, (c) narrow, convex ramp and (d) wide, convex ramp. The interval between contours is 0.025. Dotted lines denote regions of negative surface height. The initial three plots on each page have been truncated to eliminate large areas where no contours are seen (flat regions).

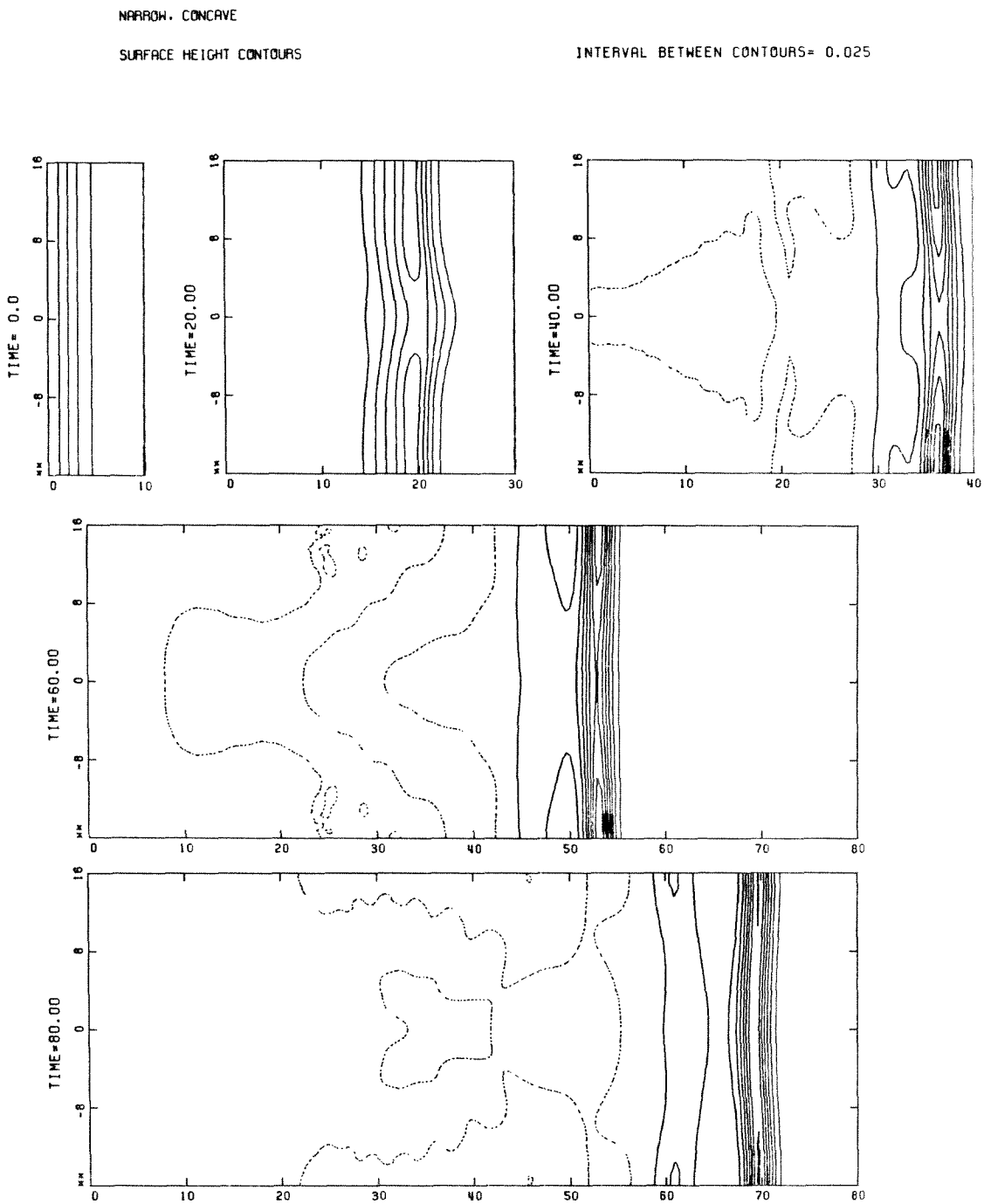
NARROW. CONCAVE
SURFACE HEIGHT CONTOURS
INTERVAL BETWEEN CONTOURS= 0.025
TIME= 0.0
TIME=20.00
TIME=40.00
TIME=60.00
TIME=80.00
MM
16
8
0
-8
0
10
20
30
40
50
60
70
80

Figure 4.10a

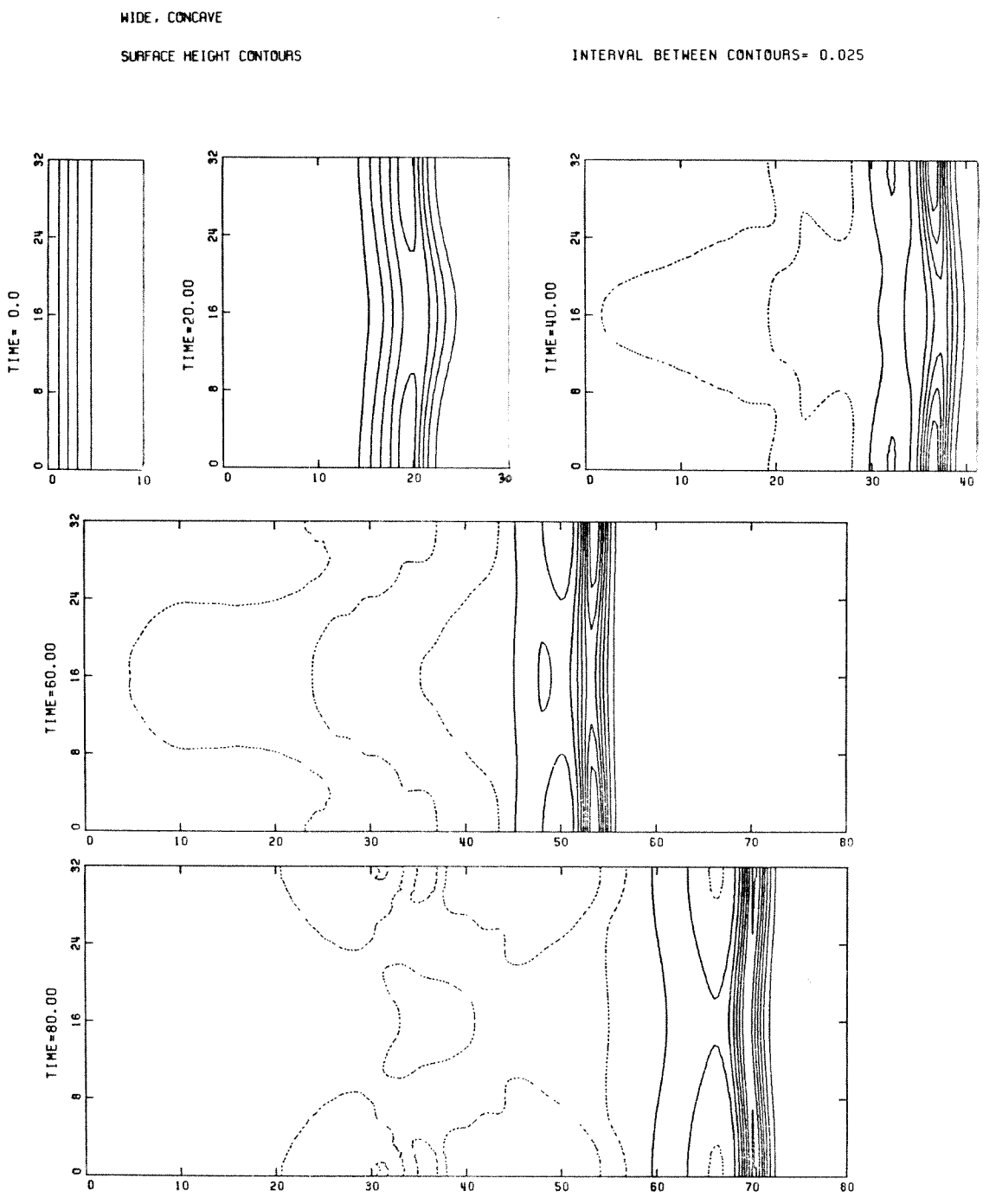
WIDE, CONCAVE
SURFACE HEIGHT CONTOURS
INTERVAL BETWEEN CONTOURS= 0.025
TIME= 0.0
TIME=20.00
TIME=40.00
TIME=60.00
TIME=80.00

Figure 4.10b

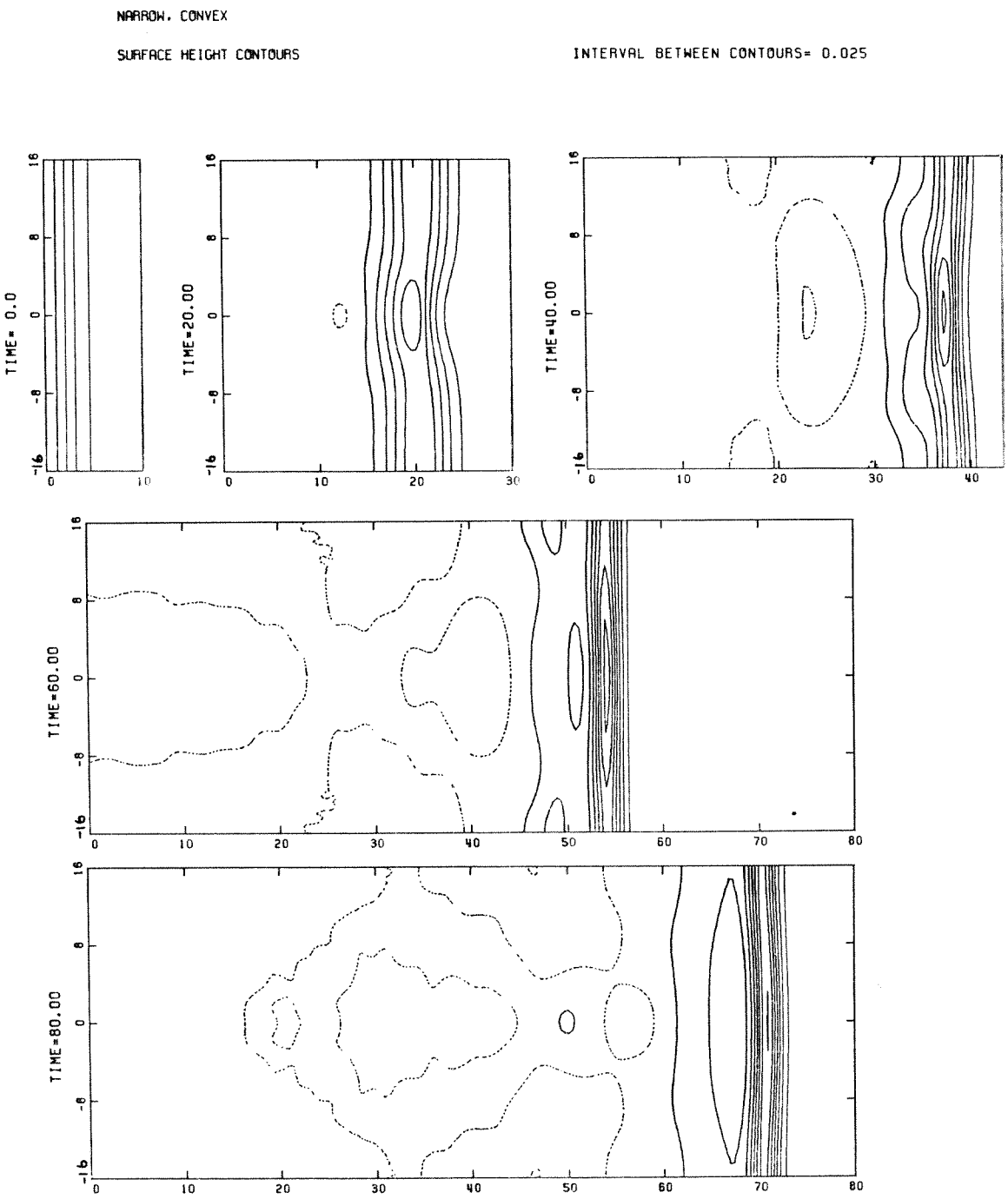
NARROW. CONVEX
SURFACE HEIGHT CONTOURS
INTERVAL BETWEEN CONTOURS= 0.025
TIME= 0.0
TIME=20.00
TIME=40.00
TIME=60.00
TIME=80.00

Figure 4.10c

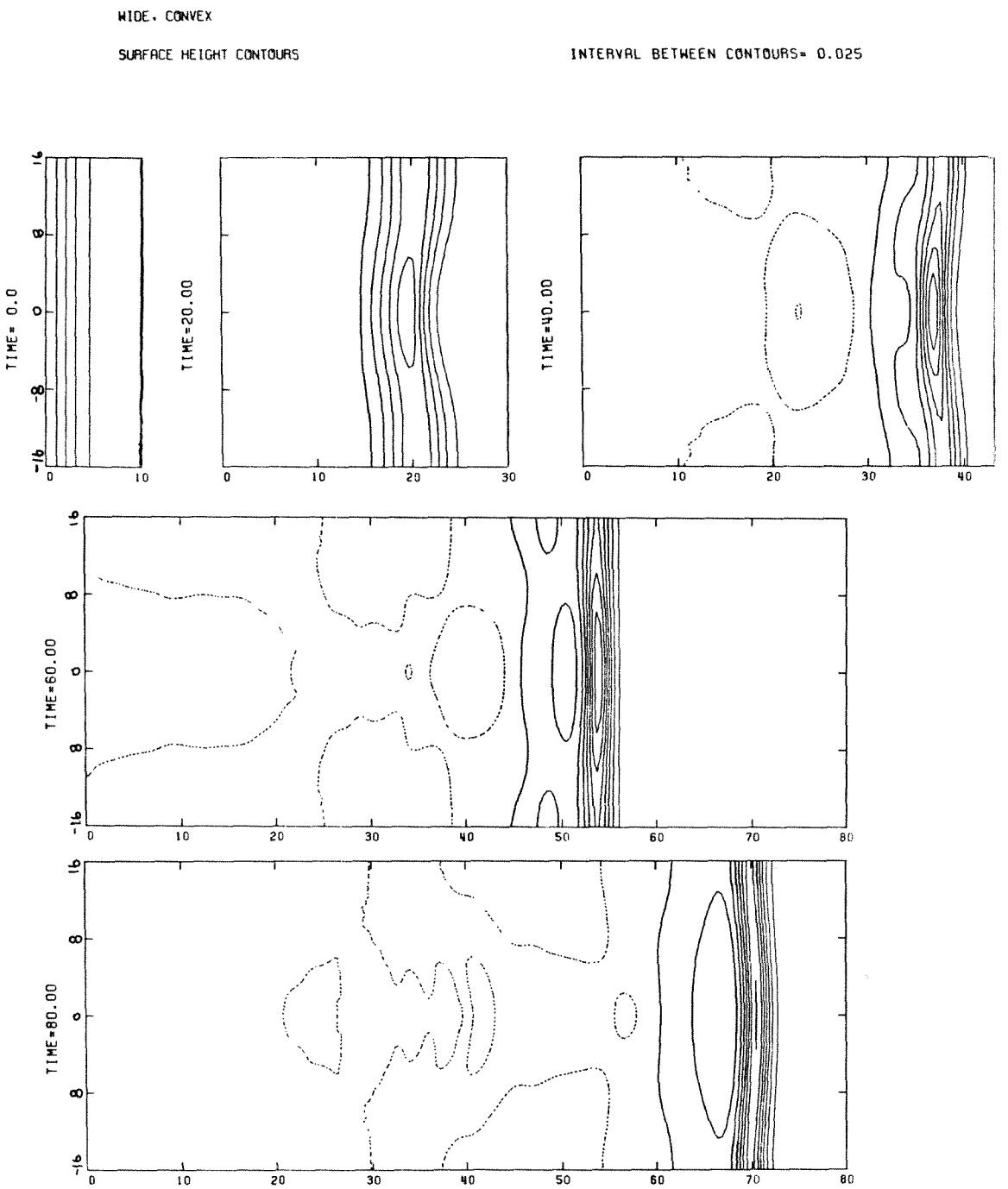
WIDE, CONVEX
SURFACE HEIGHT CONTOURS
INTERVAL BETWEEN CONTOURS= 0.025
TIME= 0.0
TIME=20.00
TIME=40.00
TIME=60.00
TIME=80.00

Figure 4.10d

deeper region, indicating that the wavelength is smaller on the shelf. This can be clearly seen in Figures 4.10a through 4.10d in which the contour lines become more closely packed as the wave moves up onto the shelf. The dotted lines on the contour plots indicate that the primary and secondary solitons are followed by rather extensive, but shallow, regions which dip below the undisturbed water line. It is not known whether these features of large extent but small amplitude are true features of the solution, or whether they are brought on by the numerical scheme. Additional testing at decreased stepsize would be required to confirm these features.

4.3 Comparison with Linear, Nondispersive Theory

In order to gauge the importance of nonlinearity and dispersion in our numerical experiments, we re-examined the case of a wide concave ramp (IW) by numerically solving the linear nondispersive long wave equations . (For convenience, we will refer to these equations as linear theory.) This was a simple matter, since these equations (as we have discussed in Section 2.5) are a subset of the full nonlinear dispersive equations. We modified the original 1HD and 2HD by setting all nonlinear and dispersive terms to zero; no other changes were made in the programs. The 1HD program for linear theory was used to test for convergence of the computed solutions as the stepsize was decreased and the scheme was found to be satisfactory: the effect of step size on peak degradation and excess mass was found to be similar to the 1HD test cases described in Section 3.1. The 2HD program for linear theory retrieved the 1HD linear theory results identically when required to converge within a small enough tolerance.

Figure 4.11 is a three-dimensional perspective view of the surface height obtained at various time steps by solving the linear equations. As mentioned above, the bottom topography used for this experiment was the wide concave

Figure 4.11 Three-dimensional perspective view of the surface height at various times for the case using linear nondispersive theory. The bottom topography is the wide concave ramp (IW) pictured in Fig. 4.5b. Initial conditions are the same as in cases (IN), (IW), (ON) and (OW).

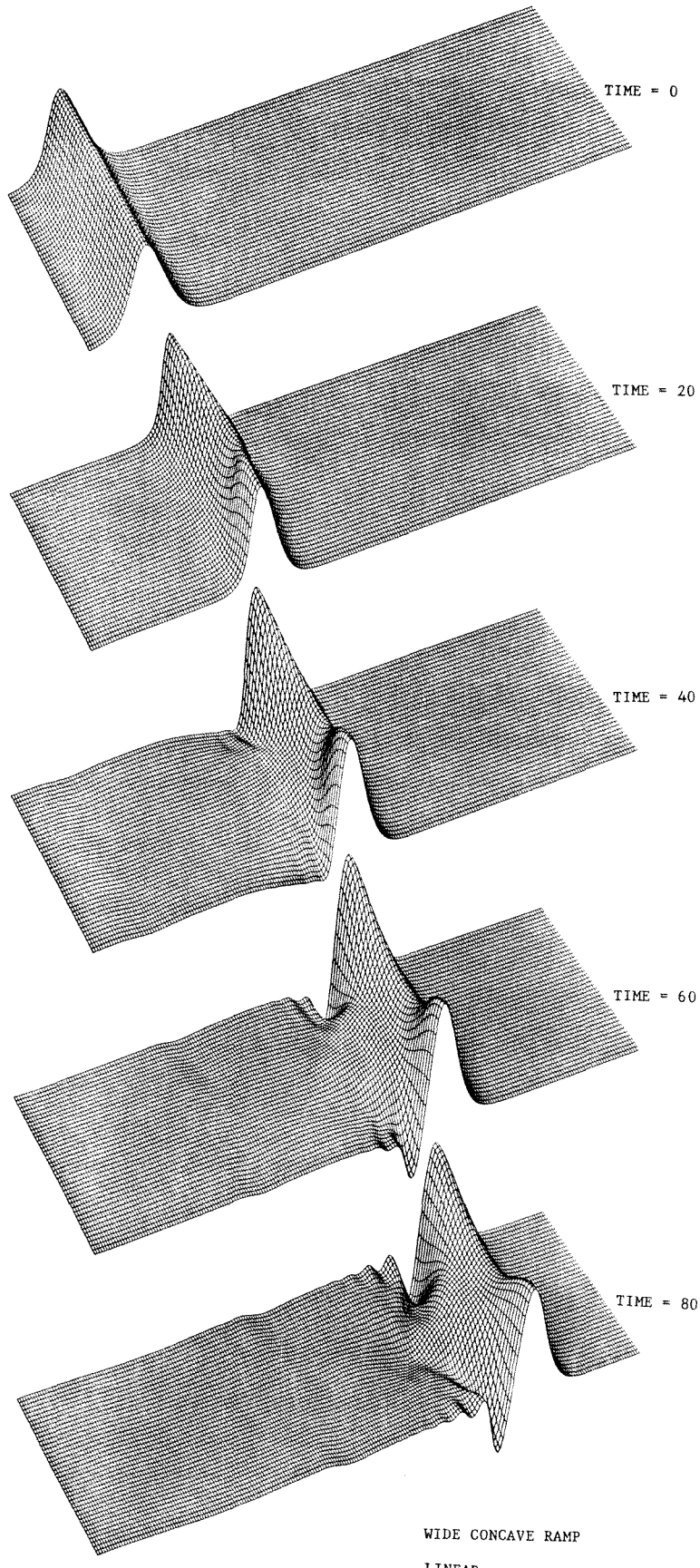

WIDE CONCAVE RAMP

LINEAR
NONDISPERSIVE THEORY

Figure 4.11

ramp (IW). Comparison of figure 4.11 with the corresponding figure 4.6b for nonlinear dispersive solution shows grossly different wave forms at the end of computation. Figure 4.12 shows profiles for the centerline and wall at various times. The corresponding figure for nonlinear dispersive theory is 4.8b. These profiles show that along the wall the wave achieves a smaller height than in the nonlinear dispersive calculation. No additional solitons are formed and a rather deep trough forms at the rear face of the wave. The back of the wave is seen to be steeper than the front at the last 3 times displayed for the wall cut. The centerline cut profiles show a peak amplitude much lower than that for the nonlinear dispersive theory. The final wave form computed looks poorly formed and possesses a wavelength roughly 3-4 times larger than that computed for the primary soliton in the nonlinear dispersive theory. The waves do not travel as fast as those calculated using the full nonlinear, dispersive theory, as should be expected.

We may compare the peak amplitudes along three longitudinal lines vs. time through Figure 4.13. This figure also emphasizes the differences between the linear theory and the nonlinear, dispersive theory. Here the wave peaks computed from linear theory are seen to achieve lower amplitudes than in the previously computed cases. Similar to the curves in Fig 4.9b, the curves in 4.13 also appear to approach each other but much less rapidly than seen before. Preliminary computations performed for a larger stepsize and longer time did not evidence that a crossing occurs before $t \approx 100$. Thus our results suggest that, if a cross-channel ringing is set up, the period would be much longer than indicated by the results of the nonlinear dispersive theory.

Finally we examine Figure 4.14, the contour plots of surface height for the linear case. These plots clearly show that the wavelength of the progressing wave is not compressed as much as in the previously computed case, shown in

Figure 4.12 Surface height profiles for the case using linear, nondispersive theory. Surface heights are shown for two longitudinal cuts (along centerline and wall) at various times. Bottom topography is the wide concave ramp. Along the centerline, the ramp extends from 16 to 26; along the wall the ramp extends from 6 to 16.

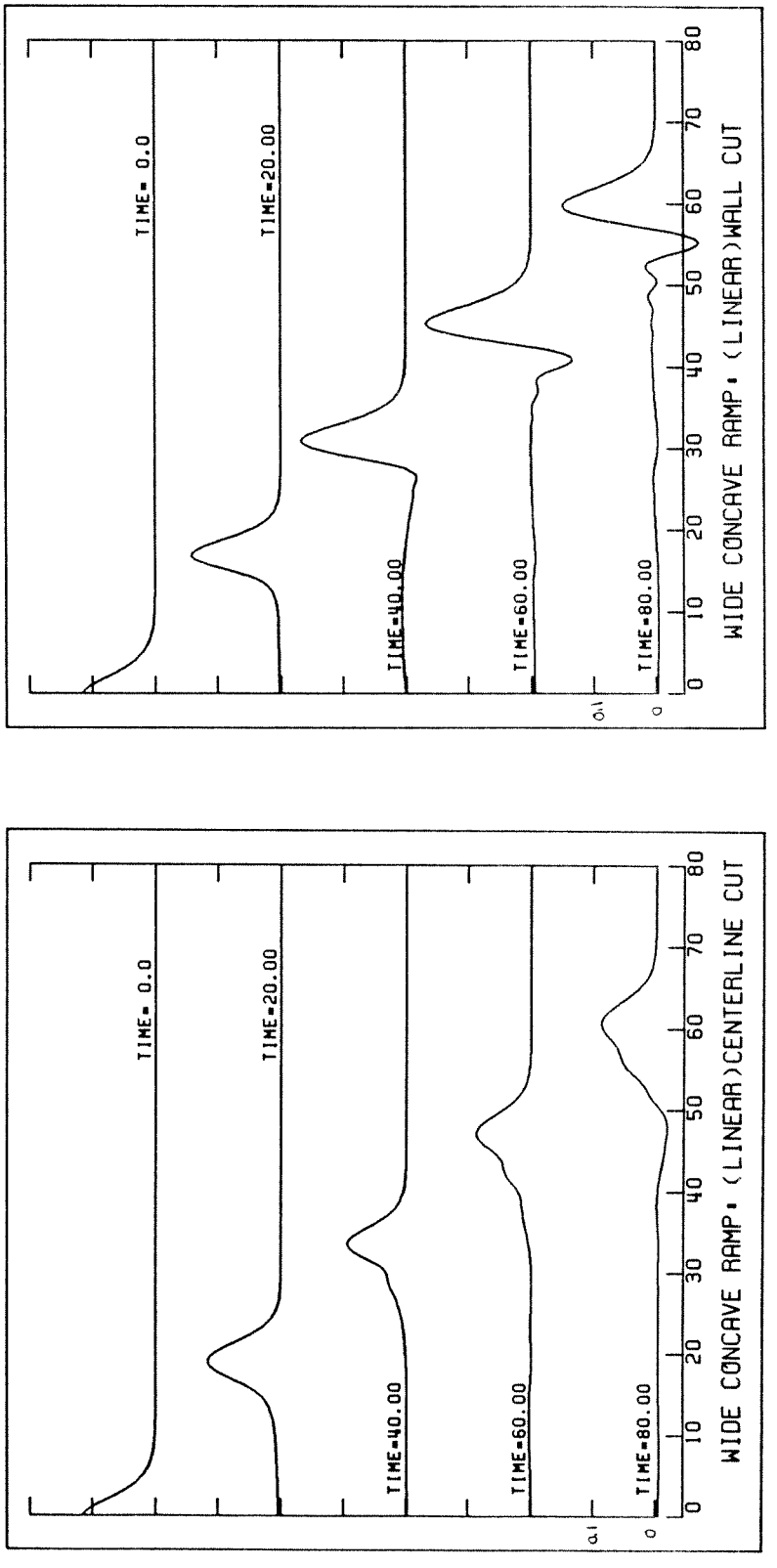
TIME= 0.0
TIME=20.00
TIME=40.00
TIME=60.00
TIME=80.00
WIDE CONCAVE RAMP, (LINEAR)CENTERLINE CUT
0.1
0
0
10
20
30
40
50
60
70
80
TIME= 0.0
TIME=20.00
TIME=40.00
TIME=60.00
TIME=80.00
WIDE CONCAVE RAMP, (LINEAR)WALL CUT
0.1
0
0
10
20
30
40
50
60
70
80

Figure 4.12

Figure 4.13 The peak amplitude as a function of time along three longitudinal lines for the case using linear nondispersive theory. Bottom topography is the wide, concave ramp.

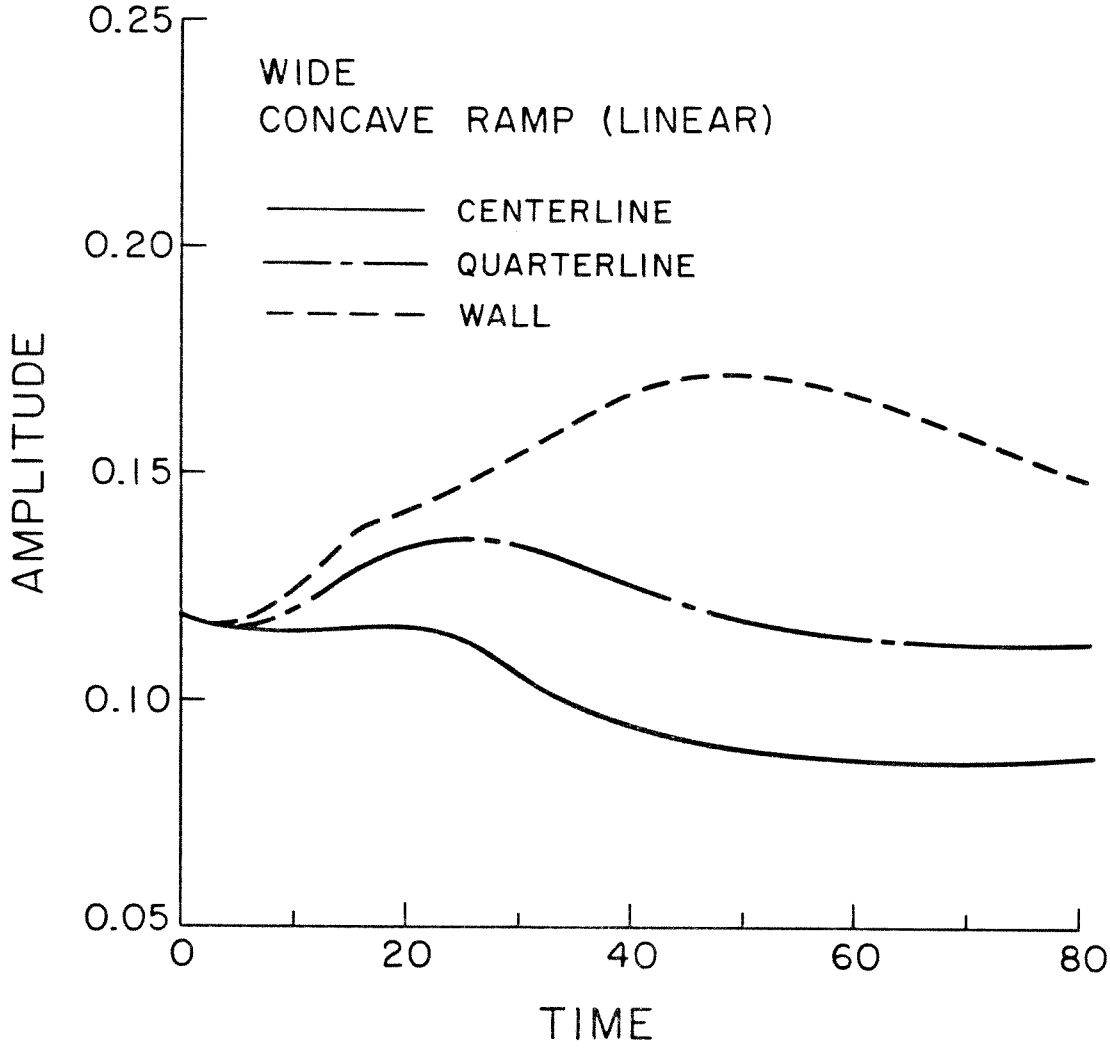
WIDE
CONCAVE RAMP (LINEAR)
CENTERLINE
QUARTERLINE
WALL
AMPLITUDE
0.25
0.20
0.15
0.10
0.05
0
20
40
60
80
TIME

Figure 4.13

Figure 4.14 Contour plots of computed surface height at various times for the case using linear nondispersive theory. First three plots are truncated as remarked in Fig. 4.10. Bottom topography is the wide, concave ramp.

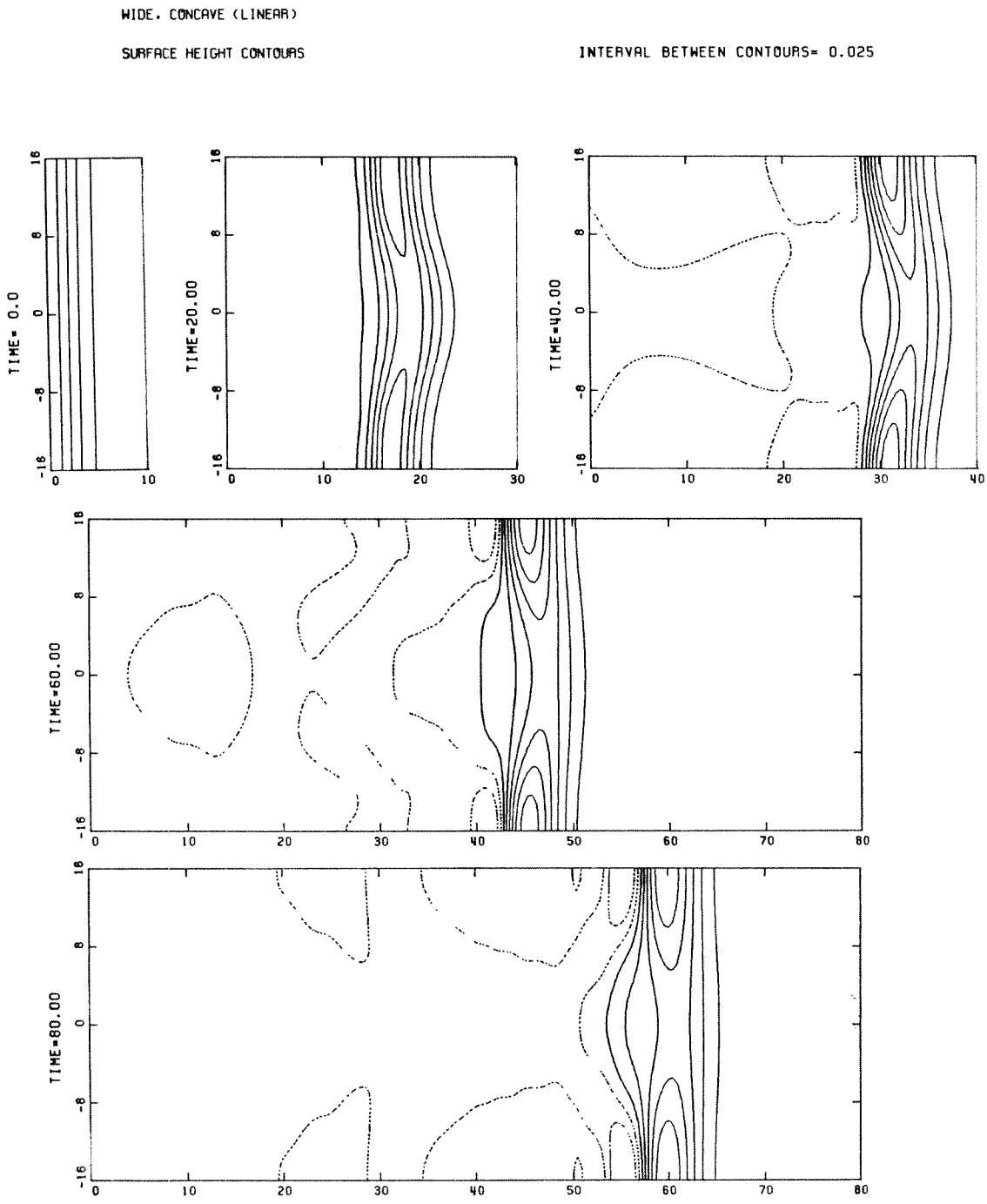
WIDE. CONCAVE (LINEAR)
SURFACE HEIGHT CONTOURS
INTERVAL BETWEEN CONTOURS= 0.025
TIME= 0.0
TIME=20.00
TIME=40.00
TIME=60.00
TIME=80.00

Figure 4.14

Figure 4.10b. The wave contours look quite similar at time=20, but are markedly different by the end of the computation.

The above results indicate that, for the present case, the linear theory fails to adequately describe the overall three-dimensional character of the interaction between the wave and the bottom topography. The linear theory appears unable to satisfactorily predict crest amplification, soliton formation, cross-channel effects and overall wave shape. Therefore, to obtain reliable information about 2HD problems such as those considered here, application of a more appropriate model (such as the present nonlinear dispersive theory) is required.

CHAPTER 5

Summary and Conclusions

In this thesis, a new formulation of the model equations for finite amplitude dispersive long waves has been presented. The major improvement in this new formulation stems from the introduction of the irrotational layer-mean velocity in Section 2.4 and the subsequent translation of the classical Boussinesq equations into this new variable. The transformed equations were written in terms of the velocity potential and surface height and in addition these two equations were combined to obtain a single equation for the potential. The combined equation can fully model depth variations in space and time, as well as wave propagation in two horizontal dimensions including wave reflection. We have examined the resultant, single, Boussinesq-class equation for permanent form solutions in constant depth. Permanent-form solutions were determined for the potential and surface height, and the shape of the permanent form wave was found to be slightly wider than the classical KdV result.

The permanent-form solution permitted verification of the numerical scheme developed in Chapter 3. This numerical method, which uses an implicit finite-difference formulation, was examined for test cases in one and two horizontal dimensions and found to be satisfactory for the initial conditions prescribed in this study. Estimates were made on the errors in peak amplitude, shape deformation and wave speed induced by the finite grid spacing. In particular, errors due to insufficient mesh refinement were evidenced by peak amplitude degradation, excess mass variations and the development of an oscillatory tail. The observed undular tail was attributed to numerical dispersion resulting from the finite grid spacing and was clearly seen to

diminish as the grid spacing was refined.

The combined equation was used in a group of numerical experiments to model a wave progressing over a ramp and onto a shelf in one horizontal dimension. Solitons were produced on the shelf and our results for soliton amplitudes show good agreement with theoretical predictions and numerical computations based on the variable-coefficient KdV equation, even though the ramp reflects about 15% of the excess mass. These results suggest that the variable-coefficient KdV theory may be applicable to study of the transmitted wave on the shelf.

Another group of numerical experiments were performed to examine wave propagation in two horizontal dimensions over a curved submerged ramp. The curving ramp bottom topographies had a focussing effect on the wave as evidenced by enhanced primary crest amplification. Soliton formation was also apparent on the shelf, with the exception that the formation of the second soliton was delayed at certain locations in the channel. Indications of an cross-channel oscillatory mode with nodal points at the quarter and three-quarter lines were presented.

For comparison, computations for an identical case were performed using linear nondispersive theory. The waves were seen to evolve quite differently, and although the wave was clearly being focussed by the submerged curved ramp, the effects were not as great as in the nonlinear, dispersive case (as would be expected). No additional solitons were formed on the shelf and a trough developed near the back of the wave, steepening that side. Finally, the linear theory solution was seen to travel more slowly than the waveform computed through nonlinear dispersive theory. For the kinds of cases we considered here the linear nondispersive theory was inadequate for the characterization of the amplitude, shape and wave speed of the nonlinear dispersive solution.

From the information obtained through this study, our principal conclusions are:

- The combined governing equation derived in Chapter 2 is a convenient and straightforward replacement for the more cumbersome, two-equation Boussinesq models used previously.
- The combined equation has the advantage of an exact, easily-obtained permanent form solution which can be used to check the accuracy of a numerical approximation to the equation and as initial conditions for solitary wave studies.
- Special attention must be paid to the stepsize convergence tests in a numerical scheme developed to solve Boussinesq-class equations. In particular, the appearance of an oscillatory tail must be considered suspect until testing at reduced stepsizes can confirm its validity.
- For the gradual slopes considered here, it is not necessary to include reflection to obtain a satisfactory representation of the wave transmitted onto the shelf. A KdV-type formulation seems to fairly well describe the waveform propagated onto the shelf, however, our computed results fall slightly below the KdV theory. The somewhat smaller amplitudes on the shelf are attributed to the effect of reflection from the ramp which causes only about 85% of the excess mass to be transmitted onto the shelf.
- For the curving bottom topographies and initial wave amplitudes used in this study, linear nondispersive theory is inadequate. The linear nondispersive theory fails to accurately describe crest amplification, soliton formation, cross-channel effects and overall three-dimensional wave shape.

APPENDIX A

Derivation of the Transport Theorem

In Chapter 2, the following transport theorem (Eq. 2.6) was presented:

$$\int_{-h}^{\zeta} \frac{df}{dt} = \frac{\partial}{\partial t}\int_{-h}^{\zeta} f\, dz + \nabla\cdot\int_{-h}^{\zeta} \mathbf{u}f\, dz.$$

In order to prove this transport theorem, let us consider the material derivative of a flow quantity, $f(\mathbf{X},t)$, integrated over a material volume V. It is well known (e.g., Serrin [1959]) that, for an incompressible fluid,

$$\frac{d}{dt}\int_V f\, dV = \int_V \left(\frac{df}{dt} + f\,\nabla_0\cdot\mathbf{U}\right)dV = \int_V \frac{df}{dt}\, dV,$$

where $\frac{d}{dt}\left(\equiv \frac{\partial}{\partial t}+\mathbf{U}\cdot\nabla_0\right)$, ∇_0, $\mathbf{U}$, and other quantities are fully described in Chapter 2 (Section 2.1). If we choose a material volume V which at time t coincides with a vertical column having horizontal cross-section S_c then

$$\begin{aligned}\int_V \frac{df}{dt}dV &= \int_{S_c} dS\int_{-h}^{\zeta}\left(\frac{\partial f}{\partial t} + \mathbf{U}\cdot\nabla_0 f\right)dz \\ &= \int_{S_c} dS\int_{-h}^{\zeta}\left[\frac{\partial f}{\partial t} + \nabla_0\cdot(\mathbf{U}f)\right]dz. \end{aligned} \tag{A.1}$$

The transformation of the inner integral in Eq. A.1 is possible because the fluid is incompressible: $\nabla_0\cdot\mathbf{U} = 0$.

If we expand and evaluate the inner integral in A.1, we have

$$\begin{aligned}\int_{-h}^{\zeta}\left[\frac{\partial f}{\partial t} + \nabla_0\cdot(\mathbf{U}f)\right]dz = \frac{\partial}{\partial t}\int_{-h}^{\zeta} f dz - f_\zeta\frac{\partial\zeta}{\partial t} - f_{-h}\frac{\partial h}{\partial t} + \nabla\cdot\int_{-h}^{\zeta}(\mathbf{u}f)dz \\ - (uf)_\zeta\frac{\partial\zeta}{\partial x} - (uf)_{-h}\frac{\partial h}{\partial x} - (vf)_\zeta\frac{\partial\zeta}{\partial y} - (vf)_{-h}\frac{\partial h}{\partial y} + (wf)_\zeta - (wf)_{-h}.\end{aligned} \tag{A.2}$$

Here f_{-h} indicates the quantity $f(\mathbf{X},t)$ evaluated at $z = a$. On substituting from the boundary conditions and replacing Eq. A.2 into Eq. A.1, we find

$$\int_{S_c} dS \int_{-h}^{\zeta} \frac{df}{dt} dz = \int_{S_c} dS \left[\frac{\partial}{\partial t} \int_{-h}^{\zeta} f dz + \nabla \cdot \int_{-h}^{\zeta} (\mathbf{u}f) dz - f_{\zeta} \frac{d\zeta}{dt} + (wf)_{\zeta} - f_{-h} \frac{dh}{dt} - (wf)_{-h} \right]$$

$$= \int_{S_c} dS \; \frac{\partial}{\partial t} \int_{-h}^{\zeta} f dz + \nabla \cdot \int_{-h}^{\zeta} (\mathbf{u}f) dz.$$

The transport theorem (3.6) follows immediately since the area S_c is arbitrary.

APPENDIX B

Listing of the 1HD FORTRAN Program

To complement the description of the numerical procedure in Section 3.1, we present the following FORTRAN program used in the 1HD problems. Many comment cards have been added to make the program easier to understand. A flowchart of this program is presented in Figure 3.1.

```
      IMPLICIT REAL*8(A-H,O-Z)
      COMMON/STEPS/DX,DT,NODEX,MAXT,NODEX1
      COMMON/WAVEH/ETA(850),ALF,U,BETA,AU,NXZERO
      COMMON/TWHERE/KTIME,KOUNT
C
C       PROGRAM TO SOLVE PARTIAL DIFFERENTIAL EQUATION (3.1)
C
C ***CAVEAT* THE STEP SIZES HAVE ALL BEEN TAKEN TO BE THE SAME!***
C
C   THE SCALARS ARE:
C
C        DX    -- STEPSIZE IN X-DIRECTION.
C        DT    -- STEPSIZE IN TIME: SAME AS DX.
C        NODEX -- NUMBER OF NODEX IN THE X-DIRECTION.
C        MAXT  -- NUMBER OF TIME STEPS TO BE COMPUTED.
C        NXZERO -- NODAL LOCATION OF INITIAL WAVE PEAK.
C        ALF   -- THE AMPLITUDE OF THE INITIAL WAVE.
C        DEEP  -- WATER DEPTH IN DEEP REGION.
C        SHALLO -- WATER DEPTH IN SHALLOW REGION.
C        SL    -- RAMP SLOPE.
C        NSTART -- NODAL STARTING LOCATION OF RAMP.
C        NEND  -- NODAL ENDING LOCATION OF RAMP.
C        TOLER -- CONVERGENCE TOLERANCE COMPARISON PARAMETER
C
C   THE ARRAYS ARE:
C
C        ETA   -- VECTOR ARRAY OF SURFACE HEIGHT, COMPUTED FROM
C                 SUBROUTINE SURFIT.
C        PHI   -- ARRAY CONTAINING THE POTENTIAL AT THE PREVIOUS
C                 TIME STEP PHI( ,1) AND PRESENT TIME STEP PHI( ,2).
C        PHIOLD -- FIRST OR PREVIOUS APPROXIMATION FOR PHI AT THE
C                 NEW TIME STEP.
C        PHINEW -- CURRENT APPROXIMATION FOR PHI AT THE NEW TIME
C                 STEP.
C        DERX  -- DOUBLY SUBSCRIPTED ARRAY CONTAINING THE FIRST
C                 SPATIAL DERIVATIVE OF PHI AT THE PREVIOUS TIME
C                 STEP DERX( ,1); THE PRESENT TIME STEP DERX( ,2);
C                 AND THE NEW TIME STEP DERX( ,3).
C        DXX   -- DOUBLY SUBSCRIPTED ARRAY CONTAINING THE SECOND
C                 SPATIAL DERIVATIVE OF PHI. SECOND SUBSCRIPT
C                 DENOTES TIME STEP AS IN DERX ABOVE
C        TRI   -- DOUBLY SUBSCRIPTED ARRAY CONTAINING THE COEFFICIENTS
C                 OF THE TRIDIAGONAL MATRIX. TRI( ,1) IS THE LOWER
C                 DIAGONAL, TRI( ,2) IS THE DIAGONAL, AND TRI( ,3)
C                 IS THE UPPER DIAGONAL.
C        REDRHS -- THE VECTOR ARRAY CONTAINING THE REDUCED RIGHT-
C                 HAND SIDE. COMPUTED ONCE PER TIME STEP.
C        FULRHS -- THE VECTOR ARRAY CONTAINING THE REDUCED RIGHT-
C                 HAND SIDE PLUS THE NONLINEAR CORRECTION. COM-
C                 PUTED AT EACH ITERATION IN EACH TIME STEP.
C        H,HX,HXX -- THREE VECTOR ARRAYS CONTAINING THE WATER DEPTH
```

```
C                (VARIES WITH X), THE FIRST DERIVATIVE OF THE WATER
C                DEPTH AND AND THE SECOND DERIVATIVE OF THE WATER
C                DEPTH, RESPECTIVELY. THESE ARRAYS ARE FILLED AT THE
C                BEGINNING OF COMPUTATION.
C         UPTRIA  -- UPPER TRIANGULAR MATRIX USED IN 'L-U' DECOMPOSITION.
C                COMPUTED ONCE.
C         DOTRIA  -- LOWER TRIANGULAR MATRIX USED IN 'L-U' DECOMPOSITION.
C                COMPUTED ONCE.
C
C
C...READ IN THE NUMBER OF CASES
      READ(5,149) NCASE
  149 FORMAT(I5)
      DO 500 ICASE=1,NCASE
C...READ IN INPUT VALUES AND WRITE OUT HEADERS
      CALL READVL(ICASE,TOLER,ITMAX)
C...SET UP THE BOTTOM TOPOGRAPHY
      CALL RAMP
C...SET UP THE COMPUTABLE CONSTANTS
      CALL CONSET
C...THE INITIAL CONDITIONS ON PHI, ALSO INITIAL X-DERIVATIVES
      CALL START
C...SET UP THE TRIDIAGONAL MATRIX FOR THE CURRENT TIME STEP
      CALL DIAGIT
      DO 10 KTIME=1,MAXT
      KOUNT=0
C...SOLVE THE REDUCED EQUATION (3.4).
      CALL SOLRED
C...ITERATION LOOP:  COMPUTE NEW RHS VECTOR AND
C.....SOLVE THE FULL EQUATION (3.1).
    5 IF(KOUNT.GT.ITMAX) GO TO 1000
      KOUNT=KOUNT+1
      CALL FULSOL
C.....CHECK FOR CONVERGENCE:
C.....KRIT=1 MEANS CONVERGED;  KRIT=0 MEANS NOT CONVERGED.
      CALL COMPAR(TOLER,KRIT)
      IF(KRIT.EQ.0) GO TO 5
      TIME=(KTIME-1)*DT
C...COMPUTE THE SURFACE HEIGHT
      CALL SURFIT(KTIME)
C...COMPUTE THE EXCESS MASS
      CALL EXCESS(VOLM,BELOW,ABOVE)
C...GET WAVE PEAK AND PEAK LOCATION
      CALL SIFT3(PEAK,XPEAK)
C...WRITE RESULTS.  UNIT 17 IS THE TAPE.
      WRITE(6,164) TIME,VOLM,BELOW,ABOVE,PEAK,XPEAK,KOUNT
  164 FORMAT(1X,F8.2,3X,1P3D15.6,8X,1PD15.6,4X,1PD15.6,8X,I2)
      KOMPAR=5*( (KTIME-1)/5 )
      IF(KOMPAR.EQ.KTIME-1)
     1  WRITE(17) TIME,VOLM,BELOW,ABOVE,PEAK,XPEAK,KOUNT
C...PREPARE TO MOVE TO NEXT TIME STEP
      CALL SWITCH
   10 CONTINUE
  500 CONTINUE
```

```
      STOP
 1000 WRITE(6,1600)
 1600 FORMAT(1X,'MAXIMUM ITERATION COUNT EXCEEDED')
      STOP
      END

      BLOCK DATA
      IMPLICIT REAL*8(A-H,O-Z)
      COMMON/XDERV/DERX(850,3),DXX(850,3)
      DATA DERX,DXX/2550*0.0,2550*0.0/
C...INITIALIZE THE DERIVATIVES TO ZERO
      END

      SUBROUTINE READVL(ICASE,TOLER,ITMAX)
      IMPLICIT REAL*8(A-H,O-Z)
      COMMON/STEPS/DX,DT,NODEX,MAXT,NODEX1
      COMMON/WAVEH/ETA(850),ALF,U,BETA,AU,NXZERO
C...READ IN THE CHANGEABLE CONSTANTS
      READ(5,150) DX,DT,ALF,HGT,TOLER,MAXT,NODEX,NXZERO,ITMAX
  150 FORMAT(4F8.3,1PD15.6/4I5)
C...WRITE OUT HEADER INFORMATION
      WRITE(6,160) ICASE,DX,DT,ALF,TOLER,MAXT,NODEX,NXZERO
  160 FORMAT(1H1///25X,'**** CASE NUMBER: ',I3,' ****',5X//1X,
     1 'SPACING:',10X,'DX=',F6.2/19X,'DT=',F6.2//1X,
     2 'PEAK AMPLITUDE=',1PD10.1/1X
     3 'CONVERGENCE TOLERANCE=',1PD10.1/1X,
     4 'NODE INFORMATION:',5X,'MAX TIME:',I5,5X,'X NODES:',I5/23X,
     5 'PEAK LOCATED AT NODE:',I5/)
C...TAPE WRITES
      IF(ICASE.NE.1) CALL WRTNF(17)
      WRITE(17) DX,DT,ALF,HGT,TOLER,MAXT,NODEX,NXZERO,ITMAX
      RETURN
      END

      SUBROUTINE CONSET
      IMPLICIT REAL*8(A-H,O-Z)
      COMMON/STEPS/DX,DT,NODEX,MAXT,NODEX1
      COMMON/WAVEH/ETA(850),ALF,U,BETA,AU,NXZERO
      COMMON/DIGONL/TRI(850,3),REDRHS(850),FULRHS(850)
C...COMPUTES ALL THE NECESSARY CONSTANTS
      U =DSQRT(1.0+ALF)
      BETA =DSQRT(3.*ALF/(4.*U*U))
      AU = ALF/U
      NODEX1=NODEX-1
      RETURN
      END

      SUBROUTINE START
      IMPLICIT REAL*8(A-H,O-Z)
      COMMON/STEPS/DX,DT,NODEX,MAXT,NODEX1
      COMMON/WAVEH/ETA(850),ALF,U,BETA,AU,NXZERO
      COMMON/POTEN/PHI(850,2),PHIOLD(850),PHINEW(850)
      COMMON/XDERV/DERX(850,3),DXX(850,3)
C...PLACE TWO SETS OF INITIAL CONDITIONS IN ARRAY PHI
```

```
C...ALSO COMPUTE THE FIRST AND SECOND SPATIAL DERIVATIVES OF PHI
C...INTIAL CONDITIONS DO NOT ASSUME ANY DEPTH VARIATION
      DO 10 J=1,2
      T=(J-2)*DT
      DO 10 I=1,NODEX
      X=(I-NXZERO)*DX
      CHI      = BETA*(X-U*T)
      PHI(I,J)  =DSQRT(4.*ALF/3.)*DTANH( CHI )
      IF(CHI.GT.44.) GO TO 10
      DERX(I,J) = AU/(DCOSH(CHI)*DCOSH(CHI))
      DXX(I,J)  = -2.0*BETA*DERX(I,J)*DTANH(CHI)
   10 CONTINUE
    1 RETURN
      END

      SUBROUTINE DIAGIT
      IMPLICIT REAL*8(A-H,O-Z)
      COMMON/STEPS/DX,DT,NODEX,MAXT,NODEX1
      COMMON/WAVEH/ETA(850),ALF,U,BETA,AU,NXZERO
      COMMON/SLOPE/H(850),HX(850),HXX(850)
      COMMON/DIGONL/TRI(850,3),REDRHS(850),FULRHS(850)
C...SETS UP THE DIAGONALS OF THE TRIDIAGONAL MATRIX
      TRI(1,1)    = 0.0
      TRI(1,3)    = 0.0
      TRI(NODEX,1) = 0.0
      TRI(NODEX,3) = 0.0
      TRI(1,2)    = 1.0
      TRI(NODEX,2) = 1.0
      DO 10 I=2,NODEX1
      HGT=H(I)
      CF=DT*DT*HGT/2. + HGT*HGT/3.
      TRI(I,1)= -CF/(DX*DX)  +HGT*HX(I)/(4.*DX)
      TRI(I,2)=1.0 + 2.0*CF/(DX*DX)
   10 TRI(I,3)= -CF/(DX*DX)  -HGT*HX(I)/(4.*DX)
      RETURN
      END

      SUBROUTINE SOLRED
      IMPLICIT REAL*8(A-H,O-Z)
      COMMON/STEPS/DX,DT,NODEX,MAXT,NODEX1
      COMMON/WAVEH/ETA(850),ALF,U,BETA,AU,NXZERO
      COMMON/DIGONL/TRI(850,3),REDRHS(850),FULRHS(850)
      COMMON/POTEN/PHI(850,2),PHIOLD(850),PHINEW(850)
      COMMON/XDERV/DERX(850,3),DXX(850,3)
      COMMON/UPNDO/UPTRIA(850,3),DOTRIA(850,3)
      COMMON/TWHERE/KTIME,KOUNT
      COMMON/SLOPE/H(850),HX(850),HXX(850)
C...COMPUTES THE RHS FOR THE REDUCED EQUATION
C...AND
C...SOLVES THE REDUCED EQUATIONS TO YIELD PHIOLD
      DX32=(2.*DX*DX*DX)
      DO 10 I=2,NODEX1
      HGT=H(I)
      HDX=HX(I)
```

```
      C1 = HDX*(DT*DT - HGT)
      C2 = HGT*HDX/2.
      C3 = -(HGT*HGT/3.)*(2.0 + DT*DT*HXX(I)/2.)
      C4 = HGT*DT*DT/2. + HGT*HGT/3.
      IF(I.EQ.2.OR.I.EQ.NODEX1) GO TO 11
      C5 = -DT*DT*HGT*HGT*HDX/6.
      DXXX=(PHI(I+2,2)-2.*PHI(I+1,2)+2.*PHI(I-1,2)-PHI(I-2,2))/DX32
      REDRHS(I) =2.*PHI(I,2)    - PHI(I,1)
     1      + C1*DERX(I,2) + C2*DERX(I,1)
     2      + C3*DXX(I,2)  + C4*DXX(I,1) + C5*DXXX
      GO TO 10
   11 REDRHS(I) =2.*PHI(I,2)    - PHI(I,1)
     1      + C1*DERX(I,2) + C2*DERX(I,1)
     2      + C3*DXX(I,2)  + C4*DXX(I,1)
   10 CONTINUE
      REDRHS(1)   = 2.*PHI(1,2)    - PHI(1,1)
      REDRHS(NODEX)= 2.*PHI(NODEX,2) - PHI(NODEX,1)
      CALL TRISOL(TRI,REDRHS,PHIOLD)
      DO 20 I=2,NODEX1
      DERX(I,3)=(PHIOLD(I+1)-PHIOLD(I-1))/(2.*DX)
      DXX(I,3) =(PHIOLD(I+1)-2.0*PHIOLD(I)+PHIOLD(I-1))/(DX*DX)
   20 CONTINUE
      DERX(1,3 )   =(PHIOLD(2)-PHIOLD(1))/DX
      DXX(1,3)     =0.0
      DERX(NODEX,3) =(PHIOLD(NODEX)-PHIOLD(NODEX1))/DX
      DXX(NODEX,3)  =0.0
      RETURN
      END

      SUBROUTINE TRISOL(TRI,RHS,PHI)
      IMPLICIT REAL*8(A-H,O-Z)
      DIMENSION TRI(850,3),RHS(1),PHI(1)
      COMMON/UPNDO/UPTRIA(850,3),DOTRIA(850,3)
      COMMON/STEPS/DX,DT,NODEX,MAXT,NODEX1
      COMMON/TWHERE/KTIME,KOUNT
C...SOLVES A TRIDIAGONAL MATRIX BY 'L-U' DECOMPOSITION. LOWER AND UPPER
C...TRIANGULAR MATRICES ARE COMPUTED ONLY ONCE
      UPTRIA(1,2)=TRI(1,2)
      UPTRIA(1,3)=TRI(1,3)
      PHI(1) = RHS(1)
      IF(KTIME.GT.1) GO TO 500
      IF(KOUNT.GT.1) GO TO 500
      DO 10 I=2,NODEX
      I1    = I-1
      DOTRIA(I,2) = 1.
      UPTRIA(I,3) = TRI(I,3)
      DOTRIA(I,1) = TRI(I,1) / UPTRIA(I1,2)
      UPTRIA(I,2) = TRI(I,2) - DOTRIA(I,1)*UPTRIA(I1,3)
      IF(DABS(UPTRIA(I,2)).LT.1.D-29) GO TO 35
   10 CONTINUE
  500 DO 20 I=2,NODEX
   20 PHI(I)    = RHS(I) - DOTRIA(I,1) * PHI(I-1)
      PHI(NODEX) = PHI(NODEX) / UPTRIA(NODEX,2)
      I=NODEX
```

```
   25 I1=I-1
      PHI(I1)= (PHI(I1) - UPTRIA(I1,3) * PHI(I)) / UPTRIA(I1,2)
      I=I-1
      IF(I.EQ.1) GO TO 15
      GO TO 25
   15 RETURN
   35 WRITE (6,7)
    7 FORMAT (//5X,'A  REQUIRES PIVOTING OR IS SINGULAR')
      STOP
      END

      SUBROUTINE FULSOL
      IMPLICIT REAL*8(A-H,O-Z)
      COMMON/STEPS/DX,DT,NODEX,MAXT,NODEX1
      COMMON/WAVEH/ETA(850),ALF,U,BETA,AU,NXZERO
      COMMON/DIGONL/TRI(850,3),REDRHS(850),FULRHS(850)
      COMMON/POTEN/PHI(850,2),PHIOLD(850),PHINEW(850)
      COMMON/XDERV/DERX(850,3),DXX(850,3)
      COMMON/TWHERE/KTIME,KOUNT
      COMMON/UPNDO/UPTRIA(850,3),DOTRIA(850,3)
C...COMPUTES RHS FOR FULL EQN AND SOLVES THE FULL EQUATION (3.1)
C...FOR PHINEW
C...KEEPS THE SAME BOUNDARY CONDITION ON LEFT AND RIGHT
      DO 10 I=2,NODEX1
      FULRHS(I) = REDRHS(I) - DT*DERX(I,2)*(DERX(I,3)-DERX(I,1))
     1        - DT*DXX(I,2)*(PHIOLD(I)-PHI(I,1))/2.
   10 CONTINUE
      FULRHS(1)    =REDRHS(1)- DT*DERX(1,2)*(DERX(1,3)-DERX(1,1))
      FULRHS(NODEX)=REDRHS(NODEX)
     1        - DT*DERX(NODEX,2)*(DERX(NODEX,3)-DERX(NODEX,1))
      CALL TRISOL(TRI,FULRHS,PHINEW)
      DO 20 I=2,NODEX1
      DERX(I,3)=(PHINEW(I+1)-PHINEW(I-1))/(2.*DX)
      DXX(I,3) =(PHINEW(I+1)-2.0*PHINEW(I)+PHINEW(I-1))/(DX*DX)
   20 CONTINUE
      DERX(1,3)    =(PHINEW(2)-PHINEW(1))/DX
      DXX(1,3)     =0.0
      DERX(NODEX,3) =(PHINEW(NODEX)-PHINEW(NODEX1))/DX
      DXX(NODEX,3)  =0.0
      RETURN
      END

      SUBROUTINE COMPAR(TOLER,KRIT)
      IMPLICIT REAL*8(A-H,O-Z)
      COMMON/STEPS/DX,DT,NODEX,MAXT,NODEX1
      COMMON/POTEN/PHI(850,2),PHIOLD(850),PHINEW(850)
C...COMPUTES THE CONVERGENCE CRITERION
C...AND
C...COMPARES IT TO THE USER SELECTED TOLERANCE
      KRIT=0
      DFITER=0.0
      DFTIME=0.0
      DO 10 I=1,NODEX
      DFITER=DFITER+(PHIOLD(I)-PHINEW(I))*(PHIOLD(I)-PHINEW(I))
```

```
      DFTIME=DFTIME+(PHI(I,2)-PHINEW(I))*(PHI(I,2)-PHINEW(I))
   10 CONTINUE
      COMTOL=DSQRT(DFITER)/DSQRT(DFTIME)
      IF(COMTOL.LT.TOLER) KRIT=1
      DO 20 I=1,NODEX
   20 PHIOLD(I)=PHINEW(I)
      RETURN
      END

      SUBROUTINE SURFIT(KTIME)
      IMPLICIT REAL*8(A-H,O-Z)
      COMMON/STEPS/DX,DT,NODEX,MAXT,NODEX1
      COMMON/WAVEH/ETA(850),ALF,U,BETA,AU,NXZERO
      COMMON/POTEN/PHI(850,2),PHIOLD(850),PHINEW(850)
      COMMON/XDERV/DERX(850,3),DXX(850,3)
      COMMON/SLOPE/H(850),HX(850),HXX(850)
C...COMPUTES THE SURFACE HEIGHT BASED ON THREE TIME LEVELS OF PHI
      DO 10 I=1,NODEX
      HGT=H(I)
      PDXXT=(DXX(I,3)  - DXX(I,1) )/(2.0*DT)
      PDXT =(DERX(I,3) - DERX(I,1))/(2.0*DT)
      ETA1 =(PHINEW(I) - PHI(I,1) )/(2.0*DT)
      ETA(I)= - ETA1 - DERX(I,2)*DERX(I,2)/2.0
     1   + (HGT*HGT/3.)*PDXXT  + (HGT*HX(I)/2.)*PDXT
   10 CONTINUE
      KOMPAR=5*( (KTIME-1)/5 )
C     IF(KOMPAR.EQ.KTIME-1)      WRITE(17) KTIME,ETA,PHINEW
      IF(KTIME.EQ.MAXT) GO TO 2
      KCHK=50*( (KTIME-1)/50 )
      IF(KCHK.NE.KTIME-1) RETURN
    2 TIME=(KTIME-1)*DT
      WRITE(6,160) TIME
  160 FORMAT(1X,' SURFACE HEIGHT AT TIME = ',F7.2)
      WRITE(6,161) (ETA(I),I=1,NODEX)
  161 FORMAT(10(1X,F10.6))
      RETURN
      END

      SUBROUTINE EXCESS(SUMEX,BELOW,ABOVE)
      IMPLICIT REAL*8(A-H,O-Z)
      COMMON/STEPS/DX,DT,NODEX,MAXT,NODEX1
      COMMON/WAVEH/ETA(850),ALF,U,BETA,AU,NXZERO
      COMMON/RAMPPM/DEEP,SHALLO,SL,NSTART,NEND
      SUMEX=0.0
C...INTEGRATES THE EXCESS MASS
      NE1=NEND-1
      BELOW = 0.0
      DO 10 I=1,NE1
   10 BELOW = BELOW + ETA(I)*DX
      ABOVE = 0.0
      DO 20 I=NEND,NODEX
   20 ABOVE = ABOVE + ETA(I)*DX
      SUMEX=BELOW+ABOVE
      RETURN
```

```
      END

      SUBROUTINE SIFT3(PEAK,XP)
      IMPLICIT REAL*8(A-H,O-Z)
      DIMENSION P(3),X(3),IP(3)
      COMMON/STEPS/DX,DT,NODEX,MAXT,NODEX1
      COMMON/WAVEH/ETA(850),ALF,U,BETA,AU,NXZERO
C...FINDS WAVE PEAK AND PEAK POSITION
C...SEARCHES FOR THE THREE HIGHEST VALUES AND THE FITS A QUADRATIC
      DO 5 L=1,3
      P(L) = 0.0
    5 IP(L)= 0
      DO 10 I=1,NODEX
      IF (P(1).GT.ETA(I)) GO TO 12
        DO 100 M=1,2
        P(4-M) = P(3-M)
  100   IP(4-M)=IP(3-M)
      P(1) =ETA(I)
      IP(1)=I
      GO TO 10
   12 IF(P(2).GT.ETA(I)) GO TO 13
      P(3) = P(2)
      IP(3)=IP(2)
      P(2) = ETA(I)
      IP(2)= I
      GO TO 10
   13 IF(P(3).GT.ETA(I)) GO TO 10
      P(3) = ETA(I)
      IP(3)= I
   10 CONTINUE
      DO 20 M=1,3
   20 X(M)=(IP(M)-NXZERO)*DX
      A=((P(1)-P(2))/(X(1)-X(2))-(P(1)-P(3))/(X(1)-X(3)))/(X(2)-X(3))
      B=(P(1)-P(3))/(X(1)-X(3)) - A*(X(1)+X(3))
      C= P(1) - A*X(1)*X(1) -B*X(1)
      XP=-B/(2.*A)
      PEAK=A*XP*XP + B*XP + C
      RETURN
      END

      SUBROUTINE SWITCH
      IMPLICIT REAL*8(A-H,O-Z)
      COMMON/STEPS/DX,DT,NODEX,MAXT,NODEX1
      COMMON/POTEN/PHI(850,2),PHIOLD(850),PHINEW(850)
      COMMON/XDERV/DERX(850,3),DXX(850,3)
C...BUMPS ALL PHI AND PHI DERIVATIVES DOWN ONE TIME STEP TO
C...PREPARE FOR NEXT TIME STEP COMPUTATION
      DO 10 I=1,NODEX
      PHI(I,1)=PHI(I,2)
      PHI(I,2)=PHINEW(I)
      DERX(I,1)=DERX(I,2)
      DERX(I,2)=DERX(I,3)
      DXX(I,1) =DXX(I,2)
   10 DXX(I,2) =DXX(I,3)
```

```
      RETURN
      END

      SUBROUTINE RAMP
      IMPLICIT REAL*8(A-H,O-Z)
      DIMENSION HRAW(850)
      COMMON/STEPS/DX,DT,NODEX,MAXT,NODEX1
      COMMON/SLOPE/H(850),HX(850),HXX(850)
      COMMON/RAMPPM/DEEP,SHALLO,SL,NSTART,NEND
C...SETS THE BOTTOM TOPOGRAPHY
C...READ IN THE RAMP START NODE, RAMP END NODE, DEEP DEPTH, SHALLOW DEPTH,
C...AND THE SLOPE OF THE RAMP
      READ(5,150) NSTART,NEND,DEEP,SHALLO,SL
  150 FORMAT(2I5,3F10.5)
C...WRITE OUT
      WRITE(17) NSTART,NEND,DEEP,SHALLO,SL
      WRITE(6,160) NSTART,NEND,DEEP,SHALLO,SL
  160 FORMAT(1X,'RAMP PARAMETERS:',6X,'START NODE=',I5,5X,
     1  'END NODE:',I5/23X,'DEEP WATER DEPTH=',F6.2/23X,
     2  'SHALLOW WATER DEPTH=',F6.2/23X,'SLOPE=',1PD11.2//)
      NS1=NSTART+1
      NE1=NEND+1
C...SET UP THE HEIGHTS
      DO 10 I=1,NSTART
   10 HRAW(I)=DEEP
      DO 20 I=NS1,NEND
   20 HRAW(I)=DEEP - SL*(I-NSTART)*DX
      DO 30 I=NE1,NODEX
   30 HRAW(I)=SHALLO
C...SMOOTH THE PROFILE
      NODEX1=NODEX-1
      DO 35 I=2,NODEX1
   35 H(I)=(HRAW(I-1)+HRAW(I)+HRAW(I-1))/3.
      H(1)=HRAW(1)
      H(NODEX)=HRAW(NODEX)
C...COMPUTE THE DERIVATIVES
      DO 40 I=2,NODEX1
      HX(I) =(H(I+1)-H(I-1))/(2.*DX)
   40 HXX(I)=(H(I-1)-2.*H(I)+H(I-1))/(DX*DX)
      HX(1)    =0.0
      HXX(1)   =0.0
      HX(NODEX) =0.0
      HXX(NODEX)=0.0
      RETURN
      END
```

APPENDIX C

Listing of the 2HD FORTRAN Program

To complement the description of the numerical procedure in Section 3.2, we present the following FORTRAN program used in the 2HD problems. This sample program can be used to solve the concave topographies described in Chapter 4. (The convex topographies have a slightly different subroutine SETRMP.) Many comment cards have been added to make the program easier to understand. A flowchart of this program is presented in Figure 3.3.

```
      IMPLICIT REAL*8(A-H,O-Z)
      COMMON/STEPS/DX,DT,NODEX,MAXT,NODEX1
      COMMON/ADDY/DY,NODEY,NODEY1,NODTOT
      COMMON/WAVEH/ETA(12341),ALF,U,BETA,AU,NXZERO
      COMMON/POTEN/PHI(12341,2),PHIOLD(12341),PHINEW(12341)
      COMMON/TWHERE/KTIME,KOUNT
C
C
C       PROGRAM TO SOLVE PARTIAL DIFFERENTIAL EQUATION (3.10)
C        DESCRIBING PROPAGATION IN TWO HORIZONTAL DIRECTIONS
C
C     PROGRAM HAS BEEN DESIGNED TO CORRESPOND AS MUCH AS POSSIBLE
C     WITH THE PROGRAM FOR PROPAGATION IN ONE HORIZONTAL DIMENSION
C
C  ***CAVEAT* THE STEP SIZES HAVE ALL BEEN TAKEN TO BE THE SAME!***
C
C  ALL SINGLY SUBSCRIPTED ARRAYS FOR THE POTENTIAL, SURFACE HEIGHT,
C   AND DERIVATIVES REPRESENT FUNCTIONS OF TWO VARIABLES, X AND Y.
C   EQUATION (3.12) GIVES THE RELATIONSHIP BETWEEN THE SEQUENTIAL
C    NOTATION USED HERE AND THE MORE PHYSICAL (X,Y) NOTATION.
C
C     THE SCALARS ARE:
C
C          DX     -- STEPSIZE IN X-DIRECTION.
C          DY     -- STEPSIZE IN Y-DIRECTION: SAME AS DX.
C          DT     -- STEPSIZE IN TIME: SAME AS DX.
C          NODEX  -- NUMBER OF NODES IN THE X-DIRECTION.
C          NODEY  -- NUMBER OF NODES IN THE Y-DIRECTION.
C          NODTOT -- TOTAL NUMBER OF NODES.
C          MAXT   -- NUMBER OF TIME STEPS TO BE COMPUTED.
C          NXZERO -- NODAL LOCATION OF INITIAL WAVE PEAK.
C          ALF    -- THE AMPLITUDE OF THE INITIAL WAVE.
C          DEEP   -- WATER DEPTH IN DEEP REGION.
C          SHALLO -- WATER DEPTH IN SHALLOW REGION.
C          SL     -- RAMP SLOPE.
C          NSTART -- NODAL STARTING LOCATION OF RAMP.
C          NEND   -- NODAL ENDING LOCATION OF RAMP.
C          MCURVE -- WIDTH OF CURVING RAMP FEATURE
C          TOLER  -- CONVERGENCE TOLERANCE COMPARISON PARAMETER
C          SOR    -- SUCCESSIVE OVER-RELAXATION PARAMETER
C
C      THE ARRAYS ARE:
C
C          ETA    -- VECTOR ARRAY OF SURFACE HEIGHT, COMPUTED FROM
C                    SUBROUTINE SURFIT.
C          PHI    -- ARRAY CONTAINING THE POTENTIAL AT THE PREVIOUS
C                    TIME STEP PHI( ,1) AND PRESENT TIME STEP PHI( ,2).
C          PHIOLD -- FIRST OR PREVIOUS APPROXIMATION FOR PHI AT THE
C                    NEW TIME STEP.
C          PHINEW -- CURRENT APPROXIMATION FOR PHI AT THE NEW TIME
C                    STEP.
```

```
C        DERX  -- DOUBLY SUBSCRIPTED ARRAY CONTAINING THE FIRST
C              X-DERIVATIVE OF PHI AT THE PREVIOUS TIME
C              STEP DERX( ,1); THE PRESENT TIME STEP DERX( ,2);
C              AND THE NEW TIME STEP DERX( ,3).
C        DERY  -- DOUBLY SUBSCRIPTED ARRAY CONTAINING THE FIRST
C              Y-DERIVATIVE OF PHI AS IN DERX ABOVE.
C        DELSQ -- DOUBLY SUBSCRIPTED ARRAY CONTAINING DEL-SQUARED
C              SECOND SUBSCRIPT DENOTES TIME AS IN DERX ABOVE.
C        REDRHS -- THE VECTOR ARRAY CONTAINING THE REDUCED RIGHT-
C              HAND SIDE. COMPUTED ONCE PER TIME STEP.
C        FULRHS -- THE VECTOR ARRAY CONTAINING THE REDUCED RIGHT-
C              HAND SIDE PLUS THE NONLINEAR CORRECTION. COM-
C              PUTED AT EACH ITERATION IN EACH TIME STEP.
C        HEIGHT,DHDX,DHDY,DDH -- FOUR DOUBLY-SUBSCRIPTED ARRAYS
C              CONTAINING RAMP INFORMATION: THE WATER DEPTH IN
C              THE RAMP REGION, THE FIRST X AND Y DERIVATIVES OF
C              DEPTH, AND DEL-SQUARED OF THE DEPTH.  THESE ARRAYS
C              ONLY CONCERN THE RAMP REGION AND ARE USED BY
C              THE FUNCTION SUBROUTINES FOR DEPTH AND DEPTH
C              DERIVATIVES.
C
C...INITIALIZE THE DERIVATIVE ARRAYS
      CALL BLOCK
C...READ IN THE NUMBER OF CASES TO BE COMPUTED
      READ(5,149) NCASE
  149 FORMAT(I5)
      DO 500 ICASE=1,NCASE
C...READ IN INPUT VALUES, SET RAMP CONFIGURATION
C...AND WRITE OUT HEADERS
      CALL READVL(ICASE,TOLER,ITMAX)
C...SET UP THE COMPUTABLE CONSTANTS
    1 CALL CONSET
C...THE INITIAL CONDITIONS ON PHI, ALSO GETS X-DERIVATIVES
      CALL START
      DO 10 KTIME=1,MAXT
      KOUNT=0
C...SOLVE THE REDUCED EQUATION:
      CALL SOLRED
C...ITERATION LOOP:  COMPUTE NEW RHS VECTOR; SOLVE THE FULL EQN.
    5 KOUNT=KOUNT+1
      IF(KOUNT.GE.ITMAX) GO TO 1000
      CALL FULSOL
C...CHECK FOR CONVERGENCE: CONVERGED => KRIT=1; NOT CONVERGED => KRIT=0.
      CALL COMPAR(TOLER,KRIT)
      IF(KRIT.EQ.0) GO TO 5
      TIME=(KTIME-1)*DT
      CALL SURFIT(KTIME)
      CALL EXCESS(VOLM)
      CALL SIFT3(PEAK,XPEAK)
      WRITE(6,164) TIME,VOLM,PEAK,XPEAK,KOUNT
  164 FORMAT(1X,F8.2,1PD15.6,4X,1PD15.6,4X,1PD15.6,8X,I2)
      KOMPAR=10*( (KTIME-1)/10 )
      IF(KOMPAR.EQ.KTIME-1)
     1 WRITE(17) TIME,VOLM,PEAK,XPEAK,KOUNT
```

```
      CALL SWITCH
   10 CONTINUE
  500 CONTINUE
      STOP
 1000 WRITE(6,1600)
 1600 FORMAT(1X,'MAXIMUM ITERATION COUNT EXCEEDED')
      STOP
      END

      SUBROUTINE BLOCK
      IMPLICIT REAL*8(A-H,O-Z)
      COMMON/XDERV/DERX(12341,3),DELSQ(12341,3)
      COMMON/YDERV/DERY(12341,3)
      DO 10 N=1,3
      DO 10 L=1,12341
      DELSQ(L,N) = 0.0
      DERX(L,N)  = 0.0
   10 DERY(L,N)  = 0.0
      RETURN
      END

      SUBROUTINE READVL(ICASE,TOLER,ITMAX)
      IMPLICIT REAL*8(A-H,O-Z)
      COMMON/STEPS/DX,DT,NODEX,MAXT,NODEX1
      COMMON/ADDY/DY,NODEY,NODEY1,NODTOT
      COMMON/WAVEH/ETA(12341),ALF,U,BETA,AU,NXZERO
      COMMON/DEPTH/HGT,SHELFH,SLOPE,NSTART,NEND,NSTRT1,NENDP1
      COMMON/SOPARM/SOR,SOR1
      COMMON/PROFIL/HEIGHT(55,41),DHDX(55,41),DHDY(55,41),DDH(55,41)
C...COMPUTES THE VARIOUS CONSTANTS
      READ(5,150) DX,DT,ALF,HGT,TOLER,MAXT,NODEX,NXZERO,ITMAX
  150 FORMAT(4F8.3,1PD15.6/4I5)
      READ(5,152) DY,NODEY
  152 FORMAT(F8.3,I5)
      READ(5,153) NSTART,NEND,SLOPE,SHELFH,SOR
  153 FORMAT(2I5,2F10.5/F10.5)
C...THE HEIGHT PROFILE AND ITS DERIVATIVES
      CALL SETRMP
C...PUT ALL INPUT OUT ONTO TAPE; NEW FILE IF MORE THAN ONE CASE
      IF(ICASE.NE.1) CALL WRTNF(17)
      WRITE(17) DX,DT,ALF,HGT,TOLER,MAXT,NODEX,NXZERO,ITMAX,
     1      DY,NODEY,NSTART,NEND,SLOPE,SHELFH,SOR
C...THE IDENTIFIERS FOR THIS CASE
      WRITE(6,60)
   60 FORMAT(10X,'**************************************************',
     1         '**********************************')
      WRITE(6,65)
   65 FORMAT(10X,'*',79X,'*')
      WRITE(6,70) ICASE
   70 FORMAT(10X,'*',32X,'CASE NUMBER =',I2,32X,'*')
      WRITE(6,65)
      WRITE(6,75) DX,DY,DT
   75 FORMAT(10X,'*',5X,'SPACING:',12X,'DX=',F6.3,5X,'DY=',
     1      F6.3,5X,'DT=',F6.3,17X,'*')
```

```
      WRITE(6,80) NODEX,NODEY,MAXT
   80 FORMAT(10X,'*',5X,'NUMBER OF POINTS:',3X,'X-DIR:',I3,5X,'Y-DIR:',
     1     I3,5X,'MAX TIME:',I3,14X,'*')
      XZERO=(NXZERO-1)*DX
      WRITE(6,65)
      WRITE(6,85) ALF,HGT,XZERO
   85 FORMAT(10X,'*',5X,'WAVE PARAMETERS:',5X,'AMPLITUDE:',15X,
     1       F5.3,23X,'*',1X/10X,'*',26X,'WATER DEPTH:',13X,
     1       F5.3,23X,'*',1X/10X,'*',26X,'INITIAL PEAK LOCATION',
     1     2X,F7.3,23X,'*')
      WRITE(6,65)
      ST =(NSTART-1)*DX
      END=(NEND-1)*DX
      WRITE(6,87) ST,END,SHELFH
   87 FORMAT(10X,'*',5X,'RAMP PARAMETERS:',5X,'START LOCATION:',8X,
     1       F6.2,24X,'*',1X/10X,'*',26X,'END LOCATION:',10X,
     1       F6.2,24X,'*',1X/10X,'*',26X,'DEPTH ON SHELF:',
     1     8X,F7.3,23X,'*')
      WRITE(6,65)
      WRITE(6,90) TOLER
   90 FORMAT(10X,'*',5X,'COMPUTATIONAL TOLERANCE USED:',1PD12.2)
      WRITE(6,65)
      WRITE(6,95) SOR
   95 FORMAT(10X,'*',5X,'SOR PARAMETER:',15X,1PD15.6)
      WRITE(6,65)
      WRITE(6,60)
      RETURN
      END

      SUBROUTINE CONSET
      IMPLICIT REAL*8(A-H,O-Z)
      COMMON/STEPS/DX,DT,NODEX,MAXT,NODEX1
      COMMON/WAVEH/ETA(12341),ALF,U,BETA,AU,NXZERO
      COMMON/RHSIDE/REDRHS(12341),FULRHS(12341)
      COMMON/ADDY/DY,NODEY,NODEY1,NODTOT
      COMMON/DEPTH/HGT,SHELFH,SLOPE,NSTART,NEND,NSTRT1,NENDP1
      COMMON/SQUEEZ/CF,C,C2,CD,D2,DSQ,DSQ3,DD4
      COMMON/SHELF/CFSH,CSH,C2SH,CDSH
      COMMON/SOPARM/SOR,SOR1
      COMMON/FIX/NS3
      U =DSQRT(1.0-ALF)
      BETA =DSQRT(3.*ALF/(4.*U*U))
      AU = ALF/U
      NODEX1=NODEX-1
      NODEY1=NODEY-1
      NODTOT=NODEX*NODEY
      NSTRT1=NSTART-1
      NENDP1=NEND+1
      NS3  =NSTART-3
C...FLAT ENTRY SECTION
      CF   = DT*DT*HGT/2. + HGT*HGT/3.
      C    =  -CF/(DX*DX)
      C2   =  2.0*C
      CD   =  (1.0 - 4.0*C)/SOR
```

```
C...SHELF SECTION
      CFSH   = DT*DT*SHELFH/2. + SHELFH*SHELFH/3.
      CSH    = -CFSH/(DX*DX)
      C2SH   = 2.0*CSH
      CDSH   = (1.0 - 4.0*CSH)/SOR
      D2     = DX*2.0
      DSQ    = DX*DX
      DSQ3   = DSQ*3.
      DD4    = DX*4.0
      SOR1   = 1.0 - SOR
      RETURN
      END

      SUBROUTINE START
      IMPLICIT REAL*8(A-H,O-Z)
      COMMON/STEPS/DX,DT,NODEX,MAXT,NODEX1
      COMMON/ADDY/DY,NODEY,NODEY1,NODTOT
      COMMON/WAVEH/ETA(12341),ALF,U,BETA,AU,NXZERO
      COMMON/POTEN/PHI(12341,2),PHIOLD(12341),PHINEW(12341)
      COMMON/XDERV/DERX(12341,3),DELSQ(12341,3)
      COMMON/YDERV/DERY(12341,3)
C...INTIAL CONDITIONS DO NOT ASSUME ANY DEPTH VARIATION
      DO 10 N=1,2
      T=(N-2)*DT
C...SET UP THE FIRST ROW OF VALUES
      DO 10 J=1,NODEX
      CHI       = BETA*((J-NXZERO)*DX-U*T)
      PHI(J,N)  = DSQRT(4.*ALF/3.)*DTANH( CHI )
      IF(CHI.GT.44.) GO TO 10
      DERX(J,N)  = AU/(DCOSH(CHI)*DCOSH(CHI))
      DELSQ(J,N) = -2.0*BETA*DERX(J,N)*DTANH(CHI)
   10 CONTINUE
C...SPREAD FIRST ROW ACROSS GRID
      DO 20 N=1,2
      DO 20 K=2,NODEY
      DO 20 J=1,NODEX
      L=J+(K-1)*NODEX
      PHI(L,N)   = PHI(J,N)
      DERX(L,N)  = DERX(J,N)
   20 DELSQ(L,N) = DELSQ(J,N)
      RETURN
      END

      SUBROUTINE SOLRED
      IMPLICIT REAL*8(A-H,O-Z)
      COMMON/STEPS/DX,DT,NODEX,MAXT,NODEX1
      COMMON/ADDY/DY,NODEY,NODEY1,NODTOT
      COMMON/WAVEH/ETA(12341),ALF,U,BETA,AU,NXZERO
      COMMON/DEPTH/HGT,SHELFH,SLOPE,NSTART,NEND,NSTRT1,NENDP1
      COMMON/RHSIDE/REDRHS(12341),FULRHS(12341)
      COMMON/POTEN/PHI(12341,2),PHIOLD(12341),PHINEW(12341)
      COMMON/XDERV/DERX(12341,3),DELSQ(12341,3)
      COMMON/YDERV/DERY(12341,3)
      COMMON/TWHERE/KTIME,KOUNT
```

```
      COMMON/SQUEEZ/CF,C,C2,CD,D2,DSQ,DSQ3,DD4
      COMMON/SHELF/CFSH,CSH,C2SH,CDSH
C.....C
C                                                    C
C          COMPUTES THE RHS FOR THE REDUCED EQUATION              C
C    AND CALLS THE SOLVER TO YIELD SOLUTION TO LINEARIZED EQUATION     C
C      WHICH IS THEN USED TO CALCULATE NONLINEAR TERMS AND           C
C           ALSO FUNCTIONS AS NEXT GUESS FOR SOLVER               C
C                                                    C
C                                                    C
C.....THE ENTRY AND EXIT EDGE BOUNDARIES.....-
      DO 10 JEND=1,NODTOT,NODEX
      REDRHS(JBND) = 2.*PHI(JBND,2) - PHI(JBND,1)
      JDEX=JBND+NODEX1
   10 REDRHS(JDEX) = 2.*PHI(JDEX,2) - PHI(JDEX,1)
C
C.....THE MIDDLE REGIONS.....--
C.....INITIAL FLAT SECTION.....
      C1 = -2.*HGT*HGT/3.
      B1 = HGT*DT*DT/2. + HGT*HGT/3.
      DO 30 K=1,NODEY
      DO 30 J=2,NSTRT1
      L=J+(K-1)*NODEX
   30 REDRHS(L) =2.*PHI(L,2) - PHI(L,1) + C1*DELSQ(L,2) + B1*DELSQ(L,1)
C.....SLOPING REGION.....
C              *EXCLUDING THE WALLS*
      DO 32 K=2,NODEY1
      DO 32 J=NSTART,NEND
      VHGT = H(J,K)
      VHX  = HX(J,K)
      VHY  = HY(J,K)
      VDELH= DELH(J,K)
      L=J+(K-1)*NODEX
      C1 = -(VHGT*VHGT/3.)*(2.+DT*DT*VDELH/2.)
      B1 = VHGT*DT*DT/2. + VHGT*VHGT/3.
      C3 = DT*DT-VHGT
      C4 = VHGT/2.
      C5 = - VHGT*VHGT*DT*DT/6.
   32 REDRHS(L)=2.*PHI(L,2) - PHI(L,1) + C1*DELSQ(L,2) + B1*DELSQ(L,1)
     1    + C3*(VHX*DERX(L,2)+VHY*DERY(L,2))
     2    + C4*(VHX*DERX(L,1)+VHY*DERY(L,1))
     3 + C5*(  VHX*(DELSQ(L+1,2)-DELSQ(L-1,2))
     4      + VHY*(DELSQ(L+NODEX,2)-DELSQ(L-NODEX,2))  )/(2.*DX)
C             *NOW CALCULATE ON THE WALLS*
      DO 33 I=1,2
      DO 33 J=NSTART,NEND
      K=(I-1)*NODEY1 + 1
      VHGT = H(J,K)
      VHX  = HX(J,K)
      VHY  = HY(J,K)
      VDELH= DELH(J,K)
      L=J+(K-1)*NODEX
      C1 = -(VHGT*VHGT/3.)*(2.+DT*DT*VDELH/6.)
      B1 = VHGT*DT*DT/2. + VHGT*VHGT/3.
```

```
      C3 = DT*DT-VHGT
      C4 = VHGT/2.
      C5 = - VHGT*VHGT*DT*DT/6.
   33 REDRHS(L)=2.*PHI(L,2) - PHI(L,1) + C1*DELSQ(L,2) + B1*DELSQ(L,1)
     1    + C3*(VHX*DERX(L,2)+VHY*DERY(L,2))
     2    + C4*(VHX*DERX(L,1)+VHY*DERY(L,1))
     3 + C5*(  VHX*(DELSQ(L+1,2)-DELSQ(L-1,2))  )/(2.*DX)
C
C.....FLAT SHELF SECTION.....
      C1 = -2.*SHELFH*SHELFH/3.
      B1 = SHELFH*DT*DT/2. + SHELFH*SHELFH/3.
      DO 34 K=1,NODEY
      DO 34 J=NENDP1,NODEX1
      L=J+(K-1)*NODEX
   34 REDRHS(L) =2.*PHI(L,2) - PHI(L,1) + C1*DELSQ(L,2) + B1*DELSQ(L,1)
C
C.....-PERFORM ONE PASS OF SUCCESSIVE OVER RELAXATION.....
      CALL SUCCES(PHIOLD,REDRHS)
C
C...PUT SOLUTION TO LINEAR INTO PHINEW  AS FIRST SOR GUESS
      DO 20 L=1,NODTOT
   20 PHINEW(L)=PHIOLD(L)
      RETURN
      END

      SUBROUTINE FULSOL
      IMPLICIT REAL*8(A-H,O-Z)
      COMMON/STEPS/DX,DT,NODEX,MAXT,NODEX1
      COMMON/ADDY/DY,NODEY,NODEY1,NODTOT
      COMMON/WAVEH/ETA(12341),ALF,U,BETA,AU,NXZERO
      COMMON/DEPTH/HGT,SHELFH,SLOPE,NSTART,NEND,NSTRT1,NENDP1
      COMMON/RHSIDE/REDRHS(12341),FULRHS(12341)
      COMMON/POTEN/PHI(12341,2),PHIOLD(12341),PHINEW(12341)
      COMMON/XDERV/DERX(12341,3),DELSQ(12341,3)
      COMMON/YDERV/DERY(12341,3)
      COMMON/TWHERE/KTIME,KOUNT
C... COMPUTES RHS FOR FULL EQN AND SOLVES FOR PHINEW
C...( B.C.'S ABSORBED IN DELSQ TERM)
      DO 20 K=1,NODEY
      DO 20 J=1,NODEX
      L=J+(K-1)*NODEX
      FULRHS(L) = REDRHS(L) - DT*( DELSQ(L,2)*(PHIOLD(L)-PHI(L,1))/2.
     1    +DERX(L,2)*(DERX(L,3)-DERX(L,1))
     2    +DERY(L,2)*(DERY(L,3)-DERY(L,1)) )
   20 CONTINUE
      CALL SUCCES(PHINEW,FULRHS)
    1 RETURN
      END

      SUBROUTINE COMPAR(TOLER,KRIT)
      IMPLICIT REAL*8(A-H,O-Z)
      COMMON/STEPS/DX,DT,NODEX,MAXT,NODEX1
      COMMON/ADDY/DY,NODEY,NODEY1,NODTOT
      COMMON/POTEN/PHI(12341,2),PHIOLD(12341),PHINEW(12341)
```

```
      KRIT=0
      DFITER=0.0
      DFTIME=0.0
      DO 10 I=1,NODTOT
      DFI   =PHIOLD(I)-PHINEW(I)
      DFITER=DFITER+DFI*DFI
      DFT   =PHI(I,2)-PHINEW(I)
      DFTIME=DFTIME+DFT*DFT
   10 CONTINUE
      COMTOL=DSQRT(DFITER)/DSQRT(DFTIME)
      IF(COMTOL.LT.TOLER) KRIT=1
      DO 20 I=1,NODTOT
   20 PHIOLD(I)=PHINEW(I)
      RETURN
      END

      SUBROUTINE SURFIT(KTIME)
      IMPLICIT REAL*8(A-H,O-Z)
      DIMENSION VELOC(12341)
      COMMON/STEPS/DX,DT,NODEX,MAXT,NODEX1
      COMMON/ADDY/DY,NODEY,NODEY1,NODTOT
      COMMON/WAVEH/ETA(12341),ALF,U,BETA,AU,NXZERO
      COMMON/POTEN/PHI(12341,2),PHIOLD(12341),PHINEW(12341)
      COMMON/XDERV/DERX(12341,3),DELSQ(12341,3)
      COMMON/YDERV/DERY(12341,3)
      COMMON/DEPTH/HGT,SHELFH,SLOPE,NSTART,NEND,NSTRT1,NENDP1
      COMMON/SQUEEZ/CF,C,C2,CD,D2,DSQ,DSQ3,DD4
      DO 5  K=1,NODEY
C.....INITIAL FLAT SECTION.....
      DO 10 J=1,NSTRT1
      L=J+(K-1)*NODEX
      PT   =(PHINEW(L) - PHI(L,1))/D2
      GPSQ =DERX(L,2)*DERX(L,2)+DERY(L,2)*DERY(L,2)
      PDSQT=(DELSQ(L,3) - DELSQ(L,1))/D2
   10 ETA(L)= -PT -GPSQ/2. + (HGT*HGT/3.)*PDSQT
C.....SLOPING REGION.....
      DO 12 J=NSTART,NEND
      L=J+(K-1)*NODEX
      VHGT  = H(J,K)
      VHX   = HX(J,K)
      VHY   = HY(J,K)
      PT    = (PHINEW(L) - PHI(L,1))/D2
      GPSQ  = DERX(L,2)*DERX(L,2)+DERY(L,2)*DERY(L,2)
      PDOTH = (VHX*(DERX(L,3)-DERX(L,1))+VHY*(DERY(L,3)-DERY(L,1)))/D2
      PDSQT = (DELSQ(L,3) - DELSQ(L,1))/D2
   12 ETA(L)= -PT + (VHGT*PDOTH-GPSQ)/2. + (VHGT*VHGT/3.)*PDSQT
C.....FLAT SHELF SECTION.....
      DO 14 J=NENDP1,NODEX
      L=J+(K-1)*NODEX
      PT   =(PHINEW(L) - PHI(L,1))/D2
      GPSQ =DERX(L,2)*DERX(L,2)+DERY(L,2)*DERY(L,2)
      PDSQT=(DELSQ(L,3) - DELSQ(L,1))/D2
   14 ETA(L)= -PT -GPSQ/2. + (SHELFH*SHELFH/3.)*PDSQT
    5 CONTINUE
```

```
      KOMP=10*( (KTIME-1)/10 )
      IF(KOMP.NE.(KTIME-1).AND.KTIME.NE.MAXT) RETURN
      WRITE(17)   KTIME,PHI,PHINEW,ETA
      WRITE(6,160) KTIME
  160 FORMAT(1X,'WRITING TO TAPE, KTIME=',I5)
      RETURN
      END

      SUBROUTINE EXCESS(VOLM)
      IMPLICIT REAL*8(A-H,O-Z)
      COMMON/STEPS/DX,DT,NODEX,MAXT,NODEX1
      COMMON/ADDY/DY,NODEY,NODEY1,NODTOT
      COMMON/WAVEH/ETA(12341),ALF,U,BETA,AU,NXZERO
C...INTEGRATES THE EXCESS MASS
      VOLM = 0.0
      DO 10 I=1,NODTOT
   10 VOLM = VOLM + ETA(I)*DX
      VOLM=VOLM/NODEY
      RETURN
      END

      SUBROUTINE SIFT3(PEAK,XP)
      IMPLICIT REAL*8(A-H,O-Z)
      DIMENSION P(3),X(3),IP(3)
      COMMON/STEPS/DX,DT,NODEX,MAXT,NODEX1
      COMMON/ADDY/DY,NODEY,NODEY1,NODTOT
      COMMON/WAVEH/ETA(12341),ALF,U,BETA,AU,NXZERO
      COMMON/TWHERE/KTIME,KOUNT
C...SEARCHES FOR THE THREE HIGHEST VALUES AND THE FITS A QUADRATIC
      DO 1000 K=1,NODEY,4
      DO 5 L=1,3
      P(L) = 0.0
    5 IP(L)= 0
      ISTART=1+(K-1)*NODEX
      IEND  =K*NODEX
      DO 10 I=ISTART,IEND
      IF (P(1).GT.ETA(I)) GO TO 12
       DO 100 M=1,2
       P(4-M) = P(3-M)
  100  IP(4-M)=IP(3-M)
      P(1) =ETA(I)
      IP(1)=I
      GO TO 10
   12 IF(P(2).GT.ETA(I)) GO TO 13
      P(3) = P(2)
      IP(3)=IP(2)
      P(2) = ETA(I)
      IP(2)= I
      GO TO 10
   13 IF(P(3).GT.ETA(I)) GO TO 10
      P(3) = ETA(I)
      IP(3)= I
   10 CONTINUE
      DO 20 M=1,3
```

```
 20 X(M)=(IP(M)-(K-1)*NODEX-NXZERO)*DX
    A=((P(1)-P(2))/(X(1)-X(2))-(P(1)-P(3))/(X(1)-X(3)))/(X(2)-X(3))
    B=(P(1)-P(3))/(X(1)-X(3)) - A*(X(1)+X(3))
    C= P(1) - A*X(1)*X(1) -B*X(1)
    XP=-B/(2.*A)
    PEAK=A*XP*XP + B*XP + C
    KOMP=20*( (KTIME-1)/20 )
    IF(KOMP.NE.(KTIME-1).AND.KTIME.NE.MAXT) GO TO 1000
    WRITE(6,160) K,PEAK,XP
160 FORMAT(1X,I5,1P2D15.6)
1000 CONTINUE
    RETURN
    END

    SUBROUTINE SWITCH
    IMPLICIT REAL*8(A-H,O-Z)
    COMMON/STEPS/DX,DT,NODEX,MAXT,NODEX1
    COMMON/ADDY/DY,NODEY,NODEY1,NODTOT
    COMMON/POTEN/PHI(12341,2),PHIOLD(12341),PHINEW(12341)
    COMMON/XDERV/DERX(12341,3),DELSQ(12341,3)
    COMMON/YDERV/DERY(12341,3)
    DO 10 I=1,NODTOT
    PHI(I,1)  = PHI(I,2)
    PHI(I,2)  = PHINEW(I)
    DERX(I,1) = DERX(I,2)
    DERX(I,2) = DERX(I,3)
    DERY(I,1) = DERY(I,2)
    DERY(I,2) = DERY(I,3)
    DELSQ(I,1) = DELSQ(I,2)
 10 DELSQ(I,2) = DELSQ(I,3)
    RETURN
    END

    SUBROUTINE DERSET(PASS)
    IMPLICIT REAL*8(A-H,O-Z)
    DIMENSION PASS(12341)
    COMMON/STEPS/DX,DT,NODEX,MAXT,NODEX1
    COMMON/ADDY/DY,NODEY,NODEY1,NODTOT
    COMMON/SQUEEZ/CF,C,C2,CD,D2,DSQ,DSQ3,DD4
    COMMON/SHELF/CFSH,CSH,C2SH,CDSH
    COMMON/XDERV/DERX(12341,3),DELSQ(12341,3)
    COMMON/YDERV/DERY(12341,3)
C...ENTRANCE AND EXIT BOUNDARIES HAVE DXX=0.0; DX CALC BY BACK/FWD DIFF.
C...ALL POINTS NOT LISTED ARE SET TO 0.0 BY BLOCK DATA:
C       IN GENERAL THESE ARE:
C               *ALL FIRST DER IN Y AT TOP AND BOTTOM BDYS
C               *ALL SECOND DER IN X AT RIGHT AND LEFT BDYS
C
C...ENTRANCE AND EXIT BOUNDARIES (EXCLUDING THE FOUR CORNERS)
    DO 10 K=2,NODEY1
    JB=(K-1)*NODEX + 1
    JE= K*NODEX
    DERX(JB,3)  = (PASS(JB+1)-PASS(JB) )/DX
    DERX(JE,3)  = (PASS(JE) -PASS(JE-1))/DX
```

```
      JBPN = JB+NODEX
      JBMN = JB-NODEX
      JEPN = JE-NODEX
      JEMN = JE-NODEX
      DERY(JB,3)   = (PASS(JBPN)-PASS(JBMN))/D2
      DERY(JE,3)   = (PASS(JEPN)-PASS(JEMN))/D2
      DELSQ(JB,3)  = (PASS(JBPN) - 2.*PASS(JB) + PASS(JBMN))/DSQ
      DELSQ(JE,3)  = (PASS(JEPN) - 2.*PASS(JE) + PASS(JEMN))/DSQ
   10 CONTINUE
C...THE WALL BOUNDARIES (EXCLUDING THE FOUR CORNERS)
      DO 20 JB=2,NODEX1
      JT=JB+NODEY1*NODEX
      JBP1 = JB + 1
      JBM1 = JB - 1
      JTP1 = JT + 1
      JTM1 = JT - 1
      DERX(JB,3)  = (PASS(JBP1)-PASS(JBM1))/D2
      DERX(JT,3)  = (PASS(JTP1)-PASS(JTM1))/D2
      DELSQ(JB,3) = (PASS(JBP1)-2.*PASS(JB)+PASS(JBM1)
     1           +2.*(PASS(JB+NODEX)-PASS(JB))   )/DSQ
   20 DELSQ(JT,3) = (PASS(JTP1)-2.*PASS(JT)+PASS(JTM1)
     1           +2.*(PASS(JT-NODEX)-PASS(JT))   )/DSQ
C...MIDDLE REGION, NO SPECIAL TREATMENT
      DO 30 K=2,NODEY1
      DO 30 J=2,NODEX1
      L=J+(K-1)*NODEX
      LP1 = L + 1
      LM1 = L - 1
      LPN = L + NODEX
      LMN = L - NODEX
      DERX(L,3)  = (PASS(LP1) - PASS(LM1))/D2
      DERY(L,3)  = (PASS(LPN) - PASS(LMN))/D2
   30 DELSQ(L,3) = (PASS(LP1)+PASS(LM1)+PASS(LPN)+PASS(LMN)
     1                -4.*PASS(L))/DSQ
C...FOUR CORNERS:
      NLTCOR=NODTOT-NODEX1
      DELSQ(1,3)     = 2.*(PASS(1+NODEX)-PASS(1) )/DSQ
      DELSQ(NODEX,3)  = 2.*(PASS(2*NODEX)-PASS(NODEX))/DSQ
      DELSQ(NLTCOR,3) = 2.*(PASS(NLTCOR-NODEX)-PASS(NLTCOR))/DSQ
      DELSQ(NODTOT,3) = 2.*(PASS(NODTOT-NODEX)-PASS(NODTOT))/DSQ
      RETURN
      END

      SUBROUTINE FIRGES(PASS)
      IMPLICIT REAL*8(A-H,O-Z)
      DIMENSION PASS(12341)
      COMMON/STEPS/DX,DT,NODEX,MAXT,NODEX1
      COMMON/ADDY/DY,NODEY,NODEY1,NODTOT
      COMMON/POTEN/PHI(12341,2),PHIOLD(12341),PHINEW(12341)
C...SETS UP THE INITIAL GUESS FOR SUCCES
C...ONLY DO THIS ESTIMATE IF SOLVING LINEAR (FIRST SOL EACH TIME)
      DO 10 L=1,NODTOT
   10 PASS(L)=2.*PHI(L,2)-PHI(L,1)
      RETURN
```

```
      END

      SUBROUTINE SUCCES(PASS,RHS)
      IMPLICIT REAL*8(A-H,O-Z)
      DIMENSION PASS(12341),RHS(12341)
      COMMON/STEPS/DX,DT,NODEX,MAXT,NODEX1
      COMMON/ADDY/DY,NODEY,NODEY1,NODTOT
      COMMON/XDERV/DERX(12341,3),DELSQ(12341,3)
      COMMON/YDERV/DERY(12341,3)
      COMMON/TWHERE/KTIME,KOUNT
      COMMON/DEPTH/HGT,SHELFH,SLOPE,NSTART,NEND,NSTRT1,NENDP1
      COMMON/SQUEEZ/CF,C,C2,CD,D2,DSQ,DSQ3,DD4
      COMMON/SHELF/CFSH,CSH,C2SH,CDSH
      COMMON/SOPARM/SOR,SOR1
C
C...SOLVES THE FIVE-BANDED SYSTEM BY SUCCESSIVE OVER RELAXATION
C...SOR ITERATIONS ARE INTERLEAVED WITH NON-LINEAR ITERATIONS
C...FIRST GUESS IS SUPPLIED BY SUBROUTINE CALL TO CUT DOWN ON ITERATIONS
      IF(KOUNT.EQ.0) CALL FIRGES(PASS)
C
C.....THE ENTRY AND EXIT EDGE BOUNDARIES.....-
C          (NO OFF-DIAGONALS, SIMPLE EQUALITY)
      DO 10 JBND=1,NODTOT,NODEX
      PASS(JBND) =RHS(JBND)
      JDEX=JBND+NODEX1
   10 PASS(JDEX) =RHS(JDEX)
C
C...WALL I  BOUNDARY HAS NO LEFT COMPONENT AND H HAS NO 1ST DER IN Y
C.....INITIAL  FLAT  SECTION.....
      DO 20 J=2,NSTRT1
      OFFDIA=C*(PASS(J-1)+PASS(J+1))+ C2*PASS(J+NODEX)
      PASS(J)=SOR1*PASS(J) + (RHS(J)-OFFDIA)/CD
   20 CONTINUE
C.....SLOPING REGION.....
      DO 22 J=NSTART,NEND
      VHGT   = H(J,1)
      VHX    = HX(J,1)
      CR     = -(VHGT/2. + VHGT*VHGT/DSQ3)
      CDR    = (1.0 - 4.0*CR)/SOR
      EX     = VHGT*VHX/DD4
      OFFDIA = (CR+EX)*PASS(J-1)+(CR-EX)*PASS(J+1)
     1       +2.0*CR*PASS(J+NODEX)
   22 PASS(J) = SOR1*PASS(J) + (RHS(J)-OFFDIA)/CDR
C.....FLAT SHELF SECTION.....
      DO 24 J=NENDP1,NODEX1
      OFFDIA=CSH*(PASS(J-1)+PASS(J+1))+ C2SH*PASS(J+NODEX)
   24 PASS(J) = SOR1*PASS(J) + (RHS(J)-OFFDIA)/CDSH
C
C.....THE MIDDLE REGIONS.....--
C
      DO 36 K=2,NODEY1
C.....INITIAL  FLAT  SECTION.....
      DO 30 J=2,NSTRT1
      L=J+(K-1)*NODEX
```

```
      OFFDIA=C*(PASS(L-1)+PASS(L+1)+PASS(L-NODEX)+PASS(L+NODEX))
   30 PASS(L) = SOR1*PASS(L) + (RHS(L)-OFFDIA)/CD
C.....SLOPING REGION.....
      DO 32 J=NSTART,NEND
      VHGT  = H(J,K)
      VHX   = HX(J,K)
      VHY   = HY(J,K)
      CR    = -(VHGT/2. + VHGT*VHGT/DSQ3)
      CDR   =  (1.0 - 4.0*CR)/SOR
      EX    =  VHGT*VHX/DD4
      EY    =  VHGT*VHY/DD4
      L=J+(K-1)*NODEX
      OFFDIA=(CR+EY)*PASS(L-NODEX) + (CR+EX)*PASS(L-1)
     1    + (CR-EX)*PASS(L+1)    + (CR-EY)*PASS(L+NODEX)
   32 PASS(L) = SOR1*PASS(L) + (RHS(L)-OFFDIA)/CDR
C.....FLAT SHELF SECTION.....
      DO 34 J=NENDP1,NODEX1
      L=J+(K-1)*NODEX
      OFFDIA=CSH*(PASS(L-1)+PASS(L+1)+PASS(L-NODEX)+PASS(L+NODEX))
   34 PASS(L) = SOR1*PASS(L) + (RHS(L)-OFFDIA)/CDSH
   36 CONTINUE
C...TOP BOUNDARY HAS NO RIGHT COMPONET; NO Y DERIVS IN H
C.....INITIAL  FLAT  SECTION.....
      DO 40 J=2,NSTRT1
      L = J + NODEY1*NODEX
      OFFDIA=C*(PASS(L-1)+PASS(L+1))+C2*PASS(L-NODEX)
   40 PASS(L) = SOR1*PASS(L) + (RHS(L)-OFFDIA)/CD
C.....SLOPING REGION.....
      DO 42 J=NSTART,NEND
      VHGT  = H(J,NODEY)
      VHX   = HX(J,NODEY)
      CR    = -(VHGT/2. + VHGT*VHGT/DSQ3)
      CDR   =  (1.0 - 4.0*CR)/SOR
      EX    =  VHGT*VHX/DD4
      L = J + NODEY1*NODEX
      OFFDIA=(CR-EX)*PASS(L+1)+(CR+EX)*PASS(L-1)
     1       +2.0*CR*PASS(L-NODEX)
   42 PASS(L) = SOR1*PASS(L) + (RHS(L)-OFFDIA)/CDR
C.....FLAT SHELF SECTION.....
      DO 44 J=NENDP1,NODEX1
      L=J+(NODEY-1)*NODEX
      OFFDIA=CSH*(PASS(L-1)+PASS(L+1))+C2SH*PASS(L-NODEX)
   44 PASS(L) = SOR1*PASS(L) + (RHS(L)-OFFDIA)/CDSH
C...SUPPLY THE DERIVATIVES FOR THE NEW TIME LEVEL FROM THIS SOLUTION
      CALL DERSET(PASS)
      RETURN
      END

      FUNCTION H(JX,KY)
      IMPLICIT REAL*8(A-H,O-Z)
      COMMON/DEPTH/HGT,SHELFH,SLOPE,NSTART,NEND,NSTRT1,NENDP1
      COMMON/PROFIL/HEIGHT(55,41),DHDX(55,41),DHDY(55,41),DDH(55,41)
      COMMON/FIX/NS3
      JP=JX-NS3
```

```
      H=HEIGHT(JP,KY)
      RETURN
      END
      FUNCTION HX(JX,KY)
      IMPLICIT REAL*8(A-H,O-Z)
      COMMON/DEPTH/HGT,SHELFH,SLOPE,NSTART,NEND,NSTRT1,NENDP1
      COMMON/PROFIL/HEIGHT(55,41),DHDX(55,41),DHDY(55,41),DDH(55,41)
      COMMON/FIX/NS3
      JP=JX-NS3
      HX=DHDX(JP,KY)
      RETURN
      END
      FUNCTION HY(JX,KY)
      IMPLICIT REAL*8(A-H,O-Z)
      COMMON/DEPTH/HGT,SHELFH,SLOPE,NSTART,NEND,NSTRT1,NENDP1
      COMMON/PROFIL/HEIGHT(55,41),DHDX(55,41),DHDY(55,41),DDH(55,41)
      COMMON/FIX/NS3
      JP=JX-NS3
      HY=DHDX(JP,KY)
      RETURN
      END
      FUNCTION DELH(JX,KY)
      IMPLICIT REAL*8(A-H,O-Z)
      COMMON/DEPTH/HGT,SHELFH,SLOPE,NSTART,NEND,NSTRT1,NENDP1
      COMMON/PROFIL/HEIGHT(55,41),DHDX(55,41),DHDY(55,41),DDH(55,41)
      COMMON/FIX/NS3
      JP=JX-NS3
      DELH=DDH(JP,KY)
      RETURN
      END

      SUBROUTINE SETRMP
C...THIS PROGRAM SETS UP THE HEIGHTS AND SMOOTHS THE DEPTH PROFILE
C...ALSO CALCULATES THE X, Y DERIVATIVES AND DELSQUARE.
C...RAMP LENGTH IS FIXED AT 10.
      IMPLICIT REAL*8(A-H,O-Z)
      DIMENSION HRAW(55,41)
      COMMON/PROFIL/H(55,41),HX(55,41),HY(55,41),DELH(55,41)
      DATA DX/0.4/
      DATA DEEP,SHALLO,SL/1.0,0.5,0.05/
      DATA NSTART,NEND/3,28/
      DATA MCURVE/16/
      NS1=NSTART+1
      NE1=NEND+1
C...INITIALIZE
      DO 5 J=1,55
      DO 5 K=1,41
      DELH(J,K)=0.0
      HX(J,K)=0.0
    5 HY(J,K)=0.0
C...THIS IS THE STRAIGHT RAMP PART
      DO 16 K=MCURVE,41
      DO 10 J=1,NSTART
   10 HRAW(J,K)=DEEP
```

```
      DO 12 J=NS1,NEND
   12 HRAW(J,K)=DEEP - SL*(J-NSTART)*DX
      DO 14 J=NE1,55
   14 HRAW(J,K)=SHALLO
   16 CONTINUE
C...THIS IS THE CURVED RAMP PART
      MC1=MCURVE-1
      PI2=3.14159/2.
      DO 18 K=1,MC1
      DO 18 J=1,55
      YP=(K-1)*DX
      XP=(J-1)*DX
      YM= MC1*DX
      CS=DCOS(PI2*YP/YM)
      F1=10.0*CS*CS + (NSTART-1)*DX
      F2=F1+10.0
      IF(XP.LT.F1)           HRAW(J,K)=DEEP
      IF(XP.GE.F1.AND.XP.LE.F2) HRAW(J,K)=DEEP-SL*(XP-F1)
      IF(XP.GT.F2)           HRAW(J,K)=SHALLO
   18 CONTINUE
C...SMOOTH THE PROFILE
      DO 20 K=1,41
      H(1,K) = HRAW(1,K)
      H(55,K)= HRAW(55,K)
      DO 20 J=2,54
      IF(K.EQ.1)  GO TO 21
      IF(K.EQ.41) GO TO 22
      H(J,K)=(HRAW(J+1,K)+HRAW(J,K)+HRAW(J-1,K)+
     !      HRAW(J,K+1)        +HRAW(J,K-1) )/5.
      GO TO 20
   21 H(J,K)=(HRAW(J+1,K)+HRAW(J,K)+HRAW(J-1,K)+2.*HRAW(J,K+1))/5.
      GO TO 20
   22 H(J,K)=(HRAW(J+1,K)+HRAW(J,K)+HRAW(J-1,K)+2.*HRAW(J,K-1))/5.
   20 CONTINUE
C...CALCULATE THE DERIVATIVES -- WHAT'S NOT THERE IS ZERO
C...X-DERS ARE EASY
      DO 30 J=2,54
      DO 30 K=1,41
   30 HX(J,K)  = (H(J+1,K) - H(J-1,K))/(2.*DX)
C...LEAVE Y-DERS AT WALLS TO BE ZERO
      DO 40 J=2,54
      DO 40 K=2,40
   40 HY(J,K)  = (H(J,K+1) - H(J,K-1))/(2.*DX)
C...SOME SPECIAL TREATMENT AT THE WALLS FOR DEL SQUARE
      DO 50 J=2,54
      DO 50 K=2,40
   50 DELH(J,K)= (H(J+1,K) -4.*H(J,K)+H(J-1,K)
     1         +H(J,K+1)         +H(J,K-1)  )/(DX*DX)
      DO 60 J=2,54
      DELH(J,1) = (H(J+1,1) -2.*H(J,1)+H(J-1,1)  )/(DX*DX)
   60 DELH(J,41)= (H(J+1,41) -2.*H(J,41)+H(J-1,41)  )/(DX*DX)
      RETURN
      END
```

REFERENCES

Abramowitz, M. and Stegun, I. (1964) *Handbook of Mathematical Functions* Washington: National Bureau of Standards

Airy, G.B. (1845) 'Tides and Waves" *Encyclopaedia Metropolitana*, vol. 5, London.

Boussinesq, J. (1871a), 'Theorie de L'Intumescence Liquide Appelee Onde Solitaire ou de Translation," *Comtes Rendus Acad. Sci. Paris*, vol. 72.

Boussinesq, J. (1871b), 'Theorie generale des mouvements qui sont propages dans un canal rectangulaire horizontal," *Comtes Rendus Acad. Sci. Paris* vol. 73.

Boussinesq, J. (1872), 'Theorie des ondes et des remous qui se propagent le long d'un canal rectangulaire horizontal, en communiquant au liquide contenu dans ce canal des vitesses sensiblement pareilles de la surface au fond." *J. Math. Pures Appl.* vol. 17.

Chang, P., Mellville, W.K., and Miles, J.W. (1979), "On the Evolution of a Solitary Wave in a Gradually Varying Channel," *J. Fluid Mech.*, vol. 95, pp. 401-414.

Carrier, G.F., and Pearson, C.E. (1976), *Partial Differential Equations Theory and Technique*, Chapter 14, 'Finite-Difference Equations and Numerical Methods", Academic Press, N.Y., pp. 257-283.

Chwang, A.T., and Wu, T.Y. (1976), "Cylindrical Solitary Waves," *Waves on Water of Variable Depth, Lecture Notes in Physics*, D.G. Provis and R. Radok, eds., Springer-Verlag Book Co., New York, N.Y., vol. 64, pp.80-90.

Fenton, J. (1972), "A Ninth Order Solution for the Solitary Wave", *J. Fluid Mech.*, vol. 53, Part 2, pp. 257-271.

Gardner, S.G., Greene, J.M., Kruskal, M.D., and Miura, R.M. (1967), 'Method for Solving the Korteweg-de Vries Equation", *Phys. Rev. Letters*, vol. 19, No. 19, pp. 1095-1097.

Goring, D.G. (1978), 'Tsunamis - The Propagation of Long Waves onto a Shelf," *Keck Laboratory Report No. KH-R-38*, California Institute of Technology, Pasadena, Ca.

Greenspan, D. (1974) *Discrete Numerical Methods in Physics and Engineering*, Academic Press, Inc., New York.

Grimshaw, R. (1971), 'The Solitary Wave in Water of Variable Depth. Part 2," *J. Fluid Mech.*, vol. 46, pp. 611-622.

Johnson, R.S. (1972), 'Some Numerical Solutions of a Variable-Coefficient Korteweg-de Vries Equation (with Applications to Solitary Wave Development on a Shelf)" *J. Fluid Mech.*, vol. 54, Part 1, pp. 81-91

Johnson, R.S. (1973), "On the Development of a Solitary Wave Moving Over an Uneven Bottom", *Proc. Camb. Phil. Soc.*, vol. 73, pp. 183-203.

Korteweg, D.J. and deVries, G. (1895), "On the Change of Form of Long Waves Advancing in a Rectangular Canal, and on a New Type of Long Stationary Wave," *Philosophical Mag.*, vol. 39, pp. 422-443.

Laitone, E.V. (1960) 'The Second Approximation to Cnoidal an Solitary Waves," *J. Fluid Mech.*, vol. 9, pp.430-444.

Lamb, H. (1932), *Hydrodynamics*, 6th Edition, Dover Pub., New York, N.Y.

Leendertse, J.J. (1967), "Aspects of a Computational Model for Long-Period Water-Wave Propagation", Rand Corporation, Memorandum RM-5294-PR.

Lepelletier, T.G. (1981), 'Tsunamis - Harbor Oscillations Induced by Nonlinear Transient Long Waves," Ph.D. Thesis, California Institute of Technology,

Pasadena, Ca.

Madsen, O.S., and Mei, C.C. (1969), 'The Transformation of a Solitary Wave Over an Uneven Bottom", *J. Fluid Mech.*, vol. 39, Part 4, pp. 781-791.

Madsen, O.S., and Mei, C.C. (1969), 'Dispersive Long Waves of Finite Amplitude over an Uneven Bottom," Hydraulics Laboratory Report No. 117, Department of Civil Engineering, Massachusetts Institute of Technology, Cambridge, Mass.

Miles, J.W. (1981), 'The Korteweg-de Vries Equation: a Historical Essay", *J. Fluid Mech.*, vol. 106, pp. 131-147.

O'Brien, G., Hyman, M., and Kaplan, S. (1951), "A Study of the Numerical Solution of Partial Differential Equations," *J. Math. Phys.*, vol. 29, pp. 233-251.

Peregrine, D.H. (1967), 'Long Waves on a Beach", *J. Fluid Mech.*, vol. 27, Part 4, pp. 815-827.

Rayleigh, Lord (1876) "On Waves" *Phil.Mag.*, vol. 1, pp. 257-279

Russell, J.S. (1844), *Report on Waves* British Association Reports.

Serrin, J. (1959), "Mathematical Principles of Classical Fluid Mechanics" *Handbuch der Physik* ed. S. Flugge, vol. VIII/1, Springer-Verlag, Berlin

Tappert F.D., and Zabusky N.J. (1971), "Gradient-Induced Fission of Solitons", *Phys. Rev. Letters*, vol. 27, No. 26, pp. 1774-1776.

Whitham, G.B. (1974), *Linear and Nonlinear Waves*, John Wiley and Sons, Inc., New York, N.Y.

Ursell, F. (1953), 'The Long Wave Paradox in the Theory of Gravity Waves." *Proceedings of the Cambridge Philosophical Society* vol. 49, pp. 685-694.

Vliegenthart, A.C. (1969), 'Dissipative Difference Schemes for Shallow Water

Equations" *Journal of Engineering Mathematics*, vol. 3, No.2, pp. 81-94.

Vliegenthart, A.C. (1971), "On Finite-Difference Methods for the Korteweg-de Vries Equation" *Journal of Engineering Mathematics*, vol. 5, No. 2, pp. 137-155.

Wu, T.Y. (1981), "Long Waves in Ocean and Coastal Waters," *Journal of Engineering Mechanics Division*, ASCE, vol. 107, No. EM3, **Proc. Paper 16346**, June, pp. 501-522.